The Dissertation Committee for Michael Rodgers Mand Certifies that this is the approved version of the following dissertation

Mechanisms and Consequences of ATM Activation

Committee:

Tanya Paull, Supervisor

Kevin Dalby

Jon Huibregtse

Edward Marcotte

Kyle Miller

Mechanisms and Consequences of ATM Activation

by

Michael Rodgers Mand, B.S. Bio.

Dissertation

Presented to the Faculty of the Graduate School of

The University of Texas at Austin

in Partial Fulfillment

of the Requirements

for the Degree of

Doctor of Philosophy

The University of Texas at Austin

May 2015

Dedication

I dedicate this dissertation to Beth, Luke, and Vivian. Without your help, encouragement, and smiles, this work would not have been possible.

Acknowledgements

I would first like to thank Tanya for her continual support and advice. She has provided insights into my project at key moments and helped me find new areas to explore when my research was at a crossroads. She is a constant inspiration for how a scientist should think, act, and lead.

I would also like to thank the members of my committee: Dr. Kevin Dalby, Dr. Jon Huibregtse, Dr. Edward Marcotte, and Dr. Kyle Miller. They have provided guidance with my experiments and thoughtful comments on my project.

The entire Paull lab has been immensely helpful during my studies. They made the lab a fun and sociable place to work and gave helpful remarks about my experiments. I would like to thank everyone I worked with in the lab: Sucheta Aurora, Rajashree Deshpande, Scott Ditch, Qiong Fu, Zhi Guo, Ben Hopkins, Gary Kao, Jeff Kuhnlein, Ji-Hoon Lee, Matt Nicolette, Nodar Makharashvili, Logan Myler, Chelsea Parks, Chase Pectol, Tanya Raymond, Mingjuan Shen, Lisa Sledd, Rose Stewart, Soo-Hyun Yang, Julie Zhang, Suting Zhen, and Yi Zhou. I would especially like to thank Jeff Kuhnlein and Nodar Makharashvili for keeping me in good spirits throughout the years.

I would also like to thank my family and friends for their constant support and encouragement. They have kept me focused and driven to finish. My children Luke and Vivian have given me much needed laughs when things were difficult. Finally, I would like to thank my wife Beth who supported me in many ways. Without you, I could not have done this. Thank you.

Mechanisms and Consequences of ATM Activation

Michael R. Mand, Ph.D.

The University of Texas at Austin, 2015

Supervisor: Tanya T. Paull

Mutations in the ataxia telangiectasia mutated (ATM) gene cause the disease ataxia-telangiectasia (A-T). Patients with this disease have multiple symptoms, including the eponymous ataxia and telangiectasia as well as immunodeficiency, radiation sensitivity, and increased cancer rates. The ATM protein is a kinase and is activated by multiple types of stress to affect many cellular processes.

At sites of DNA double-strand breaks (DSBs), ATM is activated by the protein complex Mre11/Rad50/Nbs1 (MRN). As part of this complex, Rad50 binds and hydrolyzes ATP and causes large conformational changes in the complex. However, the importance of this enzymatic activity in the activation of ATM has been unknown. Here I show ATP binding by Rad50 is required for ATM activation while ATP hydrolysis is dispensable.

ATM is also activated in the presence of oxidative stress. Separation-of-function mutations for the activation of ATM by DSBs and oxidative stress have been characterized in vitro. Here, the effects of expressing wild-type ATM or ATM with these different separation-of-function mutations in an ATM-deficient lymphoblast cell line have been characterized. Analysis of the proteomes of these cells and a control cell line revealed that non-functional ATM resulted in the loss of a large group of proteins by mass spectrometry. The levels of these proteins were similar in

the cells, but in the presence of non-functional ATM they showed increased levels of aggregation. Thus my results suggest ATM may function to prevent aggregation in these conditions. Notably neurodegeneration is often associated with aggregation.

In the phosphoproteomes of cells expressing the various ATM constructs, the parental cell line and cells with ATM unable to be activated by oxidative stress had lower levels of phosphopeptides predicted to be phosphorylated by CK2. This decrease in CK2 activity was also associated with increased aggregation, specifically a subunit of CK2 known as CK2β. This work provides insights into the mechanism of ATM activation by MRN and the potential involvement of ATM in the prevention of protein aggregation.

Table of Contents

List of Figures

CHAPTER 1: INTRODUCTION

DNA double-strand breaks (DSBs) are the most dangerous genetic lesions and their repair requires the coordination of many different proteins. These breaks are repaired through two main pathways, non-homologous end joining (NHEJ) and homologous recombination (HR). In NHEJ, two DNA ends undergo limited processing and are directly ligated [2]. In HR, the breaks are more extensively processed to leave long 3' ends that are able to invade and synthesize new DNA from the homologous chromosome [3]. A key event in the choice between NHEJ and HR is the processing of the DNA ends. After the 3' end has been resected for HR, a break can no longer be repaired by NHEJ [3]. This resection and the cellular response to DSBs are controlled by a signaling cascade initiated by the protein kinase *a*taxia *t*elangiectasia *m*utated (ATM) [4].

ATM is activated by multiple types of cellular stresses and regulates many pathways. In the canonical activation pathway, ATM is activated at DNA double-strand breaks (DSBs) to initiate a signaling cascade important for DNA repair through homologous recombination. More recently, ATM was shown to be activated by oxidative stress in cells and in vitro [5]. Additionally, ATM was found to be activated during various cellular conditions including hypoxia [6], hyperthermia [7], hypotonic stress [8], and mitosis [9]. Activated ATM regulates the phosphorylation of hundreds of substrates [10-12]. Initially, most of these substrates of ATM were found to function in DNA repair, cell cycle checkpoints, and gene regulation. However, ATM substrates have also been shown to be involved in other cellular functions including protein folding [12, 13], the pentose phosphate

pathway [13], autophagy [14], protein synthesis [15], and glucose uptake [16]. Although less well understood, these pathways may represent ATM functions in the absence of DNA damage.

ATAXIA TELANGIECTASIA MUTATED

The ATM gene was discovered during a search for the molecular cause of the neurodegenerative disease ataxia telangiectasia (A-T) [17]. Loss-of-function mutations in the ATM gene result in multiple symptoms including the two symptoms for which it is named – ataxia, the progressive loss of muscle coordination in affected patients, and telangiectasia, small dilated blood vessels visible in the eyes of patients. Other symptoms include immunodeficiency, radiation sensitivity, increased cancer rates, and infertility. A-T affects between 1 in 40,000 and 1 in 100,000 people and is inherited in an autosomal recessive manner. An estimated 1.4% of the population are heterozygous carriers of a mutant allele of ATM and heterozygosity has been associated with an increased risk for certain types of cancer [18, 19]. Mice heterozygous for ATM have also been shown to develop cancer at higher rates after exposure to radiation [20]. ATM knockout mice recapitulate some of the phenotypes from humans including radiation sensitivity, immunodeficiency, and infertility although neurodegeneration is not observed [21]. Notably, kinase-dead ATM is a recessive lethal gene that causes embryonic lethality in mice [22]. The cellular phenotypes of ATM deficiency include deficits in checkpoint activation, increased radiosensitivity, and higher levels of oxidative stress [4]. As the effects of the loss of functional ATM are so diverse, it appears ATM regulates many different pathways in mammalian cells.

The ATM gene was identified on chromosome 11q22-23 by positional cloning and is nearly 150,000 base pairs long [17]. The transcribed mRNA is 13,147 nucleotides and contains 66 exons that encode the 3,056 amino acids of the ATM protein. The ATM protein is a serine/threonine protein kinase in the phosphatidylinositol 3-kinase-related (PI3K) kinase (PIKK) family with a preferred recognition sequence of a serine or threonine followed by a glutamine (S/TQ) [23]. This family includes two other proteins involved in DNA repair, *A*taxia *T*elangiectasia and *R*ad3-related protein (ATR) and the *D*NA-dependent *P*rotein *K*inase *C*atalytic *S*ubunit (DNA-PKcs) [24]. In addition, the *M*ammalian *T*arget *O*f *R*apamycin (mTOR), the *S*uppressor of *M*orphogenesis in *G*enitalia-*1* (SMG-1), and the *TR*ansformation/t*R*anscription domain-*A*ssociated *P*rotein (TRRAP) proteins are also members of this family [24]. The structures and regulation of these other PIKK family members provide valuable insights into ATM.

PIKK DOMAINS

The protein kinases in the PIKK family all share a kinase domain similar to the kinase domain of the PI3K family, a group of lipid kinases that phosphorylate the 3' OH of inositol in phosphatidylinositols [25]. Although the kinase domains are similar to PI3Ks, PIKKs have only been shown to phosphorylate proteins [24]. In addition to the kinase domain, the PIKK family members share four other domains: an extensive section of α-helical repeats in the N-terminus followed by the FRAP-ATM-TRRAP (FAT) domain, the aforementioned kinase domain, the PIKK regulatory domain (PRD), and finally the FAT C-terminal (FATC) domain (Figure 1.1).

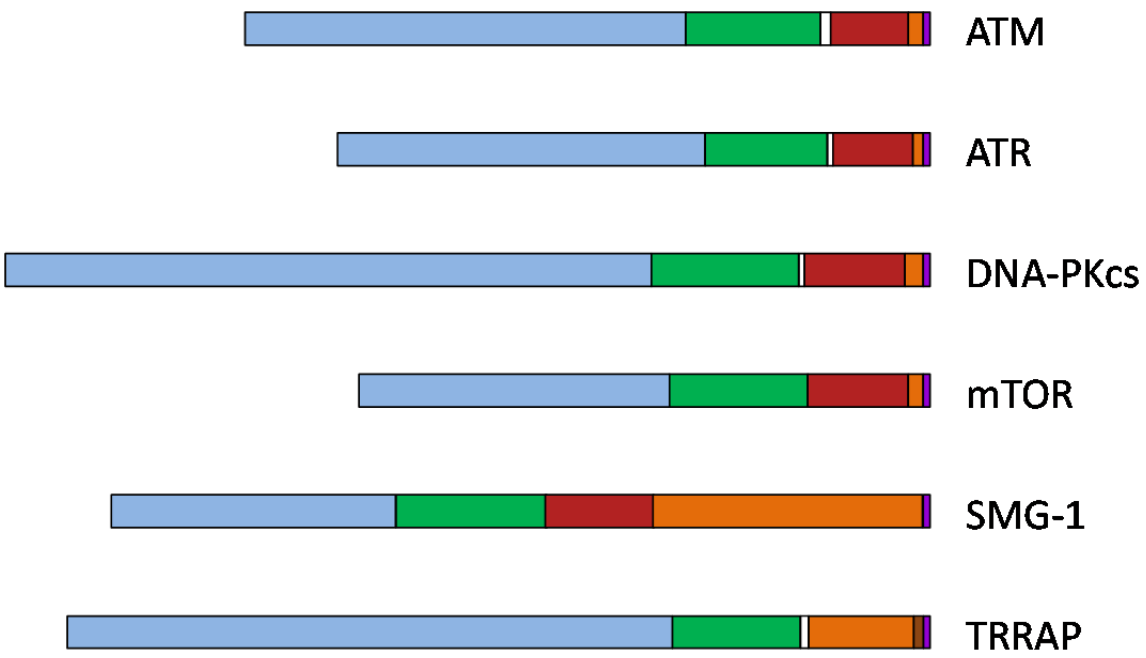

Figure 1.1 Alignment of the functional domains of PIKKs.

The colors represent domains present in the PIKKs: blue, HEAT repeats; green, FAT domain; red, PI3K-like kinase domain; orange, PIKK regulatory domain; purple, FATC domain. In ATM, the domains are defined as the following amino acids: HEAT repeats, 1-1,965; FAT domain, 1,966-2,566; kinase domain, 2,614-2,960; PIKK regulatory domain, 2,961-3,024; FATC domain, 3,025-3,056. Adapted from [26].

The α-helical repeats in the PIKKs have been predicted to be HEAT repeats with each repeat consisting of two α-helical regions of 10-20 amino acids joined by a 5-8 residue loop [27]. HEAT repeats were previously found in and named for the *H*untington, *E*longation factor 3, protein phosphatase 2*A*, and *T*OR1 proteins. In crystal structures from these and other proteins, HEAT repeats stack to form large superhelical scaffolds involved in protein-protein interactions [28-30]. Notably, ATM has been shown to interact with other proteins through its N-terminus,

including its canonical substrate p53 and Nbs1, a protein involved in recruiting ATM to DSBs [31-34].

The FAT and FATC domains always occur together and are thought to interact to regulate the activity of the PIKKs [35]. In DNA-PKcs, the stimulation of kinase activity from binding Ku70/80 and DNA also causes large conformational changes in the FAT and FATC domains [36]. The FATC domain sequence is more conserved than the FAT domain sequence suggesting a conserved function in this domain among the PIKKs [37]. Notably, the FATC domains of ATR, DNA-PKcs, and mTOR have been substituted for the FATC domain of ATM without a loss of kinase activity [38]. However, the FATC domains are not fully interchangeable as replacing the FATC domain of mTOR or ATR with the FATC domain of ATM abolishes kinase activity [39, 40]. Furthermore, deletion or mutation of even one residue of the FATC domain in mTOR has been shown to abolish kinase activity [40, 41]. In ATM, a mutation was found in an A-T patient that truncates the final 10 residues of the FATC domain and severely reduces kinase activity in vitro [5, 42, 43]. All of these results suggest the FAT and FATC domains function in the regulation of the activity of PIKKs.

The PIKK regulatory domain (PRD) is the region between the kinase domain and the FATC domain [39]. Deletion of this entire region has been shown to abolish kinase activity although shorter deletions within this region can reduce this effect or have the opposite effect [39, 44]. Post-translational modifications and protein-protein interactions in the PRD have been shown to enhance PIKK kinase activity. In ATR, Topoisomerase II-binding protein 1 has been shown to stimulate kinase activity through an interaction with the PRD [45]. Mutational analysis of DNA-PKcs

showed specific residues in the PRD were autophosphorylated and required for its role in NHEJ [39]. ATM also undergoes several post-translational modifications in this region that modulate its kinase activity. These will be discussed further in the ATM post-translational modifications section. Thus, the PRD is also important for the regulation of the kinase activity in the PIKKs.

PIKK STRUCTURES

As ATM is difficult to crystallize and thus has not been analyzed by X-ray crystallography, there is no atomic resolution structure. Llorca et al. examined ATM by electron microscopy (EM) and obtained a structure at about 30 Å resolution [46]. In the electron micrographs, most of the ATM was monomeric due to the presence of detergents in the lysis buffer and sonication of the lysate [34, 46, 47]. In this structure, ATM appears to have a distinct arm and head, possibly corresponding to the N-terminal α-helices and the FAT, kinase, PR, and FATC domains, respectively. Upon addition of DNA the arm appears to close and form a ring structure perhaps acting as a clamp [46]**.** However, the DNA binding of ATM is not thought to be relevant in the cellular setting as the recruitment of ATM to DSBs is dependent on other complexes.

Two other PIKKs – mTOR [48] and DNA-PKcs [49] – have been crystallized as well as many PI3K proteins, including PI3Kγ [50]. The mTOR structure (3.2 Å resolution) is an N-terminal truncation of mTOR such that some of the HEAT repeats are removed but the other domains remain (PDB code: 4JSV). In addition to mTOR, this structure contains the mLST8 protein from mTOR complex 1 and 2. In this structure, the kinase domain rests on the FAT domain and interacts with both the

FATC domain and the PRD. The active site is recessed and most mutations associated with mTOR hyperactivity appear to increase access to the active site [48]. The FATC domain is a kinked α-helix with a loop at the C-terminus which is similar to the FATC domain of *Saccharomyces cerevisiae* mTOR (*Sc*mTOR). However, in the *Sc*mTOR analyzed by NMR the loop at the end of FATC was shown to be stabilized by a disulfide bond linking cysteines 2460 and 2467 [51]. Although these two cysteines are conserved in humans, the disulfide is not evident in the crystal structure. This could be due to the presence of mLST8 in the human structure or differences in the preparation of the samples. Aligning the FAT, kinase, and FATC domain of this mTOR structure with porcine PI3Kγ (PDB code: 1E8X) [50] reveals the high degree of similarity between the kinase domains (Figure 1.2) . In addition, some of the α-helices from the FAT domain as well as the highly conserved FATC domain overlap with α-helices from PI3Kγ suggesting similar mechanisms of regulation.

The DNA-PKcs structure is relatively low resolution but, after refinement, the structure agrees with previous EM results [49, 52-54]. The DNA-PKcs structure includes a ring with an opening at the bottom and a crown that may correspond to the arm and head visible in the ATM structure. The HEAT repeats of DNA-PKcs form the ring and opposite the opening the other domains rest on the HEAT repeats. The structure shows the FAT, PR, and FATC domains coming together and forming a base upon which the kinase domain sits suggesting these domains could control kinase activity through direct interactions and structural rearrangements.

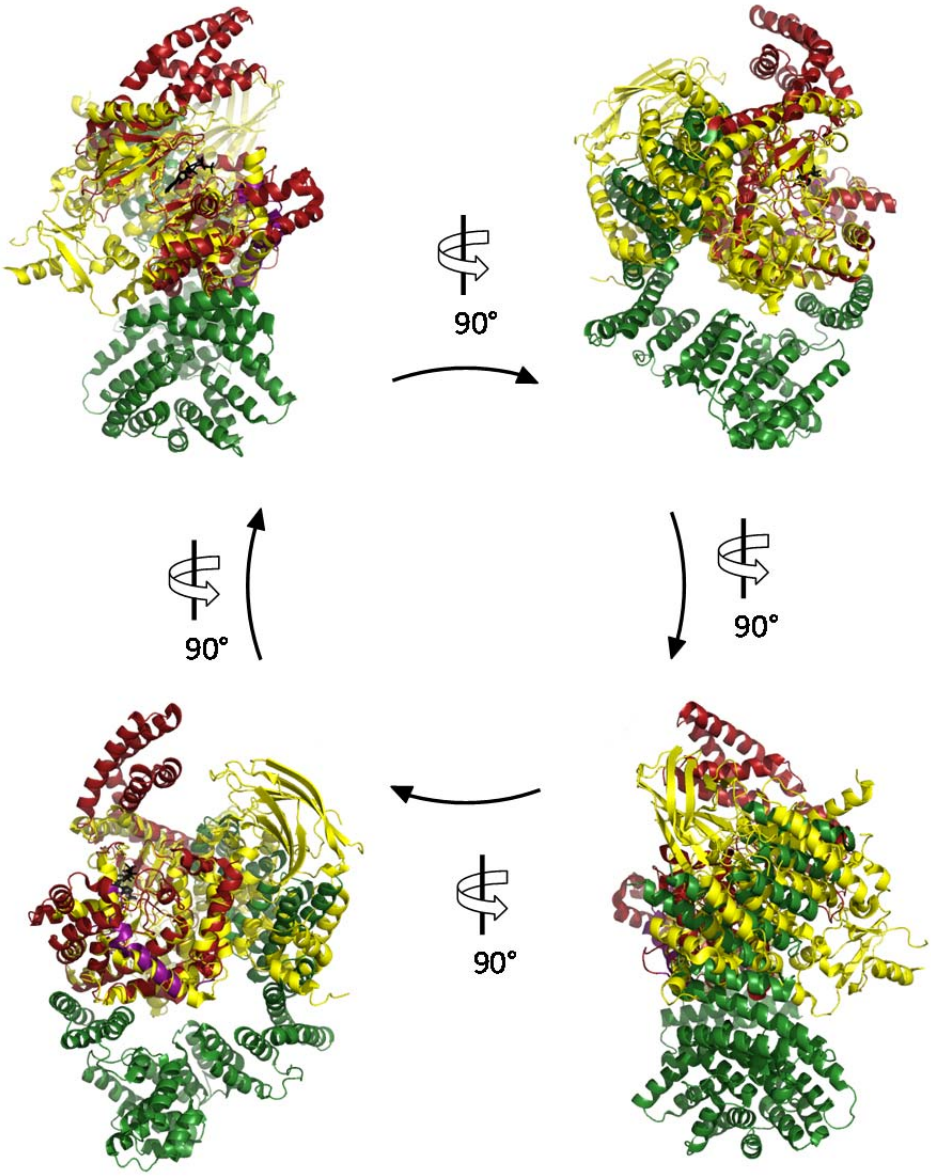

Figure 1.2 Alignment of mTOR and PI3Kγ structures reveal similarities between various domains.

Rotations of an alignment of human mTOR residues 1385-2549 and *Sus scrofa* PI3Kγ residues 142-1092. The colors represent the following: green, mTOR FAT domain; red, mTOR kinase domain; purple, mTOR FATC domain; and yellow, PI3Kγ kinase domain; black, mTOR ADP and PI3Kγ ATP. Alignments and figures were generated using Pymol version 1.3 and the PDB files mTOR (4JSV) and PI3Kγ (1E8X).

ATM Activation by DNA Double-Strand Breaks

ATM functions as a key signaling protein in the cellular response to DSBs. Following a DSB, many proteins accumulate at the site and form foci. Among the first of these proteins is Mre11/Rad50/Nbs1 (MRN), a complex consisting of dimers of the three individual proteins. After a DSB, MRN recruits ATM through an interaction with the C-terminus of Nbs1 [32-34, 55]. ATM is recruited in an inactive dimer form and then undergoes autophosphorylation and monomerization [8]. This active form of ATM then phosphorylates hundreds of substrates to activate and recruit DNA repair proteins, trigger cell cycle checkpoints, and regulate gene expression (Figure 1.3) [1, 11, 12]. As part of this process, ATM reinforces the formation of DNA damaged-induced foci through the phosphorylation of H2AX, MDC1, and BRCA1 [1, 56]. In addition to its activity at the site of the DSB, ATM also phosphorylates substrates in the nucleoplasm and cytoplasm after DNA damage [57-61].

MRN Conformational States

The Mre11/Rad50/Nbs1(Xrs2) complex in eukaryotes binds to DSBs and initiates DNA repair and signaling. Mre11 is an endonuclease important for the initiation of resection at the DSB [62, 63]. Rad50 binds DNA and also has ATPase activity that affects the structural conformation of the entire complex [64-67]. The nuclear localization of MRN is controlled by Nbs1, which also acts as a scaffold for protein interactions [55, 68, 69].

ATM activation in response to DSBs requires the MRN complex [70]. Immunodepletion experiments in *Xenopus laevis* extracts showed ATM monomerization is increased in an MRN-dependent manner [71] in agreement with

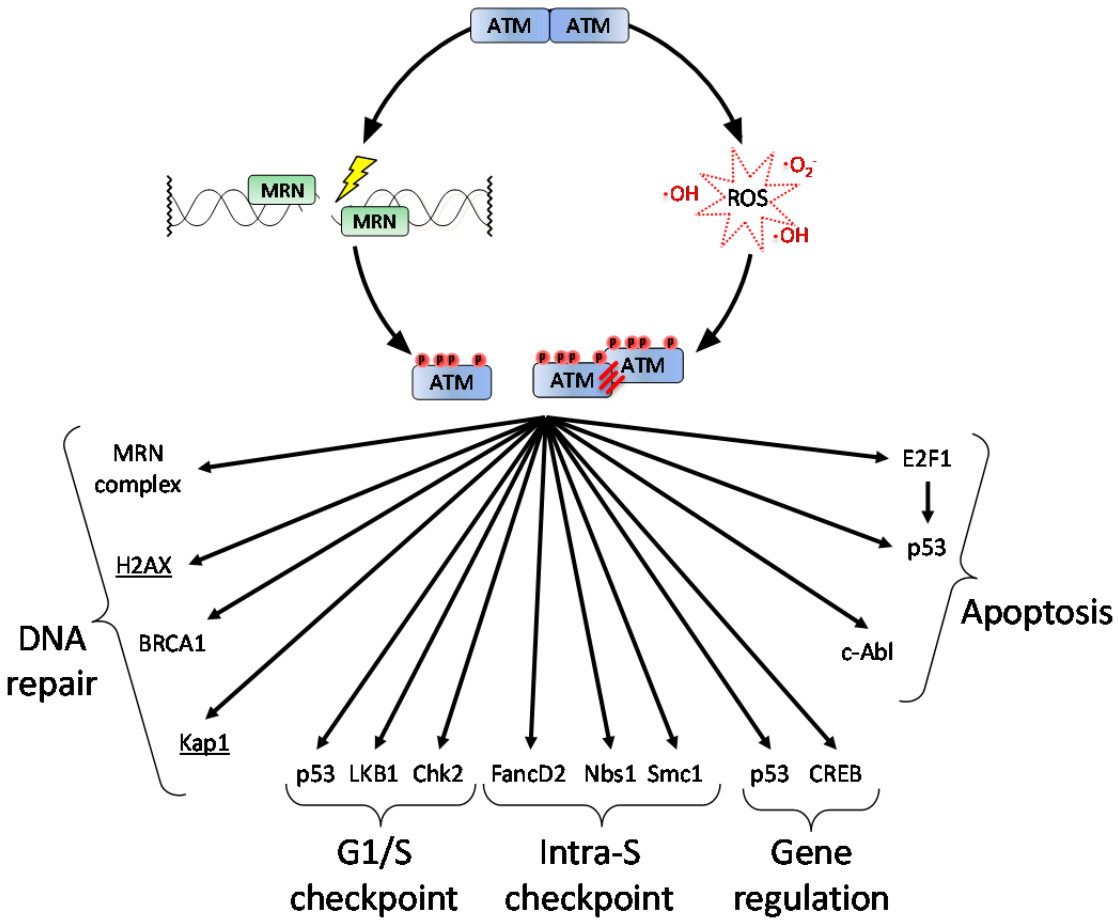

Figure 1.3 Model of downstream effectors after ATM activation.

Representative downstream effectors of ATM. After activation by DNA double-strand breaks or oxidative stress, ATM phosphorylates proteins involved in many different pathways. The underlined substrates are not phosphorylated by ATM after oxidative stress activation. Adapted from Kurz and Lees-Miller (2004) and Khalil, Tummala, Chakarov, Zhelev, and Lane (2012).

previous results using purified MRN that demonstrated MRN binding directly causes ATM autophosphorylation and monomerization [34]. Cells deficient in Mre11, Nbs1, or Rad50 show defects in ATM activation after DSBs [72-74]. Hypomorphic mutations in the MRE11, NBS1, and RAD50 genes are associated with diseases similar to A-T called AT-like disorder (ATLD), Nijmegen breakage syndrome (NBS), and NBS-like disorder (NBSLD), respectively [73, 75, 76]. However, these diseases have some unique symptoms, generally show a slower onset, and are not associated with all the symptoms of A-T suggesting MRN and ATM have related but distinct functions [73, 75, 76].

The structures and domains of the proteins in MRN have been characterized and reveal which parts are important for its function. Rad50 is a member of the structural maintenance of chromosomes (SMC) family of proteins and has an extensive antiparallel coiled-coil domain [64]. At one end of the coiled-coils, the N-termini and C-termini of 2 different Rad50 molecules bind to form globular head domains where ATP binds and is hydrolyzed. At the other end of the coiled-coils, a zinc hook tethers two Rad50 molecules together [70]. Crystal structures of Mre11 from *Pyrococcus furiosus, Thermotoga maritima*, and *Schizosaccharomyces pombe* alone or in complex with Rad50 or Nbs1 have helped characterize the Mre11 dimer interface and Rad50 and Nbs1 binding domains in Mre11 [67, 77, 78]. Many of the mutations associated with ATLD are in the Nbs1 binding domain of human Mre11 [79]. Analyses of Nbs1 have shown it interacts with many DNA-repair related proteins including Mre11, ATM, MDC1, CtIP, ATR, and WRN [80, 81]. Mutations of Nbs1 associated with NBS are mostly truncations, suggesting the C-terminus is important for Nbs1 function [76]. Notably, the C-terminus of Nbs1 contains the ATM

and Mre11 interaction domains as well as three potential nuclear localization signals [55, 82, 83].

Mre11 and Rad50 proteins are able to form a stable complex (MR) by themselves in a stoichiometry of $Mre11_2$:$Rad50_2$ or $Mre11_4$:$Rad50_4$ [84]. The structures of the complex of Mre11 and the catalytic head domain of Rad50 with shortened coiled-coils in the presence or absence of ADP and ATPγS have been described and suggest a mechanism whereby MRN is regulated (Figure 1.4) [65, 85]. The structure of *Methanococcus jannaschii* Mre11 and Rad50 (residues 1-190 and 825-1005; designated *Mj*MR^{CC}) bound to ATPγS showed Mre11 affects Rad50 dimer stabilization and key residue positioning for ATP hydrolysis [65]. Comparison between *Mj*MR^{CC} bound to ATPγS and ADP revealed large changes in the structure upon ATP hydrolysis including a rotation of the coiled-coils that could unveil the active site of Mre11 [65]. Another recent study suggests the regulation of MRN occurs through modulation of its various flexible subunits, including through the stabilization of Mre11 induced by Nbs1 binding [81].

The structure of *Thermatoga maritima* MR^{NBD} (*Tm*MR^{NBD}) (residues 1-190 and 686-852 of Rad50) in the absence of any ATP nucleotide showed an extended, open conformation [85]. Although *Tm*MR^{NBD} was unable to be crystallized in the presence of ATPγS, biochemical analyses showed a large conformational change upon the addition of ATP and DNA [85]. A later structure of *Tm*MR^{NBD} using cysteine mutations to stabilize the ATP-bound conformation showed the $Rad50^{NBD}$ flipped relative to Mre11 in the disulfide-stabilized form versus the ADP-bound form [66]. These structures demonstrate that ATP binding and hydrolysis induce large conformational shifts that affect the positioning of the proteins. However, it is

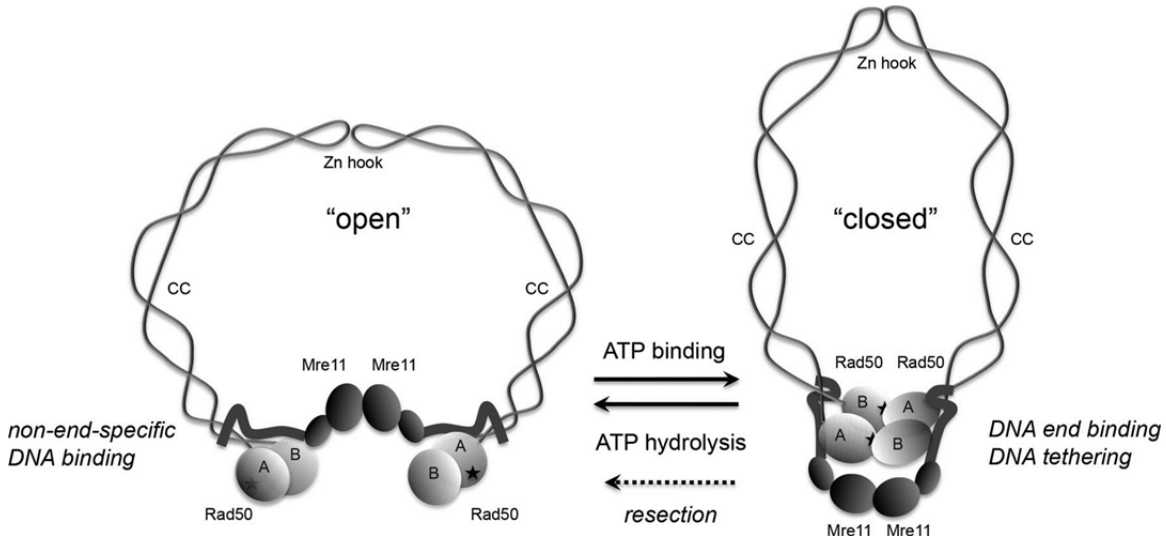

Figure 1.4 Schematic model of MRN in the absence (open) or presence of ATP (closed).

Rad50 is shown as light gray globular domains containing Walker A (A) and Walker B (B) motifs connected by intramolecular, antiparallel coiled-coils (CC), that attach to each other through the zinc hook motifs (Zn hook). Stars indicate the approximate positions of the ATP-binding residues in Rad50. Mre11 is shown as dark gray globular domains representing the nuclease/dimerization domain and the capping domain, connected to the linker that binds to the coiled-coils of Rad50. The closed state is associated with a higher affinity for DNA ends and with DNA tethering, while the movement from the closed to the open state is required for Mre11 nuclease activity and promotion of resection. The zinc hook is shown attached here, but the complex has also been observed with hooks unattached, both in solution and bound to DNA. This research was originally published in in Journal of Biological Chemistry. Lee JH, Mand MR, Deshpande RA, Kinoshita E, Yang SH, Wyman C, Paull TT. Ataxia Telangiectasia-Mutated (ATM) Kinase Activity Is Regulated by ATP-driven Conformational Changes in the Mre11/Rad50/Nbs1 (MRN) Complex. Journal of Biological Chemistry. 2013; 288:12840-12851. © the American Society for Biochemistry and Molecular Biology.

unknown which nucleotide binding state of MRN is responsible for the activation of ATM.

OXIDATIVE STRESS IN A-T AND ATM ACTIVATION

The loss of ATM kinase activity has been associated with high levels of oxidative stress. A-T patients have increased oxidative damage on lipids and DNA [86] and lower levels of antioxidants in their blood plasma [87]. Similarly, ATM knockout mice have changes in the activities of thioredoxin, catalase, and manganese superoxide indicative of high levels of reactive oxygen species (ROS) [88]. Oxidative stress from the loss of ATM may be involved in the predisposition for cancer as ATM knockout mice have higher rates of lymphoma and treatment of the mice with the antioxidant N-acetylcysteine (NAC) reduces this incidence [89]. In addition, oxidative stress may be partially responsible for immunodeficiency as NAC treatment of mice rescues the inhibition of class-switch recombination and aberrant V(D)J recombination in ATM knockout mice [90]. In A-T fibroblasts, increased sensitivity to hydrogen peroxide [91] and nitric oxide donors also suggest a high basal level of oxidative stress [92]. Notably, other neurodegenerative diseases are also associated with oxidative stress suggesting a common mechanism of neuronal loss may be responsible [93]. However, while all of these observations suggested ATM was involved in ROS regulation, the mechanism was unknown for some time.

Years after the first observation of increased oxidative stress in A-T, ATM was shown to be activated specifically in the cytoplasm by ROS [14]. In this pathway, mTORC1 activity is inhibited through a signaling cascade initiated by ATM-dependent phosphorylation of LKB1 [14]. However, the levels of hydrogen

peroxide used in this study caused γH2AX foci formation, a marker of DNA damage. In vitro activation of ATM by ROS showed a direct method for ATM activation in the absence of DNA [5]. In contrast to ATM monomerization during DSB activation, ATM forms an active disulfide cross-linked dimer after hydrogen peroxide treatment [5]. This active dimer requires cysteine 2991 in the FATC domain as replacement with leucine (C2991L-ATM) prevents activation by ROS [5]. In addition to cysteine 2991, cysteines 540, 541, 819, 1045, 1177, 1396, 1494, 1495, 2021, and 2801 were also found to form disulfide bonds after treatment with hydrogen peroxide [5]. Although individual mutations of these cysteines had no effect on kinase activity, these bonds may help stabilize the critical cysteine 2991 disulfide bond.

ATM POST-TRANSLATIONAL MODIFICATIONS

ATM undergoes multiple post-translational modifications in different domains during its activation (Figure 1.5). DNA-damage induced ATM autophosphorylation has been identified at 4 sites: serines 367, 1893, 1981, and 2996 [8, 11, 94, 95]. ATM autophosphorylated at any of these four serines was shown to localize to DSBs but each serine individually was not required for the recruitment of ATM to DSBs [94, 95]. However, the rescue of the S-phase checkpoint by wild-type ATM expression in an A-T cell line was prevented by individual mutations of serines 367 or 2996 to non-phosphorylatable alanines [95]. Furthermore, mutation of either serine 1981 or serine 2996 to alanine prevents the retention of ATM at DSBs suggesting phosphorylation of these residues is important for maintaining ATM at the repair foci [11, 96].

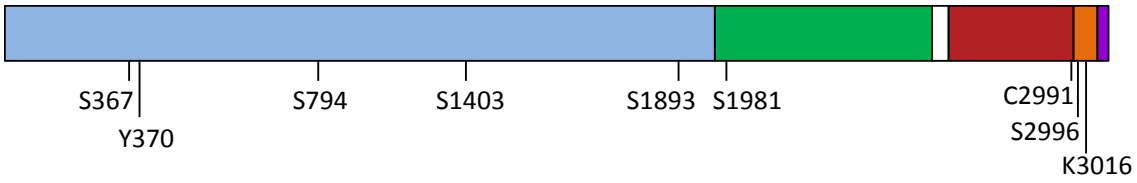

Figure 1.5 ATM domains and sites with known post-translational modifications.

Serines 367, 1893, 1981, and 2996 are autophosphorylation sites. Serines 794 and 1403 are phosphorylated by Cdk5 and Aurora-B, respectively. Tyrosine 370 is phosphorylated by EGFR. Cysteine 2991 forms a disulfide bridge and lysine 3016 is acetylated by Tip60. The colors represent domains present in ATM: blue, HEAT repeats (residues 1-1965); green, FAT domain (residues 1966-2566); red, PI3K-like kinase domain (residues 2614-2960); brown, PIKK regulatory domain (residues 2961-3024); purple, FATC domain (residues 3025-3056).

The requirement for these autophosphorylation events can vary. The phosphorylation of serine 1981 was not required for in vitro activation of human ATM [34]. In mice, autophosphorylation at the serines corresponding to 367, 1893, and 1981 have also been shown to be dispensable for ATM activation as mutating serine 1981 or all three to alanine had no phenotypic effect [97, 98]. However, all the DNA-damage induced autophosphorylation sites of ATM so far identified are important in human cells as mutation of these residues to alanine inhibits ATM signaling after DSBs and prevents rescue of ionizing radiation resistance [94, 95]. The discrepancies between the requirements for ATM autophosphorylation in humans and mice are still unresolved.

In addition to autophosphorylation at multiple sites, ATM is phosphorylated by other kinases. In neuronal cells, ATM is stimulated by cyclin-dependent kinase 5 phosphorylation of serine 794 in a DNA damage-dependent manner [99]. Recently, ATM phosphorylation by the epidermal growth factor receptor (EGFR) at tyrosine

370 was identified in response to irradiation [100]. EGFR was shown to be important for ATM activation as depletion of EGFR or addition of the EGFR inhibitor gefitinib impaired foci formation, DNA repair, and Chk2 phosphorylation [100]. ATM was also found to be activated during mitosis in the absence of DNA damage [9]. This activation required the activity of Aurora-B kinase to phosphorylate ATM on serine 1403 and was necessary for an efficient spindle assembly checkpoint in response to nocodazole [9]. ATM was also shown to constitutively associate with the tyrosine kinase c-Abl and phosphorylate c-Abl after DNA damage to activate it [101, 102], in addition to being a target of c-Abl phosphorylation [103].

Other post-translational modifications also occur on ATM, most notably acetylation. ATM and Tip60 form a stable complex and Tip60 acetylates lysine 3016 of ATM after DNA damage [104]. Knockdown of Tip60 or the mutation of lysine 3016 to arginine (K3016R) prevents DNA-damage induced activation of ATM in human cells [104, 105]. However, kinase assays with K3016R-ATM have shown this modification is not essential in vitro (JH Lee, unpublished observations). Notably, Tip60 phosphorylation by c-Abl enhances the binding of Tip60 to methylated histone H3 (H3K9me3) suggesting a positive feedback loop between ATM, c-Abl, and Tip60 after DNA damage [106].

ATM-Dependent Phosphorylation Events

Upon activation by DSBs or oxidative stress, ATM phosphorylates more than 700 substrates involved in multiple cellular processes including DNA repair, chromosomal organization, cell cycle regulation, gene regulation, apoptosis, stress responses, and RNA metabolism (Figure 1.3) [4, 10-12, 107]. Additionally, ATM

phosphorylates and activates many kinases leading to signal amplification [108]. These downstream effectors include the checkpoint kinases Chk1 and Chk2 as well as DNA-PK and AKT [109-113].

A phosphoproteomic study in an immortalized human B-cell line treated with ionizing radiation found only around 13% of phosphorylation events in the nuclei were in the canonical ATM recognition site pS/pTQ [10]. Another study showed putative ATM sites were a similar percentage of all neocarzinostatin-dependent phosphorylation events in nuclei from human melanoma cells [11]. However, in this study 60% of all the phosphorylation events were ATM-dependent as addition of an ATM inhibitor prevented phosphorylation. Both of these phosphoproteomic screens found relatively few phosphopeptides with the pS/pTQ motif (80 and 42 phosphorylation events, respectively). Matsuoka et al. enriched for ATM substrates using antibodies to known ATM phosphorylation sites and identified over 900 phosphorylation events at pS/pTQ sites upon treatment with ionizing radiation [12]. Thus there may be hundreds of direct targets of ATM and many more indirect targets through the activation of various downstream kinases.

The substrates of ATM may change depending on the method of ATM activation. In the presence of oxidative stress ATM does not phosphorylate H2AX and Kap1, substrates known to be phosphorylated after DNA damage [5]. Similarly, ATM activated by cell-cycle arrest in mitosis does not phosphorylate Smc1 or p53 at sites phosphorylated after ionizing radiation [9]. This suggests that ATM may activate specific downstream effectors in addition to common substrates depending on which cellular stress is present.

CASEIN KINASE 2

DNA double-strand breaks induce large changes in the phosphoproteome beyond the substrates of ATM. Phosphoproteomic investigations have shown that only 10% of DNA damage responsive sites conform to the ATM recognition sequence S/TQ [10, 11]. These studies showed phosphopeptides predicted to be phosphorylated by CK2 are upregulated after DNA damage [10, 11]. Notably, CK2 inhibition has been shown to suppress DNA repair, suggesting a direct role in the cellular response to DSBs [114, 115].

The CK2 holoenzyme is a heterotetramer consisting of two catalytic (α and/or α') subunits with two regulatory β subunits (Figure 1.6). Although the N-terminal catalytic domains of CK2α and CK2α' are approximately 90% identical, the α and α' subunits show some differences in substrate specificity, probably through their unrelated C-termini [116]. The holoenzyme ($\alpha_2\beta_2$, $\alpha\alpha'\beta_2$, or $\alpha'_2\beta_2$) was first described as one of the kinases responsible for the phosphorylation of casein in vitro [117, 118]. Subsequent studies have shown casein is a physiological substrate for a different kinase designated the Golgi apparatus of lactating mammary gland casein kinase (GEF-CK) [119]. However, CK2 has since been shown to phosphorylate many other proteins involved in diverse pathways.

CK2 functions as an important regulator of cell survival. In yeast, the two CK2 catalytic subunits, CKα and CKα', are functionally redundant but haploid cells with deletion of both are inviable [120]. A further analysis in a CKα deletion strain with temperature-sensitive CKα' showed cell cycle progression during G1 and G2/M requires CK2 activity [121]. In mice, CK2α and CK2β knockouts are embryonic

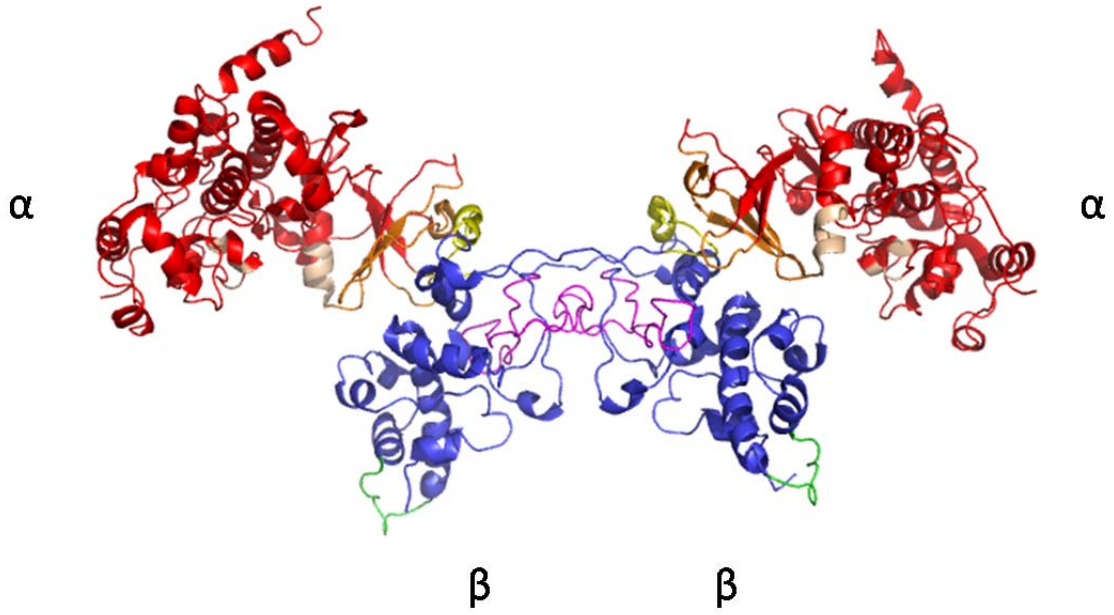

Figure 1.6 Structure of the CK2 holoenzyme.

The regulatory β subunits form a dimer and each bind an α or α' subunit to form the holoenzyme. Sections are colored as follows: red , CK2α/a'; orange, CK2α/a' β-interaction domain (residues 36-59, 69-73, 103-108); tan, CK2α/α' substrate binding domain/potential aggregation interface (residues 74-80, 191, 195, 198); blue, CK2β; magenta, CK2β dimer interface (residues 109-140); yellow, CK2β α/a'-interaction domain (residues 186-198); green, CK2β potential aggregation interface (residues 55-64). Domain boundaries defined in [116] and [128]. This figure was generated using Pymol version 1.3 from the PDB file: 1JWH.

lethal [122, 123], although CK2α' knockout in mice only causes male sterility [124]. There are no known human null mutations of CK2 but increased protein levels and kinase activity are associated with various cancers [125, 126].

CK2 SUBSTRATES

CK2 is a prolific kinase and the number of discovered substrates has risen steadily over the years. There have been over 300 proteins previously reported to be

phosphorylated by CK2 [127] and a recent phosphoproteomic approach using an in vitro CK2 kinase reaction with previously dephosphorylated lysates identified 605 phosphosites on 356 proteins of which only 36 proteins had been previously characterized [129]. The recognition site phosphorylated by CK2 is a serine or threonine surrounded by a patch of acidic residues where the amino acids at the n+1 and n+3 positions are particularly important [130]. CK2β is autophosphorylated at serines 2 and 3 which are followed by glutamates at residues 5 and 6 [131]. In addition, CK2 is able to phosphorylate tyrosine residues, including autophosphorylation sites, with a slightly different sequence preference [132-134]. The phosphorylation of CK2 substrates is generally associated with enhanced proliferation and survival [135]. These substrates are involved in many cellular functions, including transcription, translation, metabolism, signal transduction, apoptosis, and cytoskeletal maintenance (Figure 1.7) [127, 136, 137]. Notably, in all the cancers that have been examined, CK2 protein levels and kinase activity are both elevated [125, 126].

CK2 AND DNA REPAIR

CK2 localizes to DSBs and phosphorylates many proteins involved in the DSB repair pathway [138]. MRN foci at DSBs are dependent on the constitutive phosphorylation of MDC1 by CK2 as Nbs1 binds phosphorylated MDC1 through its FHA and BRCT domains [69, 139, 140]. In addition, CK2 was found to phosphorylate Mre11 constitutively at serine 649 [141]. Heterochromatin protein 1 beta is phosphorylated after IR and dissociates from DNA at DSBs in a CK2-dependent manner [142]. Finally, phosphorylation of Rad51 by Plk1 licenses CK2 to

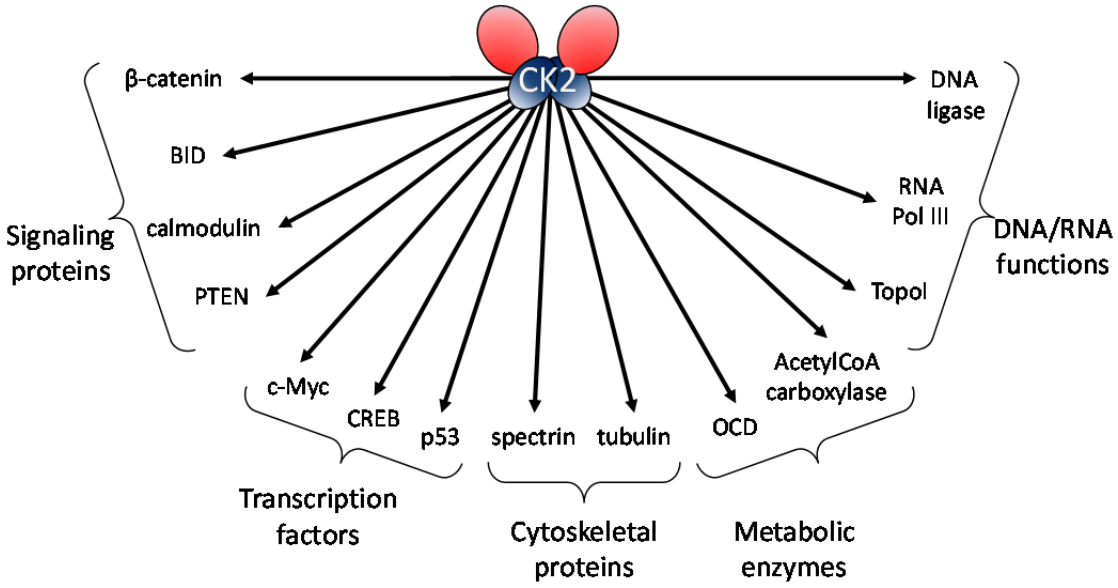

Figure 1.7 Schematic showing some of the cellular functions affected by CK2.

phosphorylate an adjacent residue to form a binding site for the FHA and BRCT domains of Nbs1 that is important for Rad51 recruitment to DSBs [143]. Conversely, in unstressed cells CK2 phosphorylates *M*urine *D*ouble-*M*inute clone *2* (MDM2) to induce the degradation of p53 [144-146]. Consistent with multiple roles in the DNA damage response, inhibition of CK2 suppresses DSB repair [114, 115].

ATM and CK2 interact in more direct ways in the DSB repair pathway also. A recent study has shown 5-diphosphoinositol pentakisphosphate binds and stimulates CK2 to phosphorylate the *T*ti1/*T*ti2/*T*el2 (TTT) complex [147]. The TTT complex is a cochaperone that binds and stabilizes PIKKs and the phosphorylation of Tti1 and Tel2 has been shown to be important for this binding [147-150]. CK2-dependent phosphorylation of TTT stimulates ATM and DNA-PK kinase activity as

measured by phosphorylation of p53 [147]. CK2 is also involved in the inhibition of *C*ylic AMP-*R*esponse *E*lement-*B*inding protein (CREB) binding to CREB-binding protein (CBP) after DNA damage [151]. A series of phosphorylation events with CK1, CK2, and ATM culminate in the crucial ATM-dependent phosphorylation of serine 121 on CREB that inhibits its interaction with CBP [151]. Similarly, constitutive phosphorylation of a residue on Structural Maintenance of Chromosome 3 (SMC3) by CK2 is important for the IR-induced activation of the intra-S phase checkpoint by ATM phosphorylation of a nearby residue [152]. ATM inhibition was shown to reduce DSB-induced CK2 activity suggesting ATM may play a direct role upstream of CK2 activity during DNA repair [11].

CK2 REGULATION

The CK2 holoenzyme has historically been characterized as having constitutive kinase activity [153]. However, in recent years different cellular stresses have been shown to alter CK2 activity and localization. CK2 phosphorylates p53 in vitro in response to UV irradiation [154]. Hypoxic conditions affect the expression and localization of CK2 and inhibitors of CK2 reduce HIF-1 transcriptional activity [155]. Similarly, heat shock induces translocation of CK2 subunits to the nucleus and a consequent rise in kinase activity there [156]. In cardiomyocytes treated with TNF-α, CK2 is oxidatively modified and has reduced kinase activity [157]. DNA damage by methyl methanesulfonate treatment or UV irradiation represses RNA polymerase III activity in *Saccharomyces cerevisiae* through the dissociation of CK2 [158, 159]. Although CK2 is often considered to be constitutively active, cellular localization, and protein-protein interactions appear to be important for modulating the effects

and substrates of CK2**.** Additionally, CK2 is known to aggregate in vivo and in vitro and this property has been shown to affect its kinase activity.

CK2 AGGREGATION

In the initial biochemical characterizations of CK2, purifications from rabbit erythrocytes and rabbit reticulocytes revealed multiple forms of CK2 with unique sedimentation rates [160, 161]. Notably, there was a salt dependent decrease in the sedimentation rate of purified *Drosophila melanogaster* CK2 (*Dm*CK2) to that of the tetrameric holoenzyme suggesting the forms with higher sedimentation rates were aggregates [162]. Furthermore, electron micrographs revealed multiple forms of *Dm*CK2 in physiologically relevant conditions, including small units and two types of filaments (Figure 1.8A) [163]. A recent study using bioluminescent resonance energy transfer technology ($BRET^2$) suggest aggregation occurs in vivo [164]. CK2α-Rluc8 and CK2α-GFP expressed in cells showed a CK2β-dependent increase in $BRET^2$ signal [164]. Overexpression of a known stable CK2-interacting protein, $G_{\alpha s}$, decreased the $BRET^2$ signal while overexpression of a transiently-interacting protein, β- arrestin2, did not [164]. Furthermore, polylysine, which was previously shown to induce disaggregation, decreased the $BRET^2$ signal [164]. The models of CK2 aggregation include a thin linear filament [165] and a thick filament consisting of stacked rings of trimers or tetramers of the holoenzyme [166, 167] (Figure 1.8B). Support for both of these models comes from their presence in the crystalline state, relatively large interface sizes, and increased kinase activity upon mutation of the putative aggregation interface [167, 168].

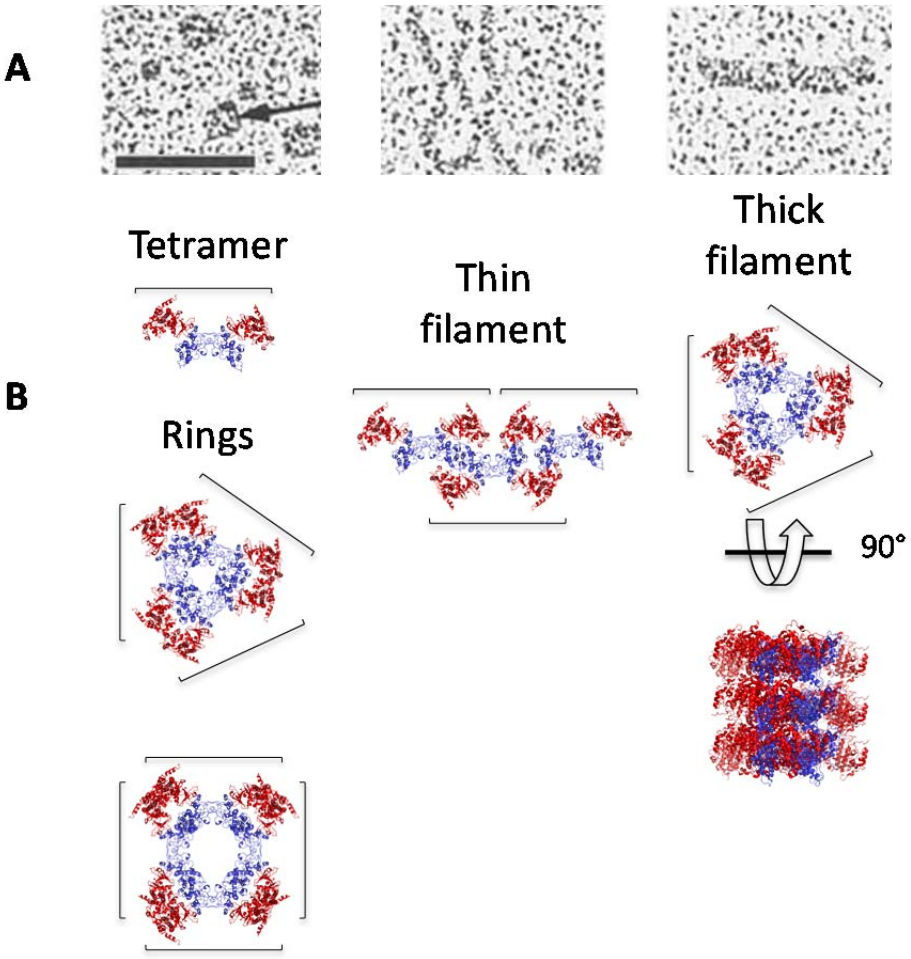

Figure 1.8 Electron microscopy and accompanying models of CK2 aggregation.

(A) Purified Drosophila melanogaster CK2 was diluted into buffer containing 10 mM Tris-HCl, pH 7.5, 1 mM DTT, 50% glycerol, and 100 mM NaCl and incubated at 4 °C for 2 hours before visualization by electron microscopy. The bar represents 100 nm. This research was originally published in Journal of Biological Chemistry. Valero E, De Bonis S, Filhol O, Wade RH, Langowski J, Chambaz EM, Cochet C. Quaternary structure of casein kinase 2. Characterization of multiple oligomeric states and relation with its catalytic activity. Journal of Biological Chemistry. 1995; 270(14):8345-52. © the American Society for Biochemistry and Molecular Biology. (B) Models of CK2 holoenzyme (PDB code: 1JWH) corresponding to structures in electron micrographs of (A). Brackets represent one tetramer.

The kinase activity of CK2 is increased in conditions that reduce aggregation suggesting aggregation inhibits CK2 kinase activity [162, 163, 169]. Several groups have proposed models of CK2 regulation by aggregation through the intermolecular binding of the basic substrate-binding region of CK2α and an acidic loop in CK2β (Figure 1.6). Notably, mutations disrupting this putative aggregation interface generate a hyperactive holoenzyme suggesting a loss of regulation [170, 171]. A study using chemical crosslinking also showed in vivo interaction of these two regions [172].

HYPOTHESES AND GOALS

The activation of ATM by DSBs is an important step in the initiation of DNA repair. ATM requires the multifunctional protein complex MRN for several roles during this activation. First, ATM is recruited to DSBs through an interaction with the C-terminus of Nbs1 [32, 74]. Once at the DSB, MRN stimulates the transition of ATM from an inactive dimer to an active monomer and increases the affinity of ATM for its substrates [34]. The Rad50 component of MRN is known to bind and hydrolyze ATP and this induces large conformational shifts in the MRN complex [65, 66, 85]. However, it has not been clear whether ATP utilization by MRN is required for the activation of ATM. Previously, there has been no simple method to separate the ATP binding and hydrolysis of Rad50 from the kinase activity of ATM as both can utilize the same pool of ATP. In this study, I use an ATM variant that is able to phosphorylate its substrates with an N^6-substituted ATP to show that ATP binding, but not hydrolysis, by Rad50 is required for the activation of ATM. This suggests

ATP binding by MRN acts as a switch through which Rad50-controlled changes in the conformation of MRN regulate the activity of ATM.

In addition to DSBs, ATM is also activated by oxidative stress [5]. There have been many studies characterizing the phosphoproteome of cells after treatment with ionizing radiation or radiomimetic drugs [10-12, 107, 173]. These studies have identified numerous pathways affected by ATM both directly and indirectly, including the phosphorylation and activation of downstream kinases. However, these studies have not examined how the different activation pathways of ATM affect its cellular role in the absence of exogenous stress. It was previously shown that ATM knockout mice recapitulate some of the symptoms of A-T, but the expression of kinase-dead ATM in mice is embryonic lethal demonstrating the presence of inactive ATM is more detrimental [21, 22]. Recently, separation-of-function mutations of ATM have been characterized that allow selective activation by either DSBs or oxidative stress [5]. In the study described here, I use an established A-T cell line to examine the effects of these separation-of-function ATM mutants. I show mutations that prevent either pathway of ATM activation affect a large group of proteins and also affect mitochondrial homeostasis. Some of these proteins appear to undergo aggregation in the absence of ATM activity. I also show a reduction in the phosphorylation of CK2 substrates in A-T cells expressing oxidative-stress-insensitive ATM that is associated with a shift higher molecular weight complexes for CK2β. These studies provide novel insights into the mechanism of ATM activation and the DNA-damage independent functions of ATM in cells.

CHAPTER 2: MATERIALS AND METHODS

CHEMICALS AND ANTIBODIES

The following antibodies were used for western blotting: rabbit anti-ACLY (GeneTex, GTX112387), rabbit anti-ACSM1 (Abgent, AP9284), rabbit anti-ALDH4A1 (Abgent, AP7875c), mouse anti-ATM (GeneTex, GTX70103), mouse anti-ATM (Santa Cruz, sc-135663), rabbit anti-β-actin (CST, 4970), rabbit anti-CBS (Santa Cruz, sc-67154), rabbit anti-CK2α (Pierce, PA1-86381), rabbit anti-CK2β (Millipore, 04-1128), rabbit anti-GPD1 (Abgent, AP8507a), mouse anti-KAP1 (Abcam, ab22553), mouse anti-LHPP (Santa Cruz, sc-376648), rabbit anti-OTC (Abgent, AP6928c), rabbit anti-pS15-p53 (EMD Biosciences, PC461), mouse anti-TPM1 (Santa Cruz, sc-376541), mouse anti-V5 (Invitrogen, R960-25), rabbit anti-V5 (Novus, NB600-381), goat anti-mouse IgG IRDye 800 Conjugated (Rockland Immunochemicals, RL-610-132-121), and goat anti-rabbit IgG IRDye 700 Conjugated (Rockland Immunochemicals, RL605-430-003). All chemicals were purchased from Sigma unless otherwise stated.

LARGE-SCALE PLASMID PURIFICATION

Single colonies from streaked plates were inoculated in small LB cultures (25 ml) in the presence of the appropriate antibiotic and shaken overnight at 30 °C. The overnight cultures were inoculated into large cultures (500 ml) at a 1:100 dilution and shaken at 30 °C. At an OD_{600} of 0.8-1, 1.5 ml 34 mg/ml chloramphenicol in 50% ethanol was added and the cells were shaken overnight at 30 °C. Pellets were made by spinning the overnight culture at 5,000 RPM for 10 minutes. The supernatant

was discarded and the pellet was resuspended in 9 ml Solution I (25 mM Tris, pH 8.0, 10 mM EDTA). The cells were lysed by the addition of 20 ml Solution II (200 mM NaOH, 1% SDS), mixed gently by inversion, and incubated for 5 minutes at room temperature. Plasmid DNA was renatured with 15 ml Solution III (3 M potassium acetate), mixed gently by inversion, and the sample was centrifuged for 30 minutes at 4 °C and 18,000 g. The supernatant was mixed with 25 ml isopropanol and centrifuged at 12,000 g for 10 minutes. The supernatant was then discarded and the pellet was resuspended in 4.4 ml TE (10 mM Tris, pH 8.0, 1 mM EDTA). Proteins were precipitated with the addition of 1.6 ml 7.5 M ammonium acetate and the solution was placed on ice for 1 hour. The sample was then centrifuged at 4,000 g for 10 minutes. The resulting supernatant was mixed with 6 ml isopropanol and centrifuged at 4,000 g for 10 minutes. The supernatant was discarded and the pellet was resuspended in 3.4 ml TE. RNA was digested with 5 µl 30 mg/ml RNase at 37 °C for 30 minutes. The sample was prepared for centrifugation by addition of 4.1 g cesium chloride and 400 µl 10 mg/ml ethidium bromide and transferred to suitable tubes for centrifugation (Beckman-Coulter, 362185). The tubes were centrifuged overnight at 300,000 g in the NVT 65.2 rotor (Beckman-Coulter). The DNA bands were visualized by long-wave UV light and the lower band (plasmid) was extracted by hand-drawn glass pipettes. The collected sample was placed in 3 inches of dialysis tubing (Pierce, 68100), and the ethidium bromide was removed by sequential 2 hour dialyses at 4 °C with 500 ml TE containing 100 mM NaCl. A final dialysis was performed overnight at 4 °C with 500 ml TE.

RESTRICTION DIGEST

Purified DNA plasmids were checked by sequencing for the first purification and by restriction digest subsequently. DNA concentration was determined on a NanoDrop 2000 (Thermo Scientific). Restriction digests were performed with New England Biolabs enzymes. Briefly, 300 ng DNA, 1 µl of the desired restriction enzyme, and appropriate amounts of buffer and/or BSA were combined in 10 µl total and incubated according to the protocol. The resulting digests were loaded alongside 250 ng of the 1 Kb Plus DNA Ladder (Life Technologies, 10787-018) on suitable percentages of agarose gels according to the size of the predicted fragments and run in TAE (40 mM Tris-HCl, 20 mM acetic acid, 1 mM EDTA) for 1 hour at 80 V. Gels were stained for 10 minutes with 5 µl 10 mg/ml ethidium bromide in water, washed for 10 minutes in water, and visualized on a Syngene G-Box.

PROTEIN EXPRESSION

Wild-type MRN complexes were expressed in Sf21 insect cells by coexpression with baculovirus prepared from the transfer vectors pTP11 (Rad50), pTP813 (Mre11), and pTP288 (Nbs1) as described previously [174-176]. pTP11 was directly transfected into Sf21 cells with linearized baculovirus DNA (BD Pharmingen) to make recombinant baculovirus, whereas the other transfer vectors were converted into bacmids pTP814 (wild-type Mre11) and pTP291 (wild-type Nbs1) and were used to make virus according to manufacturer instructions for the Bac-to-Bac system (Invitrogen). The expression construct for Flag-tagged wild-type ATM was a gift from M. Kastan. Y2755A-ATM was generated using QuikChange XL site-directed mutagenesis (Stratagene, 200516) from wild-type ATM pcDNA3 expression plasmid (sequences available upon request) with the following modifications to the protocol.

The amount of wild-type ATM DNA used as template was increased to 300 ng, DpnI was incubated for 4 hours, and the resulting digested DNA was ethanol precipitated, resuspended in 5 µl TE, and the entirety used to transform XL10-Gold Ultracompetent cells (Stratagene, 200315). The *Escherichia coli* expression constructs for GST-p53 were described previously [33].

PROTEIN PURIFICATION

Wild type MRN was purified as described [174]. Dimeric ATM was made by transient transfection of expression constructs into 293T cells using calcium phosphate and purified as described previously [177]. GST-p53 protein was expressed and purified in E. coli as described previously [33]. Protein concentrations were determined by quantification of protein preparations with standards on colloidal Coomassie-stained SDS-PAGE gels using the Odyssey system (LiCor).

IN VITRO ATM KINASE ASSAYS

ATM kinase assays with MRN and DNA were performed with 1.4 nM dimeric ATM, 150 nM GST-p53 substrate, 4.8 nM MRN, and ~140 nM 1 Kb Plus DNA Ladder (Life Technologies, 10787-018) as indicated in the figure legends. Kinase assays were performed in kinase buffer (50 mM HEPES, pH 7.5, 50 mM potassium chloride, 5 mM magnesium chloride, 10% glycerol, and 1 mM ATP) for 90 min at 30 °C in a volume of 40 µl as described previously [34]. Kinase assays with oxidative activation were performed in the absence of MRN and DNA with varying amounts of H_2O_2 as indicated. The ATP analogs N^6-(1-methylbutyl)adenosine-5′-O- triphosphate and N^6-furfuryladenosine-5′-O-triphosphate were obtained from Biolog (BLG-M027-05 and

BLG-F007-05, respectively) and used at final concentrations of 1 mM. ATM and phosphorylated S15-p53 were detected by western blot as described previously [34]. Each experiment was performed several times, and a representative example is shown in the figure.

MAMMALIAN CELL CULTURE

293T cells (ATCC, CRL-11268) were grown in DMEM (Invitrogen, 11995073) supplemented with 10% FBS (Gemini Bio Products, 900-208). AT1ABR cells and AT1ABR cells expressing the various pMAT1-ATM constructs were a gift from M. Lavin. AT1ABR cells were grown in RPMI-1640 medium (Sigma, R8758) supplemented with 15% FBS. The media for AT1ABR cells with pMAT1-ATM constructs was supplemented with 200 μg/ml hygromycin B (EMD Millipore, 400052) to select for pMAT1-ATM retention. ATM expression was induced from the metallothionein II promoter for 16 hours as described previously using 2 μM $CdCl_2$ [178].

CELL LYSIS AND PROTEIN QUANTITATION FOR MASS SPECTROMETRY

AT1ABR cell pellets were lysed in 4 volumes of cell lysis buffer (8 M urea, 50 mM Tris, pH 8, 5 mM $CaCl_2$, 30 mM NaCl, 50 mM NaF, 1 mM sodium orthovanadate, 10 mM sodium pyrophosphate, 1× mini EDTA-free protease inhibitor (Roche Diagnostics) and 1× phosSTOP phosphatase inhibitor (Roche Diagnostics). The lysate was sonciated until clear and centrifuged for 10 minutes at 20,000 g. The supernatant was collected and the protein concentration was quantitated by BCA assay (Pierce, 23227).

PROTEIN DIGESTION

Equal amounts of lysate from each cell line (1 mg) were reduced with 5 mM dithiothreitol (DTT) for 30 minutes at 37 °C. Following reduction, the cysteine residues were alkylated by the addition of 15 mM iodoacetic acid for 30 minutes at room temperature protected from light. The lysates were then reduced again with 5 mM DTT for 15 minutes at room temperature. The protein sample was diluted with 50 mM Tris, pH 8 and 5 mM $CaCl_2$ to a final concentration of 1.5 M urea. To digest the proteins, LysC (10 μg) (Wako Chemicals, 129-02541) was added and the samples were digested for 2 hours at 37 °C. Trypsin (20 μg) (Promega, V5113) was added and the samples were digested overnight at room temperature.

PEPTIDE DESALTING

Sep-Pak Accell Plus CM Vac cartridges (Waters, WAT023625) were prepared under light vacuum using the following washes (all percentages represent V/V): 3 ml 100% acetonitrile (ACN); 1 ml 70% ACN, 0.25% acetic acid (AA); 1 ml 40% ACN, 0.5% AA; 1 ml 20% ACN, 0.5% AA; and 3 ml 0.1% trifluoroacetic acid (TFA). The peptide samples were brought to pH 2 with TFA and loaded onto the pre-washed cartridge. The bound peptides were washed with 3 ml 0.1% TFA followed by 300 μl 0.5% AA. The peptides were eluted in sequential applications of 1 ml 40% ACN, 0.25% AA and by 750 μl 70% ACN, 0.25% AA and the samples were dried in a speed vacuum concentrator.

PEPTIDE TMT LABELING

The TMTsixplex Isobaric Label Reagent Set (Pierce, 90061) was used to individually tag the samples with 6 unique mass tags. The dried peptide samples were resuspended in 100 μl 200 mM tetraethylammonium bromide. TMT Label Reagents

(0.8 mg/sample) were brought to room temperature, spun down, and resuspended in 50 µl ACN. The peptide samples and TMT Label Reagents were combined and incubated at room temperature for 2 hours. The labeling reactions were quenched with 0.8 µl 50% hydroxylamine (V/V) and then shaken for 15 minutes. Aliquots (5 µl) of the samples were combined with 50 µl water and dried down and the remaining samples were immediately frozen. The aliquots of labeled peptides were resuspended in 0.2% formic acid then run on the mass spectrometer to determine the ratios of the samples to load for equal spectral counts. The frozen samples were thawed, mixed according to the determined ratios, dried down, and desalted as before.

STRONG CATION EXCHANGE FRACTIONATION

Strong cation exchange fractionation was performed at a flow rate of 3.0 mL/min using a polySULFOETHYL A column (9.4 x 200 mM, PolyLC, 209-SE05) on a Surveyor LC quaternary pump. Tagged samples were resuspended in buffer A (30% ACN, 5 mM KH_2PO_4, pH 2.6) and separated using the following gradient: 0-2 min, 100% buffer A; 2-5 min, 0-15% buffer B (30% ACN, 350 mM KCl, 5 mM KH_2PO_4, pH 2.6); 5-35 min, 15-100% buffer B. Buffer B was then held at 100% for 10 min. The column was washed with buffer C (500 mM KCl, 50 mM KH_2PO_4, pH 7.5) and water and re-equilibrated with buffer A. All fractions were collected by hand, frozen, lyophilized and de-salted over a Sep-Pak Accell Plus CM Vac cartridges (Waters, WAT023625).

PHOSPHOPEPTIDE ENRICHMENT

Phosphopeptide enrichment was performed using immobilized metal affinity chromatography with metal beads (Qiagen). Before loading the peptides, the beads were equilibrated with water and then incubated with 40 mM EDTA, pH 8.0 for 30 minutes with shaking. EDTA was removed by three successive water washes, and then the beads were incubated with 100 mM $FeCl_3$ for 30 minutes while shaking. For a final wash, the beads were washed with four rounds of 80% ACN, 0.1% TFA. Peptides were resuspended in 80% ACN, 0.1% TFA and incubated with the beads for one hour with shaking. Non-phosphorylated peptides were removed by washing the beads with 80% ACN, 0.1% TFA and these were used for the proteomic analysis. Phosphorylated peptides were eluted from the beads with 50% ACN, 0.7% NH_4OH and immediately acidified with 4% formic acid.

LC-MS/MS

Tandem mass spectrometry was performed using a NanoAcquity UPLC system (Waters) coupled to an OrbiTrap Elite (ThermoFisher). Peptides were loaded onto a 75 μm inner diameter and 360 μm outer diameter bare fused silica capillary packed with 10 cm of Magic C18 particles (Bruker-Michrom) for twelve minutes at a flow rate of 1 μL/min. Peptides were then eluted onto a 50 μm inner diameter and 360 μm outer diameter analytical column packed with 17 cm of Magic C18 particles. Peptides were separated over either a 90-minute or 120-minute gradient by ramping from 2% to 35% ACN, 0.2% formic acid at a flow rate of 0.3 μL/min. Peptides were fragmented by HCD and analyzed using the Coon OMSSA Proteomics Software Suite (COMPASS) [179]. The mass tolerance was set to 20 ppm for precursors and 0.01 Th for fragment ions. The carbamidomethylation of cysteines

and the 6 unique mass tags of TMTsixplex reagents were searched as fixed modification. Oxidation of methionine, TMTsixplex modification of tyrosine, phosphorylation of tyrosine, and phosphorylation with neutral loss on serine and threonine were searched as variable modifications. COMPASS software was used to filter peptides to a 1% FDR which were then combined and used to filter proteins at a 1% FDR.

HIERARCHICAL CLUSTERING

Protein and phosphopeptides levels were clustered in Cluster 3.0 using Hierarchical Clustering with Centered Correlation and Average Linkage [180]. Results were visualized and gene lists extracted using Java TreeView [181].

PAIRWISE COMPARISONS

Pairwise comparison graphs were made in Microsoft Excel 2010. The proteins or phosphopeptides were ranked from lowest intensity to highest intensity separately in each cell line and the Spearman's coefficients were calculated as $\rho = 1 - \frac{6\,\Sigma d_i^2}{n(n^2-1)}$, where $d_i = x_i - y_i$ is the difference in ranks for one protein between two cell lines. The t statistic for each Spearman's coefficient was calculated as $t = \rho\sqrt{\frac{n-2}{1-\rho^2}}$ and the significance at the 5×10^{-16} level was calculated using the qt() function in R version 3.0.3.

SEQUENCE ANALYSIS

Peptide sequences 6 amino acids N-terminal and C-terminal to each phosphorylated residue were extracted and formatted for submission to motif-x v1.2 10.05.06 [182, 183]. The following settings were used for analysis of the phosphoproteome: foreground format = MS/MS; extend from = IPI Human Proteome; central character

= s, t, or y in three separate runs; width = 13, occurrences = 20, significance = 0.000001; background = IPI human proteome. For the C2991 Dependent Cluster, the occurrences were reduced to 10 to reflect the smaller number of phosphopeptides.

KINASE PREDICTION

Peptide sequences 6 amino acids N-terminal and C-terminal to each phosphorylated residue were extracted and formatted for submission to Group-based Prediction System ver 3.0 (GPS) [184]. The program was run with the threshold set to high and the results for multiple kinases were combined in one table for further analysis.

KOLMOGOROV-SMIRNOV (K-S) TESTS

The empirical distribution functions (EDFs) were generated and K-S tests were performed in R version 3.0.3. Briefly, the ratios of intensities from AT1BR cells expressing wild-type-ATM and C2991L-ATM for the phosphopeptides from the entire phosphoproteome or those predicted to be phosphorylated by a specific kinase using GPS were calculated. These ratios were entered into R as a table and converted to numeric vectors. The empirical cumulative distribution function for the phosphoproteome and the phosphopeptides predicted to be substrates of a specific kinase were plotted with the plot() and ecdf() functions and the K-S test was performed using the ks.test() function.

AT1ABR TISSUE CULTURE FOR STAINING AND QPCR

AT1ABR cells and AT1ABR cells expressing wild-type-ATM or C2991L-ATM were counted using the Scepter 2.0 Handheld Automated Cell Counter (EMD Millipore, PHCC20060) with Scepter Cell Sensors, 60 μm (PHCC60250) and seeded at a density of 500,000 cells/ml in 15 ml. The following day, 4 aliquots of 1.5 ml of each cell line

were harvested for the uninduced controls. The aliquots were pelleted for 5 minutes at 100 g. The supernatant was removed and the cell pellets were washed with 1 ml PBS and pelleted again. The pellets were immediately stained or frozen in liquid nitrogen for subsequent RNA or protein extraction. The remaining cells were induced for 16 hours with 2 μM $CdCl_2$. After induction, the cells were gently spun down for 5 minutes at 100 g and resuspended in fresh media without $CdCl_2$. The cells were allowed to recover for 48 hours and 4 aliquots of 1.5 ml of each cell line were harvested and immediately stained or pelleted and frozen in liquid nitrogen for subsequent RNA or protein extraction.

H_2DCFDA, MitoTracker Green, and Propidium Iodide Staining

For staining, all centrifugation occurred for 5 minutes at 100 g unless otherwise stated. AT1ABR pellets were resuspended in PBS and stained with H_2DCFDA (Invitrogen, D-399), MitoTracker Green FM (Life Technologies, M7514), or propidium iodide as follows. For analysis of ROS levels, washed cells were incubated for 30 minutes with 1 μM H_2DCFDA, then centrifuged, and the supernatant removed. The pellets were washed 3 times with PBS and then transferred to 5 ml polystyrene round bottom tubes (VWR, 60818-496) in 0.3 – 1 ml PBS for analysis by flow cytometry. For mitochondrial mass staining, washed cells were incubated with 0.2 μM MitoTracker Green FM for 20 minutes, then centrifuged, and the supernatant removed. The pellets were washed 3 times with PBS and then transferred to 5 ml polystyrene round bottom tubes in 0.3 – 1 ml PBS for analysis by flow cytometry. For propidium iodide staining, washed cells were resuspended in 1 ml PBS in a 15 ml polypropylene, V-bottom tube on ice and allowed to cool. Cold ethanol (3 ml) was dripped onto the cells in PBS while vortexing the tube. The cells were fixed

overnight at 4 °C, pelleted at 800 g for 5 minutes, and washed twice with PBS. The fixed cells were stained with 1 ml of propidium iodide staining solution (3.8 mM sodium citrate and 40 μg/ml propidium iodide in PBS) and 50 μl 10 μg/ml RNAse A for 3 hours at 4 °C. Stained samples were stored in the 5 ml polystyrene round bottom tubes in the dark at 4 °C until all samples were prepared and then analyzed together.

FLOW CYTOMETRY

Stained samples were analyzed on a BD LSRFortessa cell analyzer using the FITC setting (excitation 488 nm/emission 515-545 nm) for samples stained with H_2DCFDA or MitoTracker Green FM, and the PE-Texas Red setting (excitation 488 nm/emission 600-620 nm) for samples stained with propidium iodide. Live cells were gated according to the forward scatter and side scatter before analysis of fluorescence. For each sample, 10,000 cells were analyzed. The median values from 4-6 biological replicates were used to calculate the means and standard deviations.

RNA EXTRACTION, RT-PCR, AND QPCR

RNA was purified from uninduced and induced AT1ABR cells using the RNeasy Mini Kit (Qiagen, 74104) and quantitated on a NanoDrop 2000 (Thermo Scientific). RNA (1 μg) was reverse transcribed using the High-Capacity cDNA Reverse Transcription Kit (Applied Biosystems, 4386614). qPCR was performed on the ViiA7 Real-Time PCR System (Applied Biosystems) using Sybr Green PCR Master Mix (Life Technologies, 4368814) as described in the protocol. Primer sequences for SLC7A11, PGC1α, and ACTB available upon request. Fold inductions and error estimates were obtained using REST 2009 [185].

VIRUS PRODUCTION

293T cells were plated in 10 cm dishes and allowed to grow to confluency. A solution of OptiMEM and plasmids was made using 20 µg pLX304 vector containing the gene of interest, 12 µg pCMV-dR8.91 (Delta 8.9), and 8 µg VSV-G and brought to 500 µl with OptiMEM. In another tube, 60 µl Lipofectamine 2000 (Invitrogen, 11668-027) was mixed 440 µl OptiMEM. The plasmid and Lipofectamine 2000 solutions were combined, incubated for 5 minutes at room temperature, and then added to the 293T cells. The media was changed the next day and left for 48 hours. The media was harvested 48 hours and replaced and then harvested again 24 hours later. The media with virus were combined, filtered with 0.45 µm filters, aliquoted in 500 µl aliquots, and stored at -20 °C for transduction. K69M-CK2α' was generated using QuikChange XL site-directed mutagenesis on the wild-type pLX304-CK2α' with the primers TP4209 and TP4210 (sequences available upon request) using the unmodified protocol.

VIRUS TRANSDUCTION

293T or U2OS cells were plated in 24-well plates and allowed to reach confluency. The media was removed and replaced with 500 µl of the viral aliquots. Polybrene (EMD Millipore, TR-1003-G) was added at a final concentration of 10 µg/ml to increase viral transduction. The cells were grown overnight and the media was replaced the next day. The following day selection agent was added, for pLX304 plasmids cells were treated with 10 µg/ml blasticidin (InvivoGen, ant-bl-1), and cells were allowed to grow for approximately one week until the control untransduced cells had died. The stable cell lines were checked for expression of V5-tagged protein and used in subsequent assays.

V5 Immunoprecipitation and Western Blotting

293T cells stably expressing V5-tagged CK2 were lysed with 1X Cell Lysis Buffer (Cell Signaling Technology, 9803) according to the protocol. Protein quantitation was performed by Bradford assay with Coomassie Plus Protein Assay Reagent (Pierce, 23236). For each immunoprecipitation, 2.5 µg lysate was combined with 4 µl mouse anti-V5 magnetic beads (Medical and Biological Laboratories, M167-9) and brought to a final volume of 50 µl with 1X Cell Lysis Buffer. Tubes were rotated for 30 minutes at 4 °C and then spun briefly. A magnetic stand was used to wash the beads 3 times with 500 µl 1X Cell Lysis Buffer. Beads were immediately used for the CK2 kinase reaction.

In Vitro CK2 Kinase Reaction

CK2 kinase assays were performed with either 1 µl CK2 (NEB, P6010L) or on the beads of immunoprecipitated CK2. The reactions were performed with 1X CK2 Reaction Buffer (NEB) (20 mM Tris-HCl, pH 7.5, 50 mM KCl, 10 mM $MgCl_2$) supplemented with 1 mM ATP, 1 µl ATP-γ-^{32}P (NEN Radiochemicals, BLU002H), and 75, 575, or 1150 ng GST-CK2 substrate. The reaction was incubated for 1 hour at 30 °C and then stopped with 6 µl 5X SDS loading buffer. Proteins were run on SDS-PAGE gels and transferred to PVDF membrane following standard protocols. V5-tagged CK2 levels were probed using rabbit anti-V5 (Novus Biologicals, NB600-381) and Alexa Fluor 680 goat anti-rabbit (Invitrogen, A21076) and scanned and quantitated on the Li-Cor Odyssey system. Then the membrane was exposed to a PhosphorImager screen for at least 16 hours. The screen was scanned using Typhoon Imager to obtain ^{32}P incorporation. For the time course, immunoprecipitated CK2β-V5 was split into 5 tubes and the reaction was stopped at

the times shown. Quantitation was performed using GelQuant and normalized to protein levels quantified through western blots. Multiple experiments were performed for each reaction and representative results are shown.

SUCROSE GRADIENT

Cell lysates were made in the presence or absence of detergent. For detergent lysis, 1X Cell Lysis Buffer (Cell Signaling Technology, 9803) was used according to the protocol. The lysis without detergent was performed with 25 mM Tris, pH 8, 100 mM NaCl, and 10% glycerol supplemented immediately before use with 1 mM DTT, 1 mM PMSF, 1 mM sodium orthovanadate, 1 mM β-glycerophosphate, and 2.5 mM sodium pyrophosphate. Lysis was performed by douncing 50 times on ice. For both methods, the protein concentration was quantitated by Bradford assay with Coomassie Plus Protein Assay Reagent (Pierce, 23236). The different concentrations of sucrose were made in 20 mM Tris, pH 7.4 and 150 mM NaCl and layered in ThinWall Ultra-Clear Tubes (Beckman-Coulter, 344059) using gravity flow from a pipet bulb. The sucrose percentages from the bottom were 50%, 45%, 40%, 35%, 30%, 25%, 20%, 15%, 10%, and 5% (W/V) and each layer was 1 ml. Between 10 µg and 2 mg of lysate in 500 µl of the appropriate cell lysis buffer was added to the top of the sucrose gradient and then spun for 16 hours at 4 °C and 180,000 g in a swinging bucket SW 41 Ti rotor (Beckman-Coulter, 331362). Fractions of 500 µl were collected by pipet. Western blots were performed with 16 or 120 µl each fraction combined with 4 or 30 µl 5X SDS and loading controls of 2.5 or 100 µg lysates were run on each blot. The blots were probed as before and the percentage of probed protein was quantitated using the Li-Cor Odyssey system.

An identical sucrose gradient was performed with molecular weight markers to determine the fractions corresponding to different size complexes. The fractions were run on a NuPage 4-12% Bis-Tris Gel (Invitrogen, NP0336BOX) and the colloidal Coomassie-stained gels. Aldolase (40 kDa monomer) appeared mostly in fractions 6 and 7. Catalase (60 kDa monomer, 240 kDa tetramer) ran in fractions 8-10. Ferritin (21 kDa monomer, 500 kDa 24-mer) and thyroglobulin (330 kDa monomer, 660 kDa dimer) showed up in the sucrose gradient starting in fraction 12. However, some amount of ferritin and thyroglobulin are present through the last fraction suggesting there are larger complexes or aggregates in the sucrose gradient.

CHAPTER 3: ATP-DEPENDENT CONFORMATIONAL CHANGES IN RAD50 CONTROL ATM ACTIVATION

This research was originally published in Journal of Biological Chemistry. Lee JH, Mand MR, Deshpande RA, Kinoshita E, Yang SH, Wyman C, Paull TT. Ataxia Telangiectasia-Mutated (ATM) Kinase Activity Is Regulated by ATP-driven Conformational Changes in the Mre11/Rad50/Nbs1 (MRN) Complex. Journal of Biological Chemistry. 2013; 288:12840-12851.

ABSTRACT

The Ataxia Telangiectasia-Mutated (ATM) protein kinase is recruited to sites of double-strand DNA breaks by the Mre11/Rad50/Nbs1 (MRN) complex, which also facilitates ATM monomerization and activation. MRN exists in at least two distinct conformational states, dependent on ATP binding and hydrolysis by the Rad50 protein. Here we use an ATP analog-sensitive form of ATM to determine that ATP binding, but not hydrolysis, by Rad50 is essential for MRN stimulation of ATM. These results show that the ATP-bound form of MRN is the critical conformation for ATM activation.

INTRODUCTION

The ATM protein kinase plays a central role in signaling the presence of DNA double-strand breaks (DSBs) in eukaryotic cells. Activation of ATM occurs very rapidly, within a few minutes of DNA break incidence [8], and is dependent on the Mre11/Rad50/Nbs1 (MRN) complex for its recruitment to sites of DNA damage

[74]. MRN also functions to promote a transition in ATM conformation from an inactive dimeric form to an active monomeric form, and increases the affinity of ATM for its substrates [34].

The MRN complex is a large, multifunctional protein assembly that possesses endo- and exonucleolytic activity through the Mre11 component and ATP binding, hydrolysis, and adenylate kinase activity through the Rad50 component. Mre11/Rad50 (MR) complexes in prokaryotes and MRN complexes in eukaryotes are important for DNA double-strand break recognition and repair [83]. The eukaryotic forms are also essential for meiotic DSB processing and telomere maintenance, as well as for signaling through the ATM kinase [63]. Rad50 has an overall domain organization that is similar to the family of Structural Maintenance of Chromosomes (SMC) proteins which regulate chromatid cohesion and chromosome condensation. The Walker A and Walker B ATP-binding domains in each Rad50 protein associate together through an antiparallel association of the coiled-coil domains (Figure 3.1). Each Rad50 protein binds to another through ATP-dependent association of the Walker A/B domains into a homodimer, and also through another association at the apex of the coiled-coils at the zinc hook domain. In addition, a dimer of Mre11 also links the ATP-binding domains of Rad50 through an association at the base of the coiled-coils.

Recent structural analysis of Mre11/Rad50 proteins from bacteria and archaea showed that the ATP-binding domains of Rad50 bound to Mre11 are in an open configuration in the absence of ATP [85]. In contrast, the ATP-bound form of the complex is a closed configuration with the Mre11 nuclease domains in a dimer underneath the Rad50 head domains [65, 66]. These results suggest that

Mre11/Rad50 complexes are in a dramatically different conformation when bound to ATP compared with the nucleotide-free conformation (Figure 3.1).

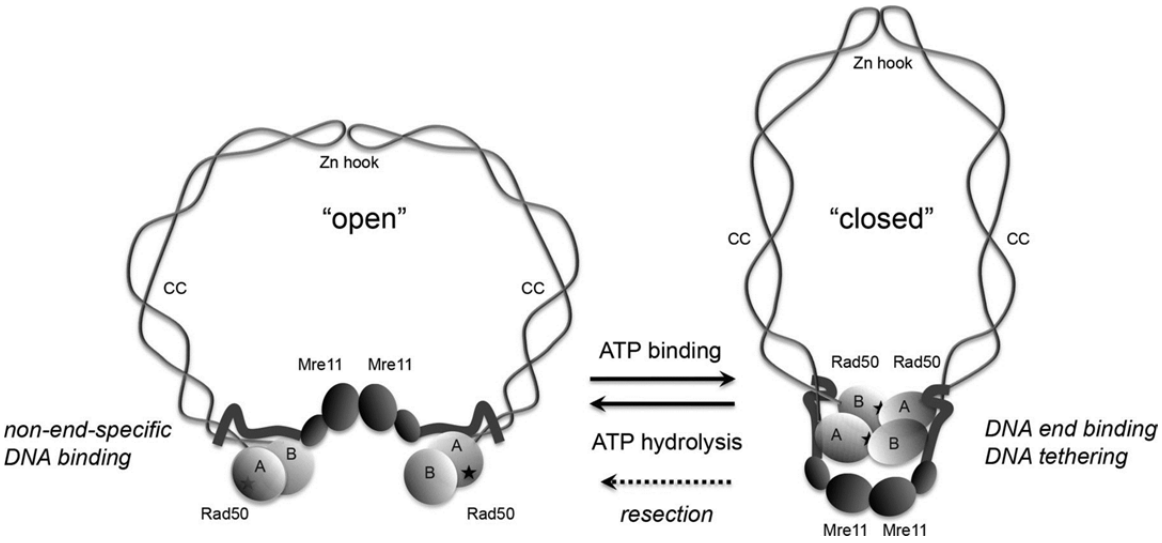

Figure 3.1 Schematic model of MRN in the absence (open) or presence of ATP (closed).

Rad50 is shown as light gray globular domains containing Walker A (A) and Walker B (B) motifs connected by intramolecular, antiparallel coiled-coils (CC), that attach to each other through the zinc hook motifs (Zn hook). Stars indicate the approximate positions of the ATP-binding residues in Rad50. Mre11 is shown as dark gray globular domains representing the nuclease/dimerization domain and the capping domain, connected to the linker that binds to the coiled-coils of Rad50. The closed state is associated with a higher affinity for DNA ends and with DNA tethering, while the movement from the closed to the open state is required for Mre11 nuclease activity and promotion of resection. The zinc hook is shown attached here, but the complex has also been observed with hooks unattached, both in solution and bound to DNA. This research was originally published in in Journal of Biological Chemistry. Lee JH, Mand MR, Deshpande RA, Kinoshita E, Yang SH, Wyman C, Paull TT. Ataxia Telangiectasia-Mutated (ATM) Kinase Activity Is Regulated by ATP-driven Conformational Changes in the Mre11/Rad50/Nbs1 (MRN) Complex. Journal of Biological Chemistry. 2013; 288:12840-12851. © the American Society for Biochemistry and Molecular Biology.

To better understand how these dynamic, ATP-driven changes in the MRN complex affect the regulation of ATM kinase activity, I employ here an analog-sensitive version of ATM to separate the nucleotide pools used by the kinase and by MRN. These experiments show that the "closed," ATP-bound state of MRN, but not ATP hydrolysis, is essential for ATM stimulation, thus explaining why it is important that MRN complexes have a slow rate of hydrolysis for signaling.

RESULTS

Both the MRN and ATM complexes utilize ATP, which cannot be removed from an in vitro kinase assay since the activity of ATM can only be assessed by monitoring ATP-dependent phosphorylation. To specifically manipulate the nucleotide pool used by ATM, I generated a mutant form of the kinase which allows the utilization of N^6-substituted-ATP analogs by generating a cavity within the ATP-binding pocket (Figure 3.2) [186]. Mutation of tyrosine 2755 in the ATP-binding pocket of ATM was previously shown to allow the kinase to accept N^6-modified ATP analogs [187].

The Y2755A mutant form of ATM was expressed and purified as previously described [177] (Figure 3.3), and tested in vitro in a kinase assay (Figure 3.4A). In this experiment, hydrogen peroxide was used to activate ATM [5], to assess the ability of ATM to utilize ATP analogs in the absence of the MRN complex. As shown previously, N^6-(1-methylbutyl)-ATP was utilized by the Y2755A-ATM, and was not utilized by the wild-type enzyme (Figure 3.4A), as measured by phosphorylation of a GST-p53 substrate and phospho-specific p53 antibody in a quantitative western blot as described previously [34]. However, further experiments showed that N^6-(1-methylbutyl)-ATP inhibited the activation of wild-type ATM by MRN/DNA, even in

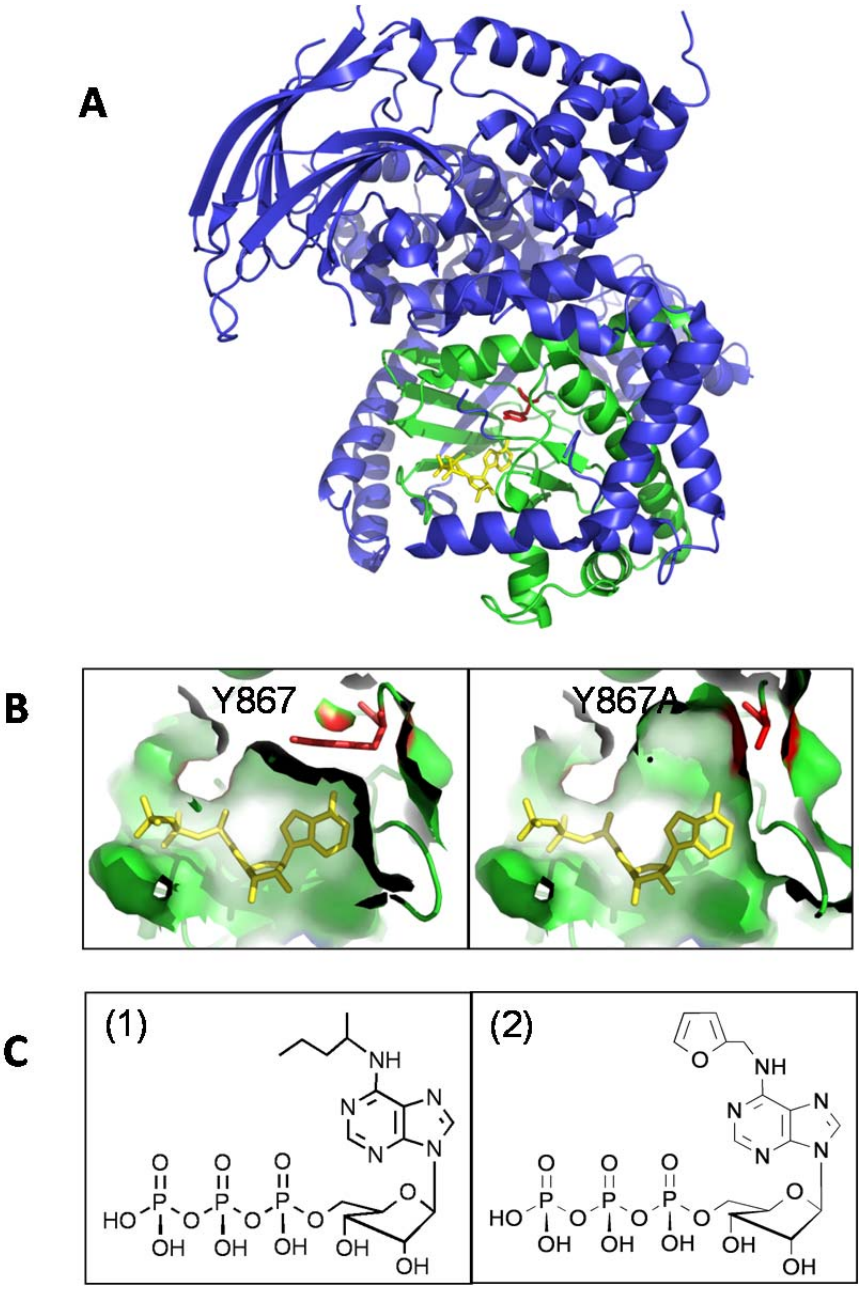

Figure 3.2 Structure of PI3Kγ and mutations in the ATP binding pocket.

(A) Structure of the Phosphatidylinositol 3-Kinase gamma subunit (PI3Kγ): ATP binding pocket, green; Y867 (ATM Y2755), red; ATP, yellow; remaining structure, blue. (B) The surfaces view of the ATP binding pocket of Y867A-PI3Kγ. (C) Structure of N^6-1-methylbutyl-ATP (1) and N^6-furfuryl-ATP (2).

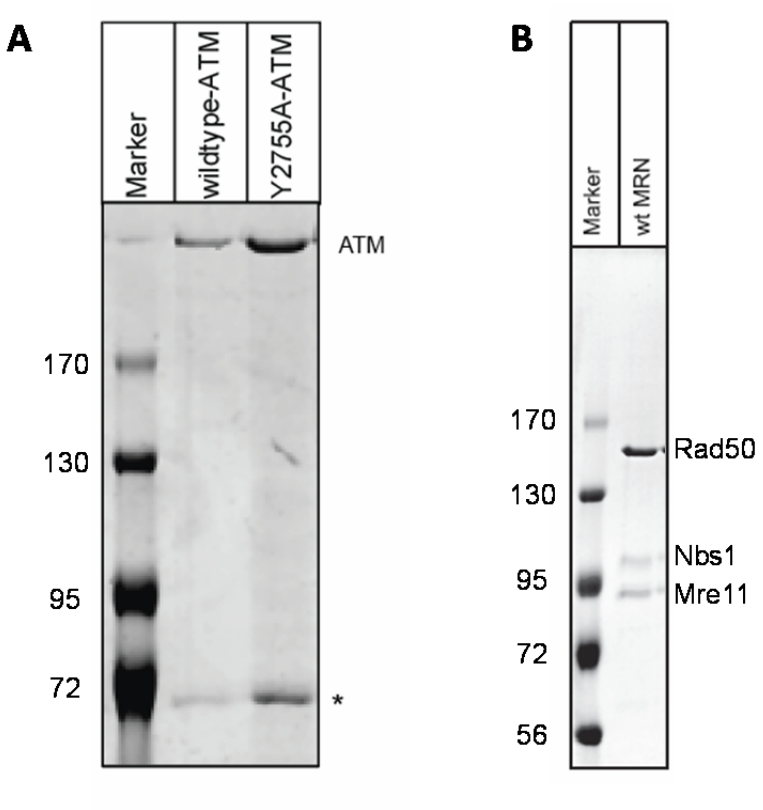

Figure 3.3 Recombinant ATM and MRN protein complexes.

(A) SDS-PAGE of purified recombinant wild-type- and Y2755A-ATM. * indicates position of Hsp70 protein that copurifies with ATM (B) SDS-PAGE of purified recombinant MRN complex with individual components labeled. Gels were stained by coomassie blue and the size (kDa) of the protein standards are shown to the left.

the presence of ATP (Figure 3.4B). This effect was specific to reactions containing MRN, so we conclude that N^6-(1-methylbutyl)-ATP is toxic to MRN function. We also found that several other N^6-modified ATP analogs were similarly toxic, with the exception of N^6-(furfuryl)-ATP. This nucleotide was utilized by Y2755A-ATM but not by wild-type ATM when activated by oxidation (Figure 3.4A) and also does not

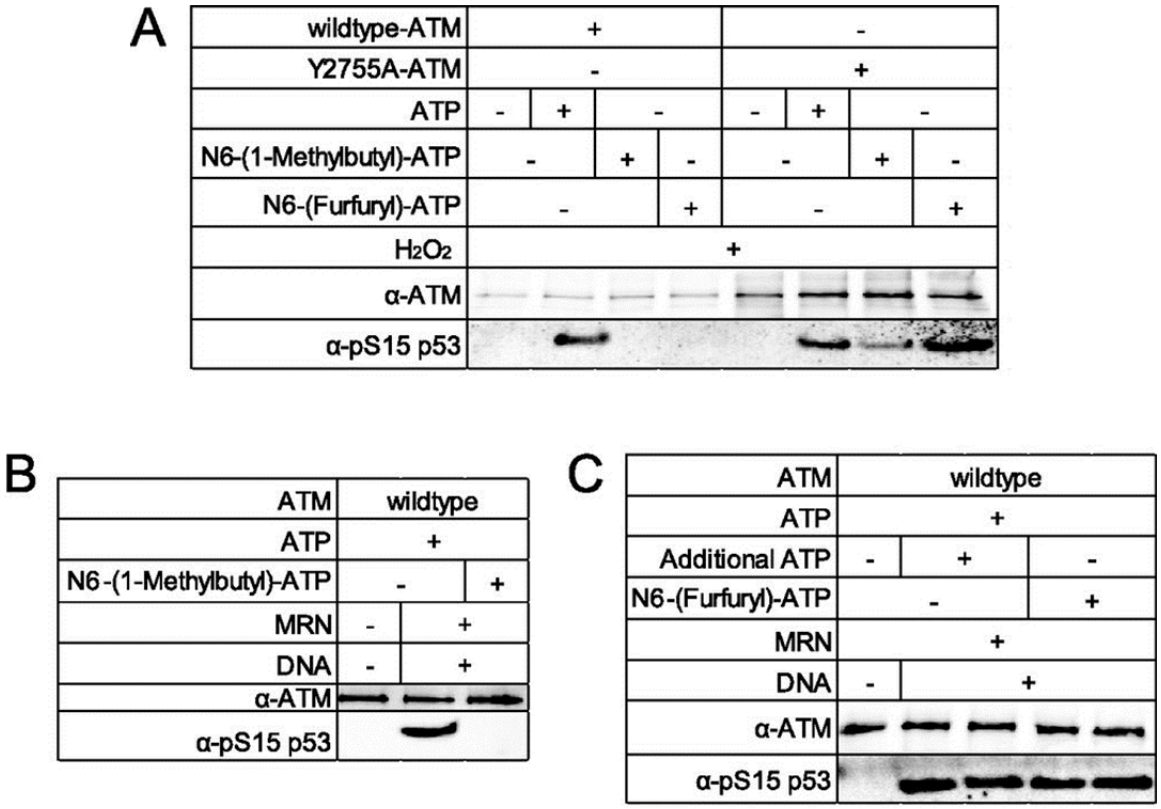

Figure 3.4 Usage of N^6-substituted ATP analogs in ATM kinase assays.

(A) Kinase assays were performed with wild-type or Y2755A-ATM and either ATP or the ATP analogs N^6(1-methylbutyl)-ATP or N^6(1-furfuryl)-ATP as indicated, using 2.7 mM H_2O_2 to activate ATM in the absence of MRN. Recombinant GST-p53(1–100) was used as the substrate, and phosphorylation of p53 Ser-15 was assessed by Western blotting and a phospho-specific antibody directed against Ser-15. (B) MRN and DNA were used to activate wild-type ATM in the presence of ATP and N^6(1-methylbutyl)-ATP as indicated. Kinase activity was assessed as in A. (C) Kinase assays were performed as in B except with N^6(1-furfuryl)-ATP as indicated.

prevent MRN/DNA activation of wild-type ATM in the presence of ATP (Figure 3.4C).

The Y2755A mutant ATM protein was tested in an MRN/DNA-dependent assay, and was found to be unable to phosphorylate p53 in the presence of N^6-

(furfuryl)-ATP alone, demonstrating that MRN requires ATP to activate ATM (Figure 3.5A). The Y2755A mutant also shows some DNA-independent activation that is only observed with ATP, not with the N^6-(furfuryl)-ATP analog. To determine if ATP hydrolysis is required by MRN, the same reaction was performed in the presence of the nonhydrolyzable ATP analog AMP-PNP (Figure 3.5B). Notably, Y2755A ATM phosphorylated p53 in the presence of MRN/DNA, N^6-(furfuryl)-ATP, and AMP-PNP while wild-type ATM was inactive under these conditions. Taken together, these results show that MRN requires ATP for ATM activation but that hydrolysis is not essential.

DISCUSSION

Here we have investigated the enzymatic functions of the MRN complex and how these affect ATM kinase activity. Clearly the MRN complex plays a very important role in ATM function, particularly considering the similarity in clinical phenotypes of patients lacking ATM (A-T) compared with patients expressing hypomorphic alleles of MRE11 or RAD50 (A-T-like Disorder) or Nbs1 (Nijmegen Breakage Syndrome) [63]. In addition, numerous studies using cell lines, extracts, and also purified systems have shown the importance of MRN for the activation of ATM by DNA DSBs [34, 74, 75, 188, 189]. MRN has several distinct activities, however, not all of which are essential for the activation of ATM.

Using separate pools of ATP for ATM and MRN we show that ATP binding, but not hydrolysis, is essential for ATM activation via MRN. This suggests that MRN is in the "closed" configuration when bound to ATM on DNA (Figure 3.1). This form of MRN is long-lived since the rate of ATP hydrolysis by Rad50 is slow, and is also

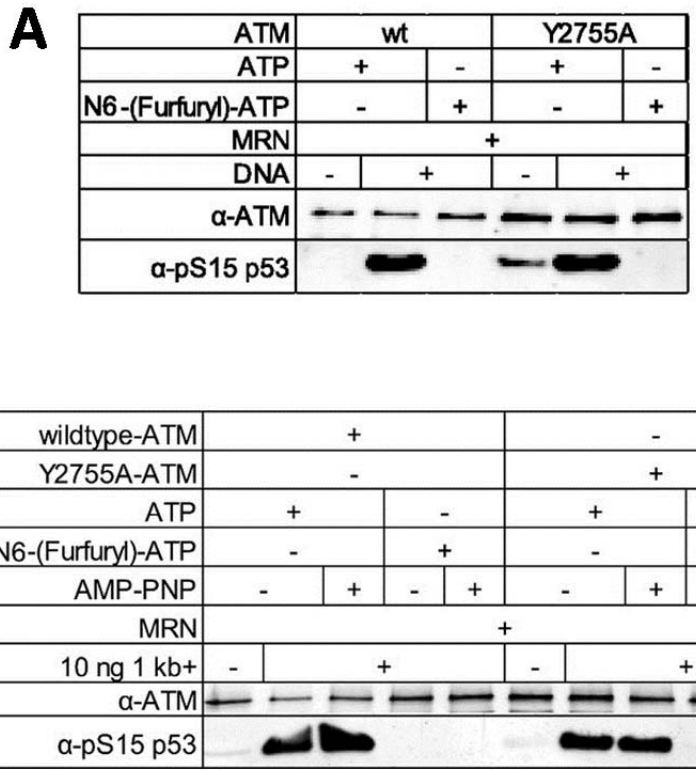

Figure 3.5. MRN stimulation of ATM activity requires ATP binding but not hydrolysis.

(A) Wild-type or Y2755A-ATM was activated by DNA and MRN in the presence of either ATP or N^6(1-furfuryl)-ATP as indicated. (B) Wild-type or Y2755A-ATM activated by DNA and MRN with either ATP or N^6(1-furfuryl)-ATP in the presence or absence of the non-hydrolyzable ATP analog AMP-PNP.

the form of MRN that functions in DNA end tethering [63] Thus many of the important functions of the MRN complex take place with ATP bound but not hydrolyzed, consistent with the idea of ATP as a switch for Mre11/Rad50 conformation rather than an energy source for mechanical work.

During the course of these experiments we found that MRN function is strongly inhibited by ATP analogs containing modifications at the N^6 position of the adenine base. This could be because the nitrogen at the N^6 position is the only solvent-exposed part of the adenine base in the Rad50 ATP-bound conformation [190], so most of these analogs would have room to bind in the ATP-binding pocket. The N^6-(furfuryl)-ATP compound was the only available N^6-modified analog that did not show this toxicity.

Recent studies with the P. furiosus MR enzyme suggest that the nuclease activity of Mre11 is triggered by the change in conformation that occurs following ATP hydrolysis, from the "closed" back to the "open" state (Figure 3.1) [62]. The enzyme in the closed state does not exhibit nuclease activity, consistent with our observation in this study that Mre11 nuclease activity is also not required for ATM activation. Analysis of a knock-in allele of the Mre11(H129N) nuclease-deficient mutant in the mouse also indicated that nuclease activity of Mre11 was not required for ATM signaling, although there are clearly essential functions of the nuclease during development since the mouse showed early embryonic lethality [191].

The rate of ATP hydrolysis by Rad50 is very slow relative to other enzymes (~0.1 molecules of ATP/minute) [174, 192]. Functionally, the reason for this appears to be that many of the activities of MRN (DNA end binding, DNA tethering, and ATM activation) occur when MRN is in the closed state in which ATP is bound but not hydrolyzed.

Schematic models of MRN function often portray Rad50 linking two broken DNA molecules, with the catalytic heads domains from one monomer bound to a distal site rather than associating with catalytic heads that are connected to it

through the zinc hook. While it is difficult to discern the conformation of structures within the tethered complexes we have observed by SFM, our data suggest that MRN would be much more likely to form catalytic domain interactions within a single dimeric unit (as depicted in Figure 3.1), particularly in the presence of ATP as illustrated previously [63, 197, 198]. Association between head domains of a Rad50 dimer is also driven by Mre11 dimerization [85, 199]. While it remains to be determined how ATP hydrolysis by Rad50 is regulated within cells, the physical characteristics of the protein support a model in which multimeric interactions are built upon the unit of a Rad50 dimer with the monomers associating within this unit at both the catalytic domains as well as the zinc hook and Mre11-binding interfaces.

In summary, our results show that the closed conformation of the human MRN complex is critical for the activation of the ATM kinase and that the structural components of the Rad50 protein that are important for this conformation are also important for the activation process. Other functions of MRN, including the stimulation of DNA end resection, are promoted by the conformational change from the closed to the open state that occurs during ATP hydrolysis but are not required for ATM activation. Thus there is a temporal sequence of DNA end tethering/ATM activation followed by DNA end resection that is orchestrated by MRN binding and hydrolysis of ATP.

CHAPTER 4: PROTEOMIC AND PHOSPHOPROTEOMIC ANALYSIS OF ATM SEPARATION-OF-FUNCTION MUTATIONS

ATM is activated by both DNA double-strand breaks (DSBs) and oxidative stress to initiate a robust signaling cascade [26]. Previous studies have looked at changes in the phosphoproteome after DNA damage using ionizing radiation (IR) or radiomimetic drugs [10-12, 107, 173]. As these treatments may generate both DSBs and oxidative stress, it is not possible to examine the effects of ATM activated by only one of these cellular stressors. Notably, separation-of-function mutations in ATM have been identified that allow the activation of ATM by only one mechanism [5] (JH Lee, unpublished observations). Expression of these constructs in A-T cells lacking functional ATM will show which cellular processes ATM is important for in the absence of exogenous stress.

The separation-of-function mutations in ATM prevent activation by either oxidative stress or DSBs in vitro. Guo et al. identified a cysteine (C2991) in the PIKK regulatory domain that was required for activation by oxidative stress [5]. Mutation of this cysteine to leucine (C2991L-ATM) abolished in vitro activation of ATM by oxidative stress but not DSBs (Figure 4.1A) [5]. The separation-of-function mutation that prevents ATM activation by DSBs was found by comparison with a method of mTOR activation. Fang et al. identified in mTOR a key arginine residue N-terminal of the kinase domain that was important for mTOR activation by phosphatidic acid [200]. This arginine was in a double arginine motif that was also present in ATM a similar distance from conserved residues in the kinase domain. Mutation of both of these arginines to alanine in ATM (R2579A/R2580A-ATM) prevents activation by MRN and DNA in vitro (Figure 4.1B)

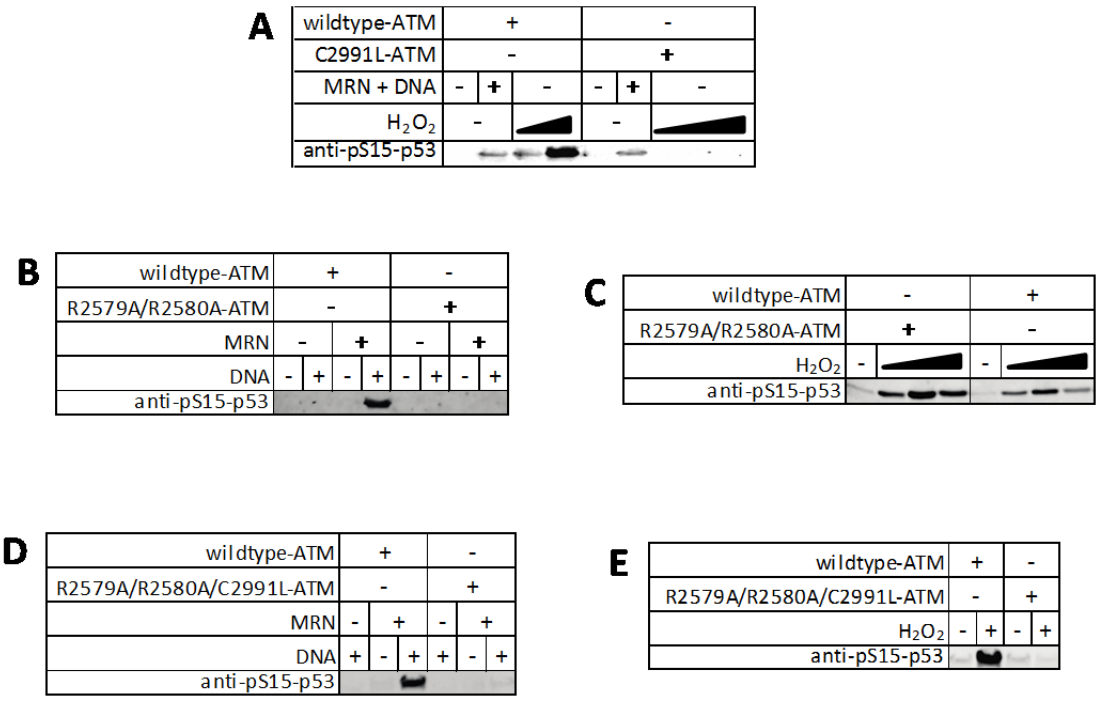

Figure 4.1 Mutations in ATM cause differential activation by DNA double strand breaks and reactive oxygen species in vitro.

(A) In vitro kinase ATM kinase activity performed with 0.2 nM recombinant purified wild-type-ATM or C2991L-ATM proteins in the presence of 3.6 nM MRN and 10 ng DNA or a titration of H_2O_2 (0.27 and 0.81 mM for wild-type-ATM and 0.27, 0.81, and 2.7 mM H_2O_2 for C2991L-ATM). Kinase activity was measured by western blot for phospho-p53. From "ATM Activation by Oxidative Stress" (Guo, Kozlov, Lavin, Person, & Paull, 2010). Reprinted with permission from AAAS. (B) In vitro kinase assay performed as in (A) with wild-type-ATM or R2579A/R2580A-ATM. (C) In vitro kinase assay performed as in (A) with wild-type-ATM or R2579A/R2580A-ATM and a titration of H_2O_2 (0.27, 0.81, and 2.7 mM H_2O_2). (D) In vitro kinase assay performed as in (A) with wild-type-ATM or R2579A/R2580A/C2991L-ATM. (E) In vitro kinase assay performed as in (A) with wild-type-ATM or R2579A/R2580A/C2991L-ATM and 2.7 mM H_2O_2. Figures (B) – (E) were provided by JH Lee.

but allows normal activation by oxidative stress (Figures 4.1C) (JH Lee, unpublished observations). Purified ATM combining all three separation-of-function mutations (R2579A/R2580A/C2991L-ATM) lacked in vitro activity in the presence of oxidative stress or DSBs (Figures 4.1D and E). The various ATM constructs and their effects on ATM activation are shown in Figure 4.2.

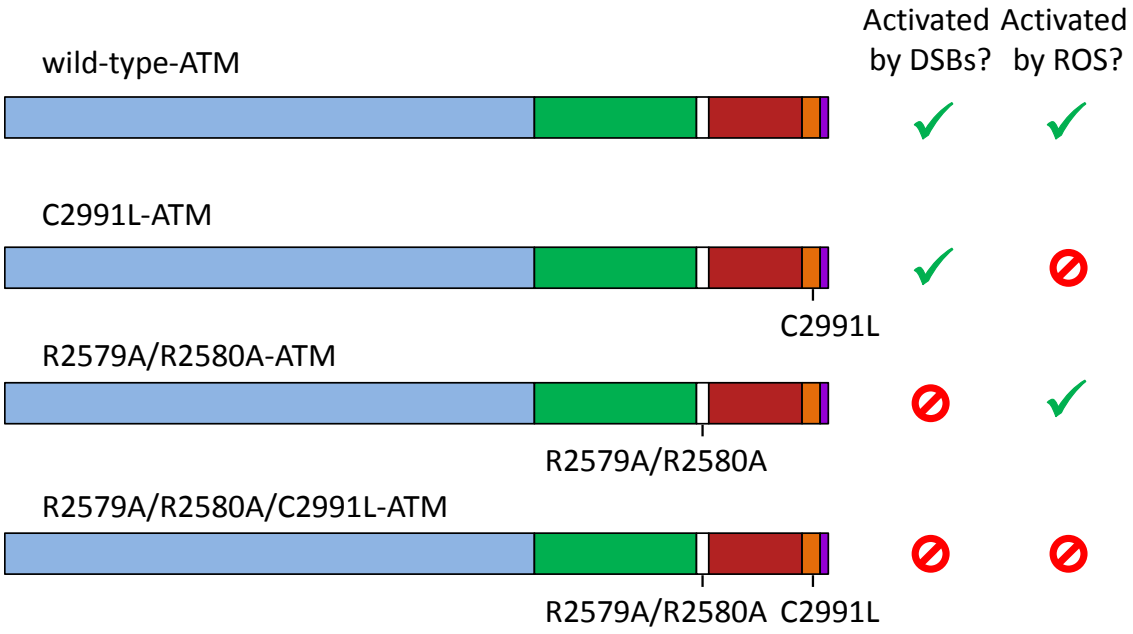

Figure 4.2 Diagrams of the ATM separation-of-function mutations that prevent activation by DSBs or ROS.

The colors represent domains in ATM: blue, HEAT repeats (residues 1-1965); green, FAT domain (residues 1966-2566); red, PI3K-like kinase domain (residues 2614-2960); orange, PIKK regulatory domain (residues 2961-3024); purple, FATC domain (residues 3025-3056).

To analyze the effects of re-expressing these different ATM constructs, I compared the proteomes and phosphoproteomes of six cell lines. Two main cell lines were used, GM07544 and AT1ABR. Both cell lines are derived from lymphoblasts that have been transformed with Epstein Barr virus. However, GM07544 cells are from a healthy individual while AT1ABR cells are from a patient with ataxia telangiectasia. The AT1ABR cells have a 9 base pair deletion in the ATM gene corresponding to amino acids 2546-2548 that abrogates kinase activity and destabilizes the protein. The AT1ABR cells were also used as the parental cell line for generating stable cells containing the four ATM constructs [17, 178]. ATM expression in these cells is under the control of the pMATII promoter and inducibly expressed with the addition of low amounts of $CdCl_2$.

All the cell lines were exposed to 2 μM $CdCl_2$ for 16 hours for protein induction and harvested. The cell pellets were lysed and total protein was quantitated. The lysates were digested with trypsin and Lys-C and the peptides were labeled with Tandem Mass Tags (TMT). After combining the tagged peptides, the samples were fractionated by strong cation exchange with or without phosphopeptide enrichment by immobilized metal affinity chromatography. The resulting samples were analyzed by quantitative LC-MS/MS (Figure 4.3).

THE PROTEOME IS ALTERED IN THE PRESENCE OF MUTANT ATM

The levels of ATM protein were compared by western blot in cells treated with or without 2 μM $CdCl_2$ (Figure 4.4A). Uninduced AT1ABR cells all showed low levels of ATM. There was a visible induction of ATM in the AT1ABR cell lines with the ATM constructs while the parental cell line showed no change in the presence of $CdCl_2$.

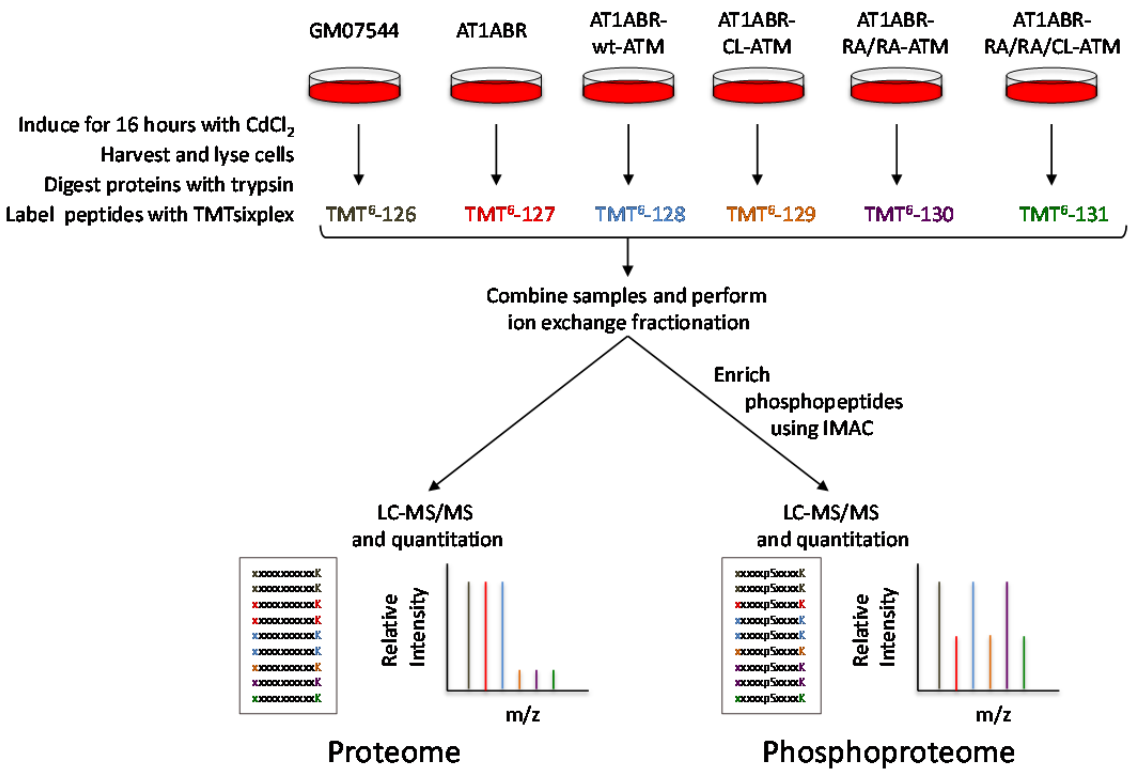

Figure 4.3 Flowchart of sample preparation and mass spectrometry.

The ATM constructs are abbreviated as follows: wt: wild-type; CL: C2991L; RA/RA: R2579A/R2580A, RA/RA/CL: R2579A/R2580A/C2991L.

AT1ABR cells expressing wild-type ATM had the highest amount of ATM and the three cell lines expressing ATM with the various mutations had lower levels but were similar when compared between the mutant cell lines. As expected, the ATM protein level in the normal lymphoblast cell line GM07544 was unaffected by $CdCl_2$ treatment. The amount of ATM protein in each cell line was also calculated using the TMT tags in the quantitative LC/MS-MS (Figure 4.4B). In contrast to the western blot results, GM07544 had ATM levels similar to the AT1ABR cell line. However, the AT1ABR cells that inducibly express ATM all had higher levels of ATM. The differences between the western blot and LC/MS-MS quantitation could be due to ATM fragments that do not appear on the western blot but would be digested and quantitated during LC-MS/MS.

There were 4,368 proteins identified in the different cell lines although 52 of these were not seen in the AT1ABR cells expressing C2991L-ATM. The raw intensity of each protein was normalized to the raw intensity in AT1ABR. To get a general look at what was happening in the proteome, hierarchical clustering was performed on the relative abundances of all the proteins in the remaining five cell lines. This clustering revealed a group of 362 proteins with much lower relative abundance in the AT1ABR cell lines expressing any of the three mutant ATM proteins that will be referred to as *D*own *I*n *M*utants (DIM) proteins (Figure 4.5).

A histogram of the relative intensity of each protein normalized to the levels in the AT1ABR parental cell line shows a shift in the peaks in the three cell lines expressing mutant ATM (Figure 4.6A). The loss of the DIM proteins in the cell lines expressing mutant ATM skew the rest of the proteome to the right such that there appears to be higher levels of the remaining proteins in comparison to the AT1ABR

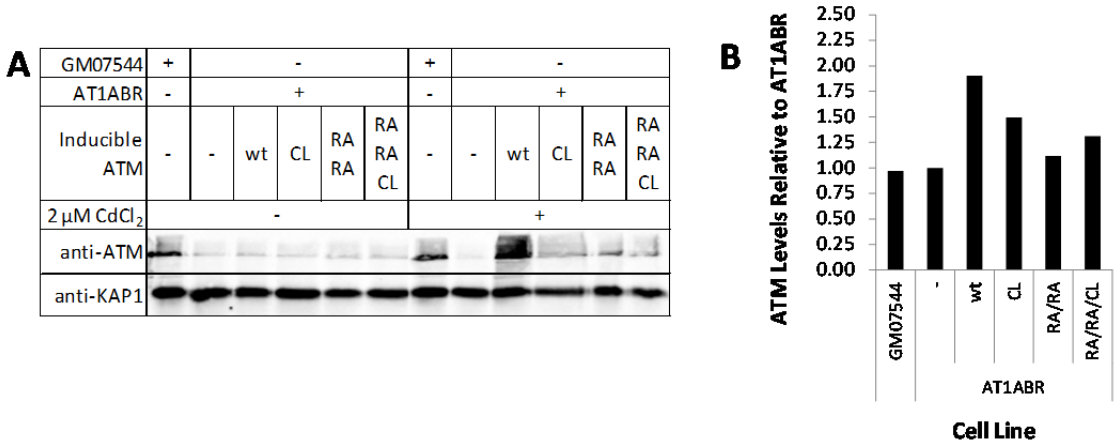

Figure 4.4 $CdCl_2$ addition causes induction of ATM in AT1ABR cells with pMATII.

(A) AT1ABR and GM07544 cells were treated with or without 2 μM CdCl2 for 16 hours and harvested. Western blots were performed on 20 μg lysate and probed for ATM and KAP1 levels. (B) Normalized values of the raw intensities of ATM from the LC-MS/MS quantitation of the cell lines after $CdCl_2$ addition. wt: wild-type; CL: C2991L; RA/RA: R2579A/R2580A, RA/RA/CL: R2579A/R2580A/C2991L.

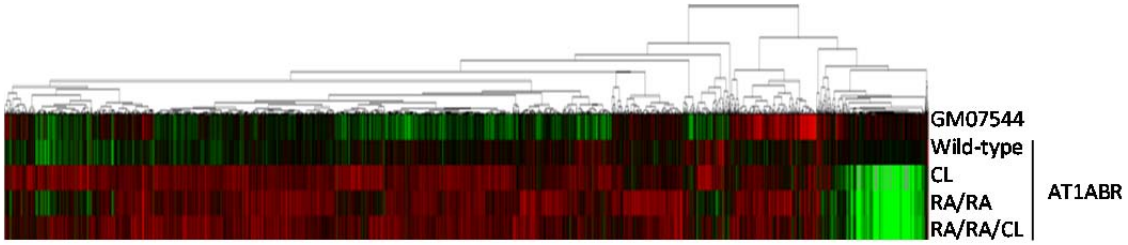

Figure 4.5 Hierarchical clustering of normalized protein levels reveals a group of proteins reduced in AT1ABR cells expressing mutant ATM.

Raw values from quantitative LC-MS/MS were normalized to the AT1ABR parental cell line and clustered using Cluster 3.0. Results were visualized using Java Treeview. Each horizontal group represents all the proteins from that cell line. Vertical lines represent the same protein in each cell line. All protein levels have been normalized to the AT1ABR parental cell line. Green represents reduced levels in the cell line listed, red represent higher levels, and proteins represented by gray were not found. CL:C2991L, RA/RA: R2579A/R2580A.

parental line. The same amount of total protein was used from each cell line but approximately 8% of the proteome (the DIM proteins) is underrepresented in the mutant ATM cell lines, some vastly so. Thus, the relative abundances of the remaining proteins seem higher and shift the peak to the right. To compare the protein levels without the DIM proteins, the protein raw intensities were normalized to the sum of the raw intensities of the proteome. Then, all the cell lines were normalized to the AT1ABR cell line and compared. This histogram with the DIM proteins removed from all the cell lines (the 4006 remaining proteins) shows similar patterns for all the cell lines (Figure 4.6B).

To investigate the differences in the levels of the DIM proteins, several of these proteins were analyzed using commercially-available antibodies. I was most interested in the comparisons between the AT1ABR lines expressing wild-type- and C2991L-ATM as these showed the largest difference in protein levels. Western blots of 5 proteins from the DIM group showed similar levels of total protein in the lysate from the AT1ABR cell lines expressing wild-type-ATM and C2991L-ATM (Figure 4.7). There are a number of reasons this could occur. First, these proteins could have post-translational modifications such that the mass spectrometry software is unable to identify the peptides to quantitate the protein. However, extensive searches of the mass spectrometry data with many post-translational modifications have not uncovered any that match the differences in intensity seen here. Another possibility is that the proteins are lost during sample processing. This could occur if the proteins were in an aggregated state and were pelleted during the centrifugation step.

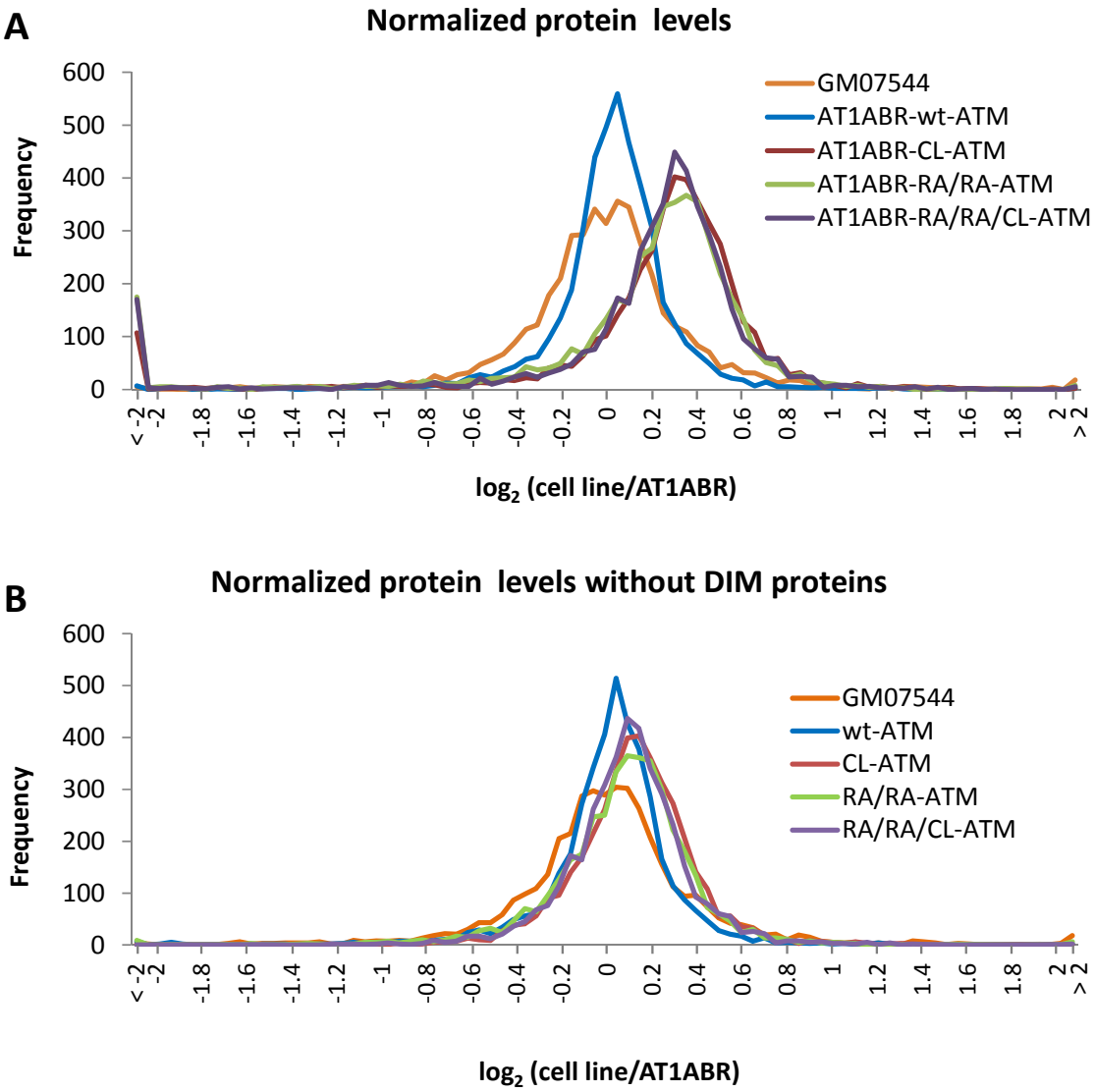

Figure 4.6 Overlapping histograms of protein levels relative to the parental cell line AT1ABR.

Histograms were generated of the protein levels of the cell lines relative to the AT1ABR cell line using (A) the entire proteome and (B) with DIM proteins removed. wt: wild-type; CL: C2991L; RA/RA: R2579A/R2580A.

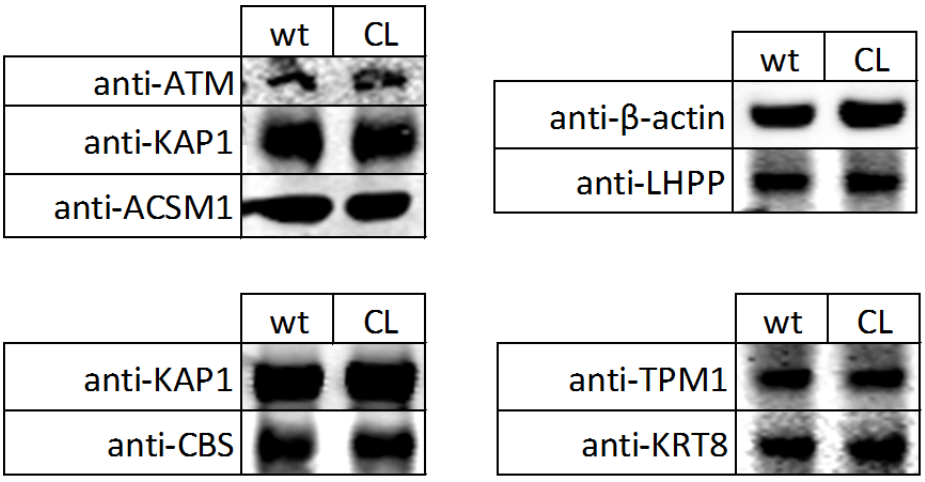

Figure 4.7 AT1ABR cells expressing wild-type-ATM or C2991L-ATM show similar total levels of a sample of proteins from the DIM group.

Cells were lysed using either the protocol for mass spectrometry or in the absence of detergent. Western blots were performed on 20 μg lysate with the indicated antibodies. ATM, KAP1, and β-actin protein levels were used as a loading control.

To examine potential aggregation, sucrose gradients were used to compare the sedimentation rates of a subset of the DIM proteins in wild-type- and C2991L-ATM expressing AT1ABR cells. The DIM proteins with commercially available antibodies that showed the largest differences between wild-type- and C2991L-ATM expressing cells were analyzed. To prevent the loss of aggregates, cells were lysed in the absence of detergent and the lysates were not pelleted. A representative western of tropomyosin 1 (TPM1) showed a large shift to the last fraction in cells expressing C2991L-ATM (Figure 4.8A). The western blots were quantitated and normalized to a sample of the lysate (Figure 4.8B). TPM1 normally interacts with the actin cytoskeleton, which was enriched in the DIM list (data not shown).

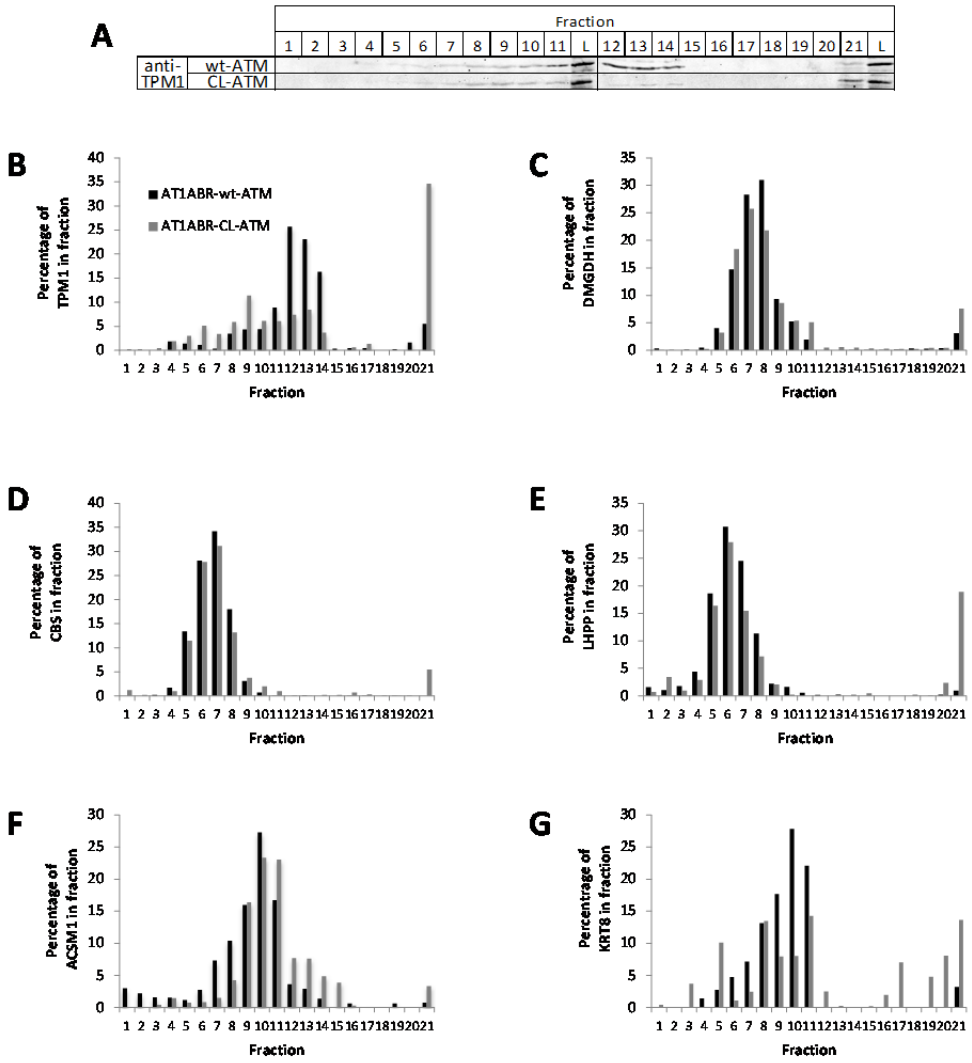

Figure 4.8 A sample of DIM proteins show a shift to the denser fractions of sucrose gradients in C2991L-ATM expressing cells.

(A) AT1ABR cells expressing wild-type-ATM (black) or C2991L-ATM (gray) were induced with 2 μM CdCl2 for 16 hours, pelleted, and lysed in the absence of detergent. The lysates (2 mg) were added to the top of sucrose gradients composed of 1 ml layers of 50% to 5% sucrose in 5% increments. After ultracentrifugation, 500 μl fractions were collected and analyzed by western blot. (A) Representative western blot for tropomyosin (TPM1, 35 kDa), (B)-(G) Quantitation of western blots for (B) TPM1; (C) DMGDH, 100 kDa; (D) CBS, 63 kDa; (E) LHPP, 29 kDa; (F) ACSM1, 65 kDa; and (G) KRT8, 45 kDa. Quantitation was performed on the Licor system using Image Studio Ver 4.0.

Previously, changes in cellular morphology of A-T cells due to alterations in the actin network have been reported [201].

In addition to TPM1, quantitation of other proteins revealed shifts to denser fractions in AT1ABR cells with C2991L-ATM relative to wild-type-ATM containing cells (Figure 4.8B-G). These proteins are involved in diverse cellular processes. Dimethylglycine dehydrogenase (DMGDH) functions in the metabolism of choline and is found in the mitochondrial matrix (Figure 4.8C). Cystathionine β-Synthase (CBS) catalyzes a crucial step in the biosynthesis of cysteine and is important for mitochondrial function as depletion causes a reduction in mitochondrial respiration and ATP synthesis (Figure 4.8D) [202]. Phospholysine phosphohistidine inorganic pyrophosphate phosphatase (LHPP) removes phosphates from imidodiphosphate, 3-phosphohistidine and 6-phospholysine (Figure 4.8E). Acyl-CoA Synthetase Medium-Chain Family Member 1 (ACSM1) is localized to the mitochondria and forms acyl-CoA from free fatty acids (Figure 4.8F). Keratin 8, another cytoskeletal protein, also showed increased levels in the denser fractions in C2991L-ATM expressing cells. However, at least one DIM protein, ATP citrate lyase (ACLY), showed more similar patterns of distribution in AT1ABR cells expressing wild-type-ATM and C2991L-ATM (Figure 4.9A). ATM, KAP1, and β-actin were used as controls in the sucrose gradient and showed no differences either (Figure 4.9B-D). Altogether, these results suggest the DIM proteins undergo changes in sedimentation rate in AT1ABR cells expressing C2991L-ATM.

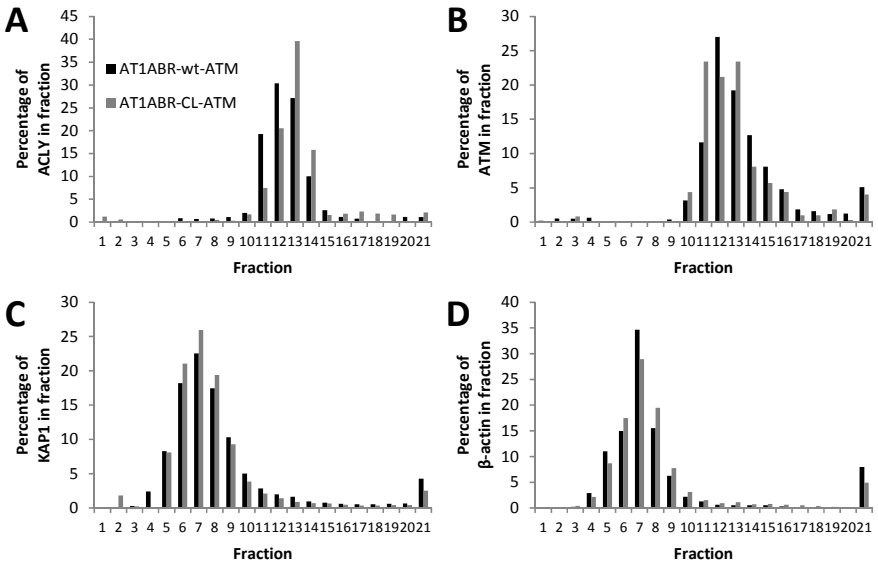

Figure 4.9 Control proteins and a DIM protein show similar patterns in sucrose gradients in both wild-type-ATM and C2991L-ATM expressing cells.

(A) Cell treatment, lysis, sucrose gradients, and western blots were performed as in Figure 4.8 for wild-type-ATM (black) and C2991L-ATM expressing cells. Quantitation of western blots for (A) ACLY, 120 kDa; (B) ATM, 350 kDa; (C) KAP1, 100 kDa; and (D) β-actin, 450 kDa are shown. Quantitation was performed on the Licor system using Image Studio Ver 4.0.

EXPRESSION OF C2991L-ATM AFFECTS THE MITOCHONDRIA

Although not all the causes of the under-representation in the mass spectrometry screen are known, analysis of the DIM proteins has uncovered some interesting features. The proteins in the DIM group were characterized using the Database for Annotation, Visualization and Integrated Discovery (DAVID) v6.7 for gene ontology analysis [203, 204]. All three domains of gene ontology – Biological Process, Cellular Component, and Molecular Function – showed significantly enriched terms for the DIM proteins (Figure 4.10). The proteins are enriched for oxidation-reduction and

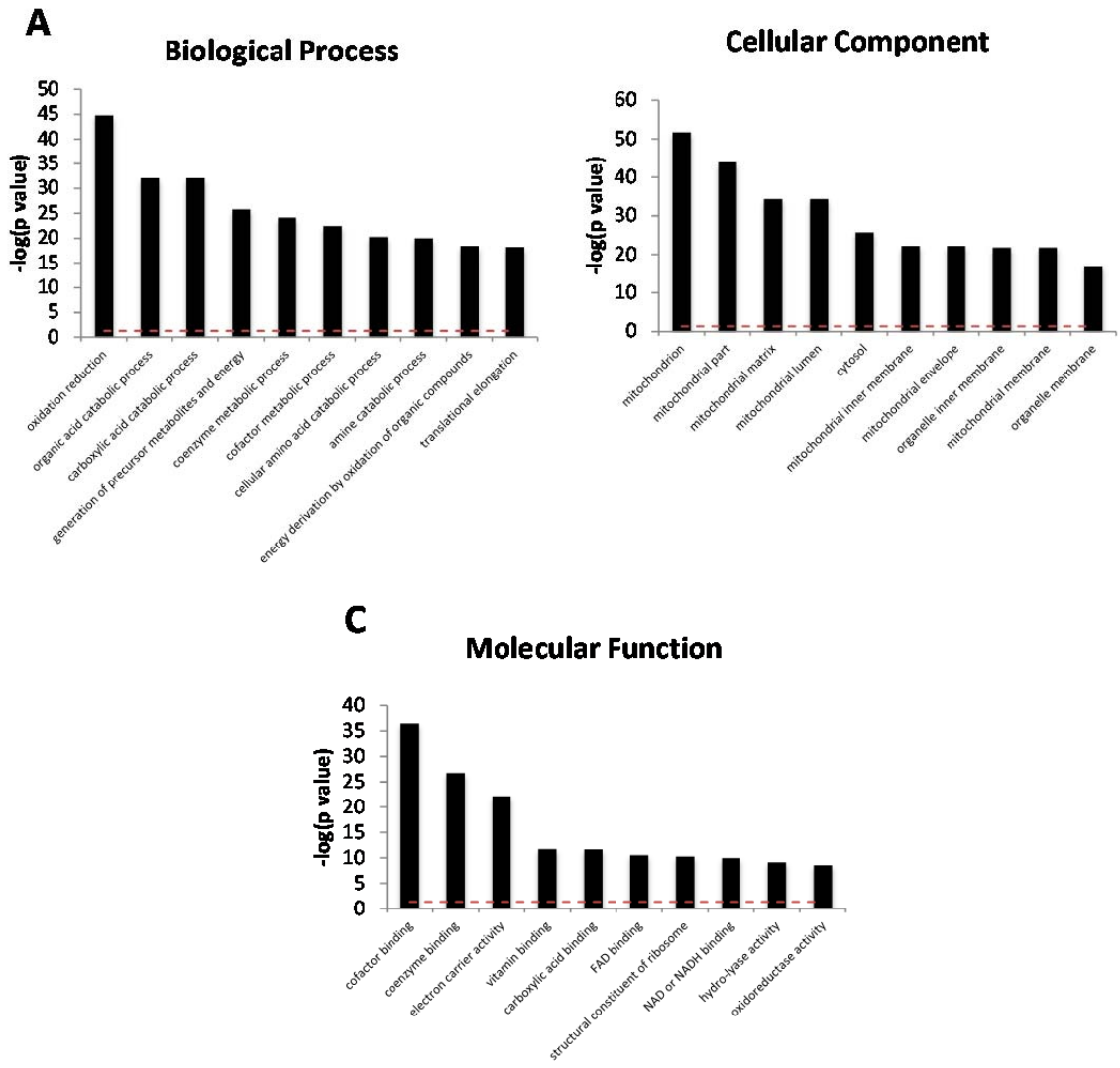

Figure 4.10 Gene ontology analysis of DIM proteins.

The list of DIM proteins was submitted to DAVID version 6.7 and the top results are shown with the -log(p value). The red line shows p value = 0.05. (A) Biological Process (B) Cellular Component and (C) Molecular Function.

various metabolic processes in the Biological Process group. In the Cellular Component group, seven of the top ten most significantly enriched terms are parts of the mitochondria. The Molecular Function group shows enrichment for cofactor binding and various specific cofactors as well as "Structural component of ribosome," Hydrolase activity," and "Oxidoreductase activity." The Cellular Component group showed DIM proteins were highly enriched for mitochondrial localization. Interestingly, the mitochondria from patients with ataxia telangiectasia have been shown to be defective [205]. Lymphoblastoid cells from patients with ataxia-telangiectasia have reduced mitochondrial membrane potentials and mitochondrial respiration rates [206]. In addition, cells lacking functional ATM are known to have higher ROS levels and increased sensitivity to ROS-inducing agents perhaps due to abnormal mitochondria [91, 207, 208].

To examine the requirements of ATM, and specifically C2991, in ROS regulation and mitochondrial homeostasis, I compared the AT1ABR parental cell line and AT1ABR cells inducibly expressing wild-type-ATM or C2991L-ATM with or without the addition of $CdCl_2$. In this experiment, the cells were allowed to recover for 2 days as there was too much variation at earlier time points. Propidium iodide staining showed all cells were in similar cell cycle phases (data not shown). The ROS levels and mitochondrial masses of the cell lines were analyzed by flow cytometry using H_2DCFDA and MitoTracker Green staining, respectively. Cells expressing C2991L-ATM showed higher levels of ROS than cells expressing wild-type ATM although both were higher than the parental AT1ABR cell line (Figure 4.11A-B). Notably, A-T cells and $ATM^{-/-}$ mouse tissues have been shown to have higher basal levels of proteins involved in oxidative-damage responsive pathways including p53,

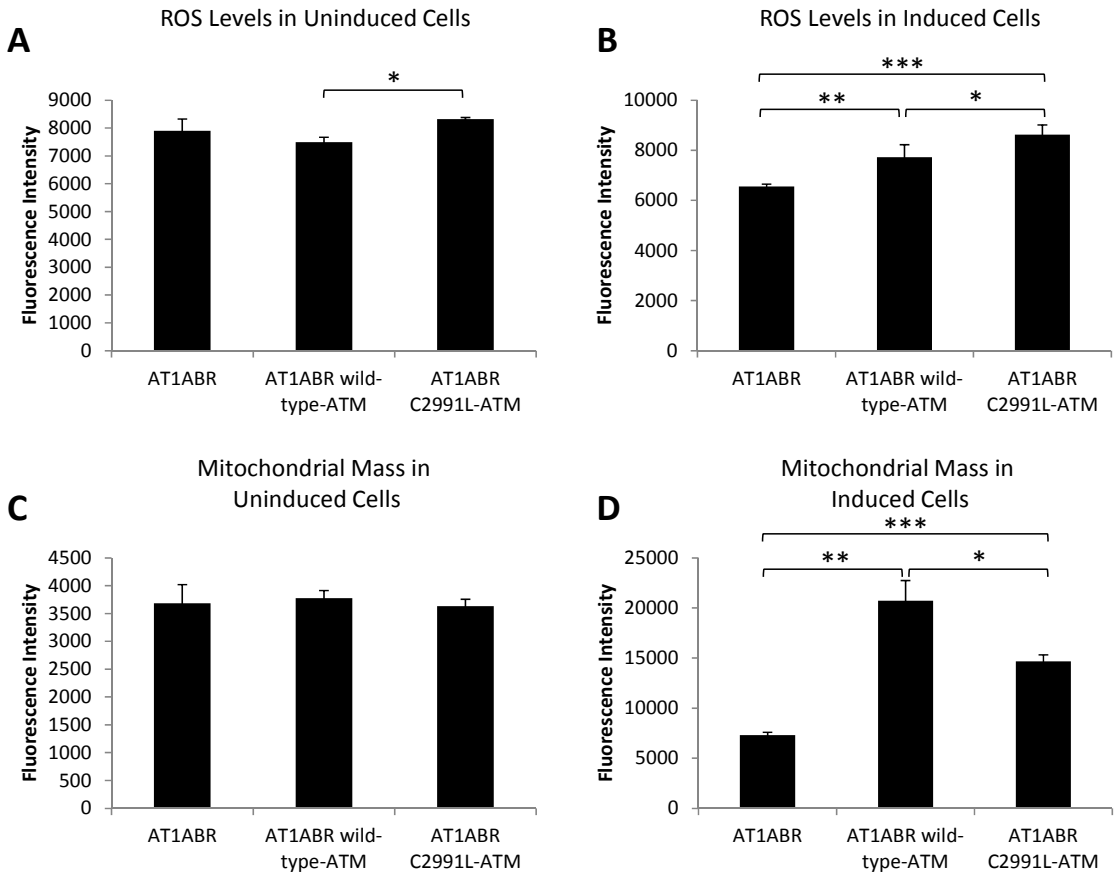

Figure 4.11 The levels of oxidative stress and mitochondrial mass in AT1ABR cells are affected by ATM expression and depend on the presence of C2991.

(A) The mitochondrial masses of uninduced AT1ABR cells were measured by MitoTracker Green staining followed by analysis using flow cytometry. (B) Cells were induced with 2 μM $CdCl_2$ then recovered for 48 hours and then treated as in (A). (C) The ROS levels of uninduced AT1ABR cells cells were measured by H_2DCFDA staining followed by analysis using flow cytometry. (D) Cells were induced with 2 μM $CdCl_2$ then recovered for 48 hours and then treated as in (C). Median values from independent replicates (n =4) were compared and used for t-tests. Error bars represent standard deviation. P-values: * < 0.05; ** < 0.005; *** < 0.0005

p21, NFκB, manganese superoxide dismutase, Gadd45, and hemeoxygenase [209-212]. Re-expression of ATM in this context could cause abnormal effects in these cells. Furthermore, other studies in our lab have shown after an inducible ATM knockout, mouse embryonic fibroblasts undergo an adaptation period with higher levels of ROS and then adjust and reduce oxidative stress to below the levels of cell heterozygous for ATM (S Zhang , unpublished observations).

As measured by MitoTracker Green, the induction of wild-type ATM greatly increased mitochondrial mass as compared to AT1ABR cells while the AT1ABR cells expressing C2991L-ATM consistently showed a level of mitochondrial mass between the AT1ABR cells and the AT1ABR cells expressing wild-type-ATM (Figure 4.11C-D). Previous studies have shown ATM activated by DNA damage can induce mitochondrial biogenesis suggesting ATM activated by either pathway may affect mitochondrial growth [213].

To examine the transcriptional effects of expressing wild-type-ATM and C2991L-ATM in AT1ABR cells, qPCR was performed with primers for SLC7A11, which encodes a cystine/glutamate transporter important for glutathione production and ROS reduction [214], and PPARGC1A, which encodes the protein PGC1α, a transcriptional coactivator of mitochondrial biogenesis [215]. The mRNA levels of SLC7A11 show an inverse pattern to the levels of ROS after the addition of $CdCl_2$ (Figure 4.12A). The parental cell line has the highest levels of SLC7A11 mRNA, AT1ABR cells expressing wild-type-ATM are intermediate, and AT1ABR cells expressing C2991L-ATM have the lowest amount of SLC7A11 transcription. A western blot showed a similar pattern in the SLC7A11 protein levels in these cells (data not shown). This suggests the parental AT1ABR cell line is able to upregulate

an antioxidant pathway more rapidly in this context. A previous study has shown SLC7A11 induction in mouse cells upon treatment with 10 μM cadmium chloride suggesting all the cells may be inducing SLC7A11 expression in response to the inducing agent [216]. A recent paper has uncovered p53-mediated inhibition of SLC7A11 expression that may explain the differences between the cell lines [217]. Here, wild-type-ATM may be activated by ROS and affect p53 activity directly. Conversely, the higher levels of ROS in C2991L-ATM cells may induce DNA damage, ATM activation, and then p53 activity.

The mRNA levels of PPARGC1A in uninduced cells were not correlated with the levels of mitochondrial mass (Figure 4.12B). Furthermore, upon addition of $CdCl_2$, levels of PPARGC1A mRNA in AT1ABR cells and AT1ABR cells expressing wild-type-ATM are increased while the amount of PPARGC1A mRNA in AT1ABR cells expressing C2991L-ATM is reduced. PPARGC1A has been shown to be regulated post-transcriptionally in mice by miRNA [218] as well as post-translationally by phosphorylation and acetylation [219]. Such mechanisms could modify or accentuate the transcriptional effects of PPARGC1A seen here. This data suggests the low levels of wild-type and C2991L-ATM in uninduced cells primes them for mitochondrial biogenesis. However, induction of more C2991L-ATM has a detrimental effect relative to the parental cell line. Notably, the levels of PGC1α, the protein encoded by PPARGC1A, followed the pattern of mitochondrial mass (data not shown).

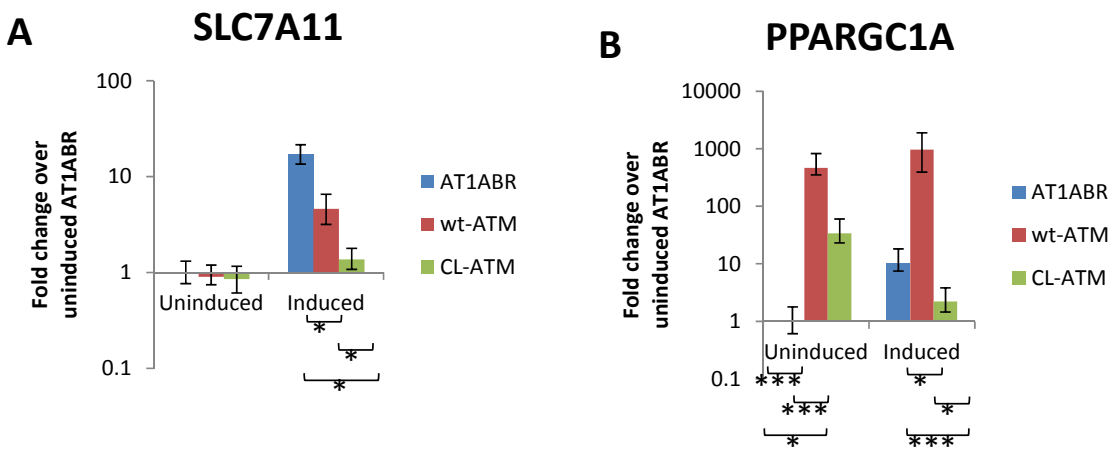

Figure 4.12 qPCR reveals SLC7A11 and PPARGC1A mRNA levels are affected by ATM expression and depend on the presence of C2991.

(A) RNA from cells treated with 2 µM $CdCl_2$ and recovered for 48 hours was reverse transcribed and the cDNA was subjected to qPCR with SLC7A11 and ACTB primers. (B) cDNA from (A) was subjected to qPCR with PPARGC1A and ACTB primers. wt: wild-type; CL: C2991L. C_t values from independent replicates (n =4) were compared and used for t-tests. Error bars represent standard deviation. P-values: * < 0.05; ** < 0.005; *** < 0.0005

PHOSPHOPROTEOME

The phosphoproteomic analysis of the GM07544 and AT1ABR cell lines identified 2,694 phosphopeptides with a false discovery rate of 1%. The phosphoproteome showed similar characteristics to previous studies, with phosphorylated serine accounting for most of the phosphorylation events followed by phosphorylated threonine and a small percentage of phosphorylated tyrosine (Figure 4.13). A histogram of the raw intensities from each cell line shows the phosphoproteomes are grossly similar, as expected (Figure 4.14). Further analysis of the AT1ABR phosphoproteomes was performed using pairwise comparisons of the log of the raw intensities of the phosphopeptides. The pairwise comparisons show with most of

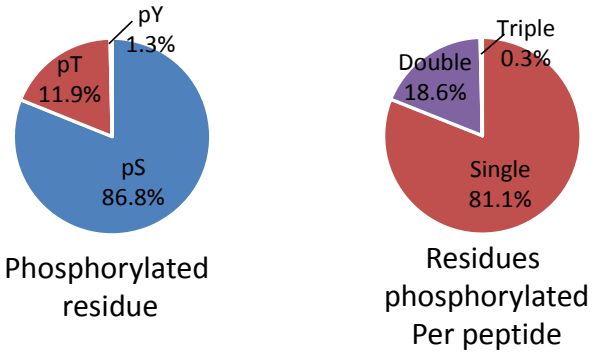

Figure 4.13 General properties of the identified phosphoproteome.

(A) Distribution of serine, threonine, and tyrosine residues. (B) Distribution of the number of phosphorylated residues on each peptide.

the phosphopeptides lie along the y = x line where the levels are similar in both cell lines (Figure 4.15). The nonparametric Spearman's rank correlation coefficient, ρ, was calculated for all the pairwise comparisons. Values of ρ closer to 1 suggest the pairwise comparisons are more similar. The ρ values were all very significant ($p < 10^{-16}$) and examination of the ρ values reveals the AT1ABR cells expressing R2579A/R2580A-ATM and C2991L-ATM were the most different while the two cell lines expressing the C2991L-ATM and R2579A/R2580A/C2991L-ATM were the most similar (Figure 4.15). C2991L-ATM cells were more similar to the parental cell line than they were to either AT1ABR-wt-ATM or AT1ABR-R2579A/R2580A-ATM cells suggesting the C2991L mutation prevents some changes in the phosphoproteome. Notably, AT1ABR- R2579A/R2580A/C2991L-ATM cells, which should have the least active ATM, were the most similar to the parental cell line. These results support our understanding of these mutations as affecting different pathways of ATM activation. Since no external DNA damaging agents were added in

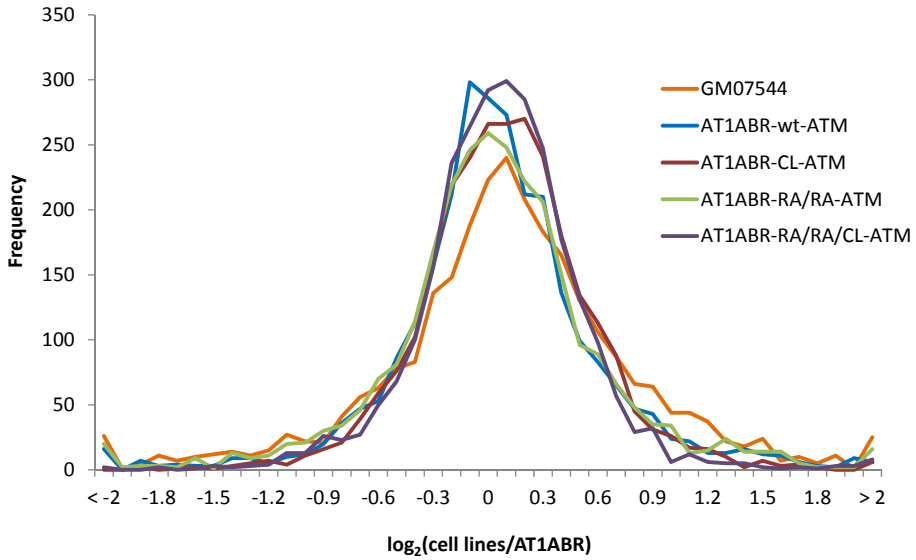

Figure 4.14 A histogram of phosphopeptide normalized values reveals overall levels of phosphorylation are similar between the cell lines.

The raw values for each cell line were normalized to the AT1ABR parental cell line and the logarithm base 2 was taken. The ATM constructs are abbreviated as follows: wt: wild-type; CL: C2991L; RA/RA: R2579A/R2580A, and RA/RA/CL: R2579A/R2580A/C2991L.

this study, the R2579A/R2580A mutations should have little effect on the activity of ATM and thus these cells will be more similar to wild-type-ATM expressing cells. On the other hand, the expression of C2991L-ATM has been shown to increase oxidative stress relative to the expression of wild-type-ATM even under conditions of normal growth [5] suggesting that ATM is activated in cells to counteract endogenous oxidative stress.

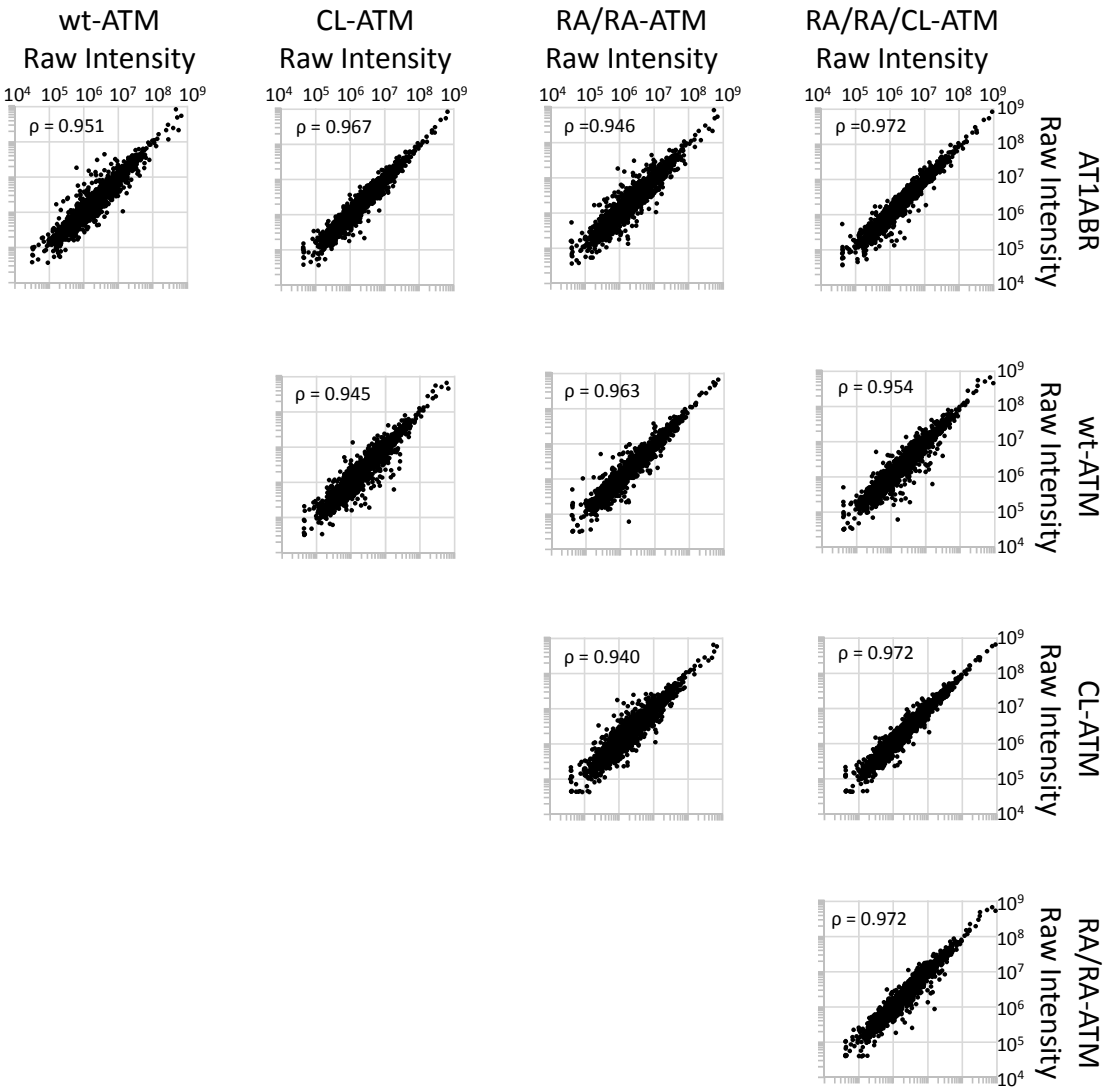

Figure 4.15 Pairwise comparisons of the phosphoproteomic raw data from AT1ABR cells with or without expression of ATM.

The raw intensity of each phosphopeptide was compared between two cell lines at a time. The cell lines and raw intensities for each graph are shown across the top and right. The Spearman's rank correlation coefficient, ρ, was calculated for each pairwise comparison and is shown. wt: wild-type; CL: C2991L; RA/RA: R2579A/R2580A, RA/RA/CL: R2579A/R2580A/C2991L.

To estimate the activities of ATM in the different cell lines, putative ATM substrates were predicted by Group-based Prediction Systems (GPS), a program which compares the 7 amino acids N-terminal and C-terminal to a phosphorylated residue with all known sites phosphorylated by a specific kinase [220]. The sequences are scored using the amino acid substitution matrix BLOSUM62 and the average value is used as the final score. The accuracy, sensitivity, and specificity vary between kinases but the false discovery rate was set at 2%. However, GPS does not limit its predictions to any certain residue in the peptide submitted so the results were curated to ensure the only predictions included were on the identified residue phosphorylated in the phosphoproteomic screen. Similar to previous phosphoproteomic experiments with enrichment for ATM substrates, I found only 53 phosphopeptides predicted to be phosphorylated by ATM under normal growth conditions [10, 11]. Of these, 35 were also predicted to be phosphorylated by one of the other PIKKs: ATR, DNAPK, or FRAP. In the remaining 18, there was a relatively stable amount of phosphorylation with AT1ABR cells expressing wildtype-ATM or C2991L-ATM as the lowest (Figure 4.16A).

Of the 53 identified direct ATM candidate proteins, twenty were previously identified in a phosphoproteomic screen by the Elledge group in peptides immunoprecipitated with antibodies to known ATM phosphorylation sites [12]. The distributions of the intensities of the putative ATM substrates are similar, suggesting there was no major effect of the C2991L or R2579A/R2580A mutations on the phosphorylation of these ATM substrates in untreated cells (Figure 4.16B).

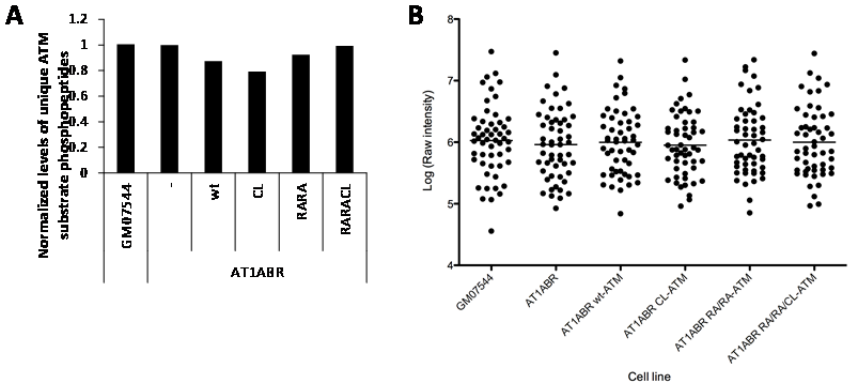

Figure 4.16 The phosphoproteome of the putative ATM substrates is not correlated with ATM protein levels and is similar among the cell lines.

(A) The raw intensities of the 18 phosphopeptides predicted to be phosphorylated by ATM and not the other PIKKs were summed and normalized to the levels in AT1ABR. (B) Grouped scatterplot of the raw intensities of all 53 putative ATM substrates with the average marked as a bar. wt: wild-type; CL: C2991L; RA/RA: R2579A/R2580A, RA/RA/CL: R2579A/R2580A/C2991L.

Analysis of the total phosphoproteome dataset by hierarchical clustering revealed a group of 315 peptides less phosphorylated in the parental AT1ABR cells and AT1ABR cells expressing ATM with the C2991L mutation, hereafter referred to as the C2991 Dependent Cluster (Figure 4.17). Only 6 of the predicted ATM substrates appear within this group. Since ATM was not the predominant kinase responsible for phosphorylating the proteins in this group, I used motif-x to extract motifs from the phosphoproteome and the C2991 Dependent Cluster to determine which kinase(s) may be phosphorylating these proteins. Nine motifs were extractedfrom the C2991 Dependent Cluster – tP, sPXK, sP, sDXE, sEXE, RXXs, sD, and sE – and the results were compared to the motifs from the whole phosphoproteome. The motifs with phosphorylated residues followed by proline or

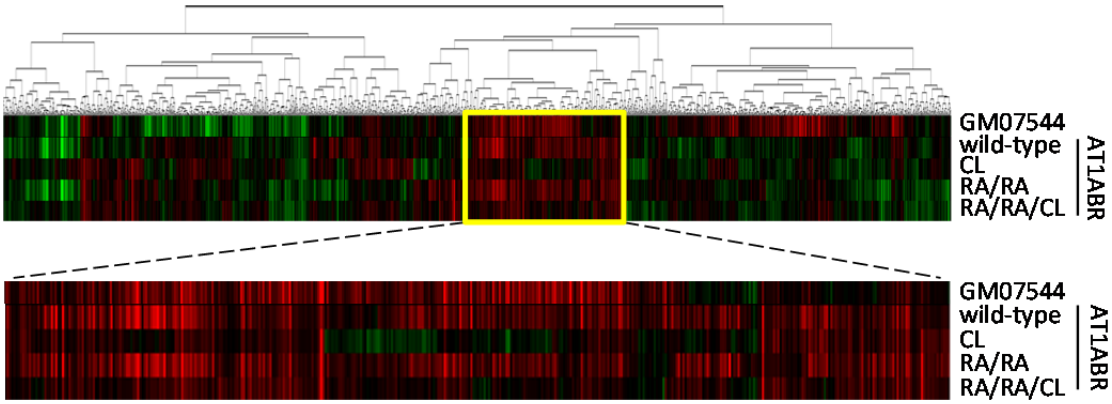

Figure 4.17 Hierarchical clustering of all the phosphopeptides reveals a cluster of phosphopeptides less phosphorylated in AT1ABR cells and AT1ABR cells expressing the C2991L mutation.

Phosphopeptide levels were normalized to the parental AT1ABR cell line. Each vertical line within a cell line is a phosphopeptide and vary from green to black to red to represent decreased, equal, and increased levels of the phosphopeptides compared to the parental AT1ABR cell line. The highlighted portion is the C2991 Dependent Cluster. wt: wild-type; CL: C2991L; RA/RA: R2579A/R2580A, RA/RA/CL: R2579A/R2580A/C2991L.

preceded three residues by an arginine showed little to no further enrichment in the C2991 Dependent Cluster (Figure 4.18). However, there was a striking enrichment for the four motifs with acidic residues following the phosphorylated residue. This motif is typical of substrates for the protein kinase CK2 but further analysis was necessary to confirm whether CK2 was specifically less active in AT1ABR cells expressing ATM with the C2991L mutation.

The two-sample Kolmogorov-Smirnov (K-S) test is a nonparametric test to determine whether two empirical distribution functions (EDFs) are from the same or separate distributions. The EDFs show the cumulative probability on the y-axis with a value less than or equal to the value on the X-axis. The K- S statistic is the

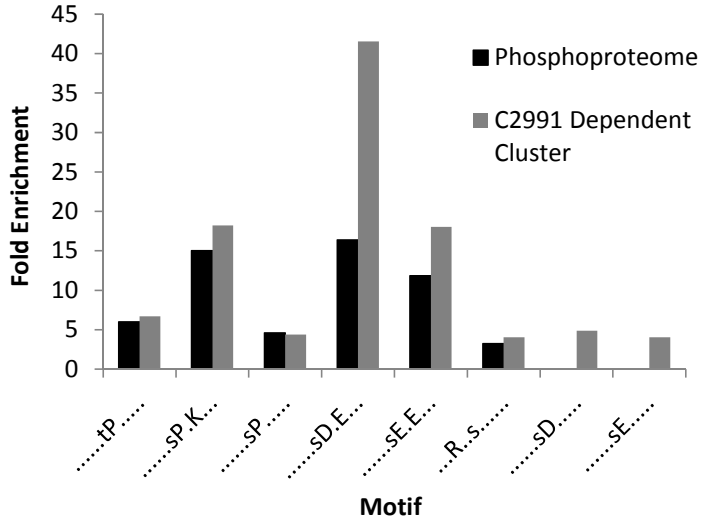

Figure 4.18 Analysis by motif-x shows an increase in enrichment of the motifs with a phosphorylation site followed by acidic residues in the C2991 Dependent Cluster.

Phosphopeptides from the phosphoproteome or the C2991 Dependent Cluster were submitted to motif-x. The sequences contained 6 residues N-terminal and C-terminal of each phosphorylation event.

largest difference between two EDFs. If the K-S statistic is above a critical value, the null hypothesis that the samples are drawn from the same distribution is rejected. Here, I used the K-S test to compare the ratios of intensities of phosphopeptides from AT1ABR cells expressing wild-type-ATM or expressing C2991L-ATM (wild-type/C2991L). If CK2 substrates are phosphorylated similarly in the AT1ABR cells expressing wild-type-ATM and C2991L-ATM, then the EDFs of the ratios of the phosphopeptides should be similar. To predict the substrates for each kinase, I analyzed the phosphopeptides in GPS. For each phosphorylation site, multiple kinases may be predicted to be responsible. These putative substrates were entered as the phosphoproteomes of the kinases and the ratios of wild-type and C2991L-

ATM expressing cells were calculated. The EDFs of the kinase phosphoproteomes and the full phosphoproteome were compared using the K-S test. A sample of the EDFs and the results from all the K-S tests are shown (Figure 4.19). The EDF of CK1 tightly overlaps the EDF of the full phosphoproteome and the K-S test has a p-value of 0.919 suggesting there is no difference in the CK1 phosphoproteome from the whole phosphoproteome (Figure 4.19A and D). However, ATM and CK2 both show a statistically significant shift to the right in their EDFs relative to the full phosphoproteome (Figures 4.19 B-D). This shift reveals the presence of more phosphopeptides with a higher wild-type/C2991L ratio demonstrating the phosphopeptides have lower intensities in the AT1ABR cells expressing C2991L-ATM. Notably, most of the other kinases are not significantly different from the full phosphoproteome (Figure 4.19D).

CK2 Activity is Reduced in the Absence of Active ATM

The holoenzyme of CK2 is a tetramer of 2 α subunits, the catalytic subunits, and 2 β subunits, the regulatory subunits (Figure 4.20A). There are two α subunits, CK2α and CK2α', and one β subunit, CK2β. The holoenzyme consists of 2 CK2β subunits bound to any combination of 2 CK2α and CK2α' subunits. To determine if the differences in the CK2 phosphoproteome were due to a change in the protein levels of the different subunits, I compared the levels of the CK2 subunits between the cell lines without the DIM proteins(Figure 4.20B). Contrary to the phosphoproteome data, the AT1ABR cell lines expressing C2991L-ATM and R2579A/R2580A/C2991L-ATM had the highest levels of expression of all three subunits. Thus the reduction in CK2 activity of AT1ABR cells expressing C2991L-ATM is not due to loss of protein.

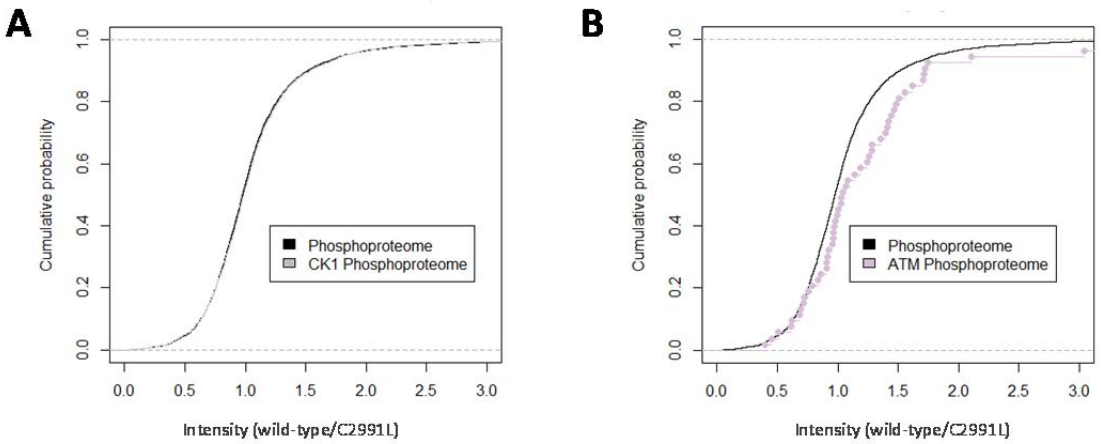

D

Kinase	Phosphopeptides	p-value
CaMK2	268	0.01331
CK2	591	0.01574
ATM	53	0.02615
DMPK	699	0.06418
DNAPK	62	0.0702
GSK3	816	0.1034
ATR	88	0.1306
IKK	295	0.1685
MAPK	695	0.1892
CDK	786	0.1956
FRAP	1323	0.3118
TK	108	0.5134
Abl	40	0.6876
RIPK	469	0.7031
RSK	535	0.8446
CK1	2068	0.9191

Figure 4.19 AT1ABR cells expressing C2991L-ATM have reduced intensities of phosphopeptides predicted to be phosphorylated by CK2 versus cells with wild-type-ATM.

Empirical cumulative distribution functions of the ratio of phosphopeptide intensities of wild-type-ATM and C2991L-ATM containing cells from (A) the phosphoproteome and the CK1 phosphoproteome, (B) the phosphoproteome and the ATM phosphoproteome, and (C) the phosphoproteome and the CK2 phosphoproteome. (D) Results from Kolmogorov-Smirnov tests. The red dotted line marks p-value = 0.05.

To determine whether there is a change in CK2 activity in the absence of ATM function, I attempted to immunoprecipitate epitope-tagged CK2 from AT1ABR cells expressing the various ATM constructs but the AT1ABR lymphoblast cells are refractory to transfection and I could not get expression. Instead, to analyze the activity of CK2 in the presence of inactive ATM, I expressed V5-tagged CK2 proteins in HEK-293T cells and left them untreated or treated them with an ATM inhibitor. The V5-tagged CK2 subunits were immunoprecipitated with V5 magnetic beads and a western blot was performed probing for V5, CK2α, and CK2β with the input and immunoprecipitated protein from each cell line (Figure 4.20C). Western blots of CK2β-V5 show a pair of bands just above 25 kDa. These separate bands could be due to post-translational modifications as CK2β is phosphorylated by the holoenzyme CK2 [131]**.** The CK2 subunits have different levels of expression in the cell lines as can be seen in the input. CK2α-V5, which had the lowest expression level, shows no pull down of endogenous CK2α' or CK2β. However, CK2α'-V5 immunoprecipitation pulls down CK2β and CK2β-V5 immunoprecipitation pulls down both CK2α and CK2α'.

To assay the kinase activity of CK2, I generated a fusion of GST and a CK2 substrate peptide, RRADDSDDDDDE. The kinase assay was first established with commercial CK2 from NEB and the incorporation of ^{32}P from ATP-γ-^{32}P was measured by PhosphorImager analysis. CK2 phosphorylated GST-CK2 substrate peptide but not GST by itself and the phosphorylation was dependent on the addition of CK2 (Figure 4.21A). The kinase assay with immunoprecipitated CK2α-V5, CK2α'-V5, and CK2β-V5 from 293T cells constitutively expressing these proteins was performed with the proteins bound to the beads (Figure 4.21B). In the CK2β-V5

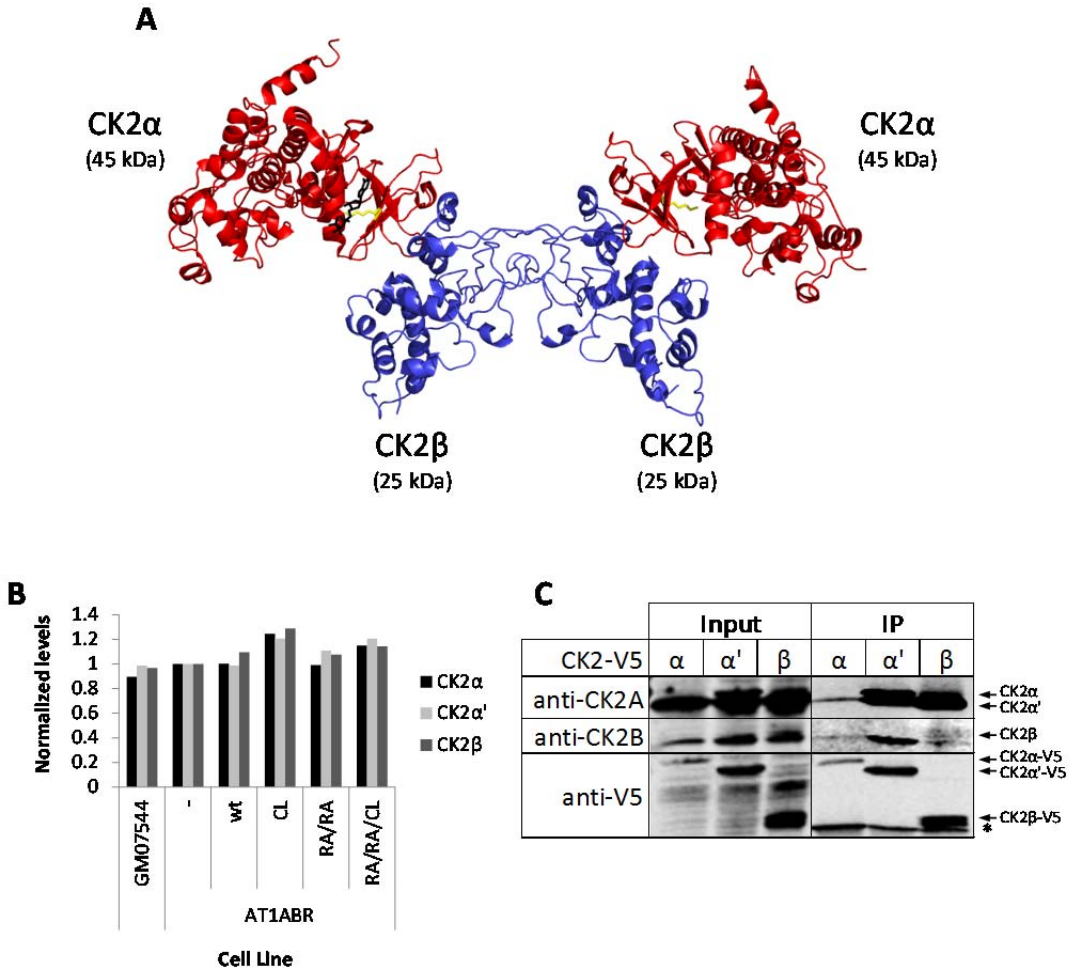

Figure 4.20 CK2 subunits are upregulated in mutant ATM expressing cells and co-immunoprecipitate other proteins from the holoenzyme.

(A) Structure of the CK2 holoenzyme ($\alpha_2\beta_2$) (PDB code: 1JWH). The regulatory β subunits form a dimer and each bind an α or α' subunit to form the holoenzyme. Sections are colored as follows: red, CK2α/a'; yellow, K68-CK2α/K69-CK2α'; blue, CK2β; black, AMPPNP. (B) CK2 levels were recalculated as a fraction of the entire proteome without the DIM group and then normalized to the levels in the parental AT1ABR cell line. wt: wild-type; CL: C2991L; RA/RA: R2579A/R2580A, RA/RA/CL: R2579A/R2580A/C2991L. (C) Lysates (20 μg) from 293T cells stably expressing CK2α-V5, CK2α'-V5, or CK2β-V5 were immunoprecipitated with magnetic anti-V5 beads and a western blot was performed with the input and immunoprecipitated protein and the indicated antibodies. * shows mouse antibody from immunoprecipitation.

immunoprecipitation, the endogenous CK2α and CK2α' subunits are pulled down and phosphorylate the GST-CK2 substrate peptide. Immunoprecipitations using any of the three subunits are able to phosphorylate GST-CK2 substrate peptide. The overall activity corresponded to the levels of protein expressed in the cells as seen in Figure 4.20B. Notably, immunoprecipitation of a previously identified kinase-dead mutant of CK2α'-V5 (K69M) showed little phosphorylation of GST-CK2 substrate peptide demonstrating the kinase activity is specifically from immunoprecipitated CK2 (Figure 4.21C) [221].

The established in vitro kinase assay was then used to compare the activities of CK2 in the presence or absence of ATM kinase activity. For this assay, 293T cells expressing CK2β-V5 were used so that both endogenous CK2α and CK2α' would be the sources of any kinase activity. 293T cells expressing CK2β-V5 were treated with 10 μM Ku-55933, an ATM inhibitor, or an equivalent amount of DMSO for 16 hours. The lysates were immunoprecipitated with V5 beads and the levels of CK2 kinase activity were assessed during an in vitro time course. The activity of immunoprecipitated CK2 increased over time in the in vitro assay, for both the untreated cells and cells exposed to ATM inhibitor (Figure 4.22A). The CK2 isolated from cells treated with inhibitor show decreased levels of phosphorylated GST-CK2 substrate peptide relative to untreated cells, but we also observed decreased levels of CK2 recovered from inhibitor-treated cells. When the kinase activity was normalized to the level of CK2β-V5 immunoprecipitated, there was little difference in the specific activity of the kinase with or without ATM inhibitor (Figure 4.22B). The decrease in CK2β-V5 immunoprecipitated was similar between multiple experiments (Figure 4.22C). This effect was reproducible and occurred despite a

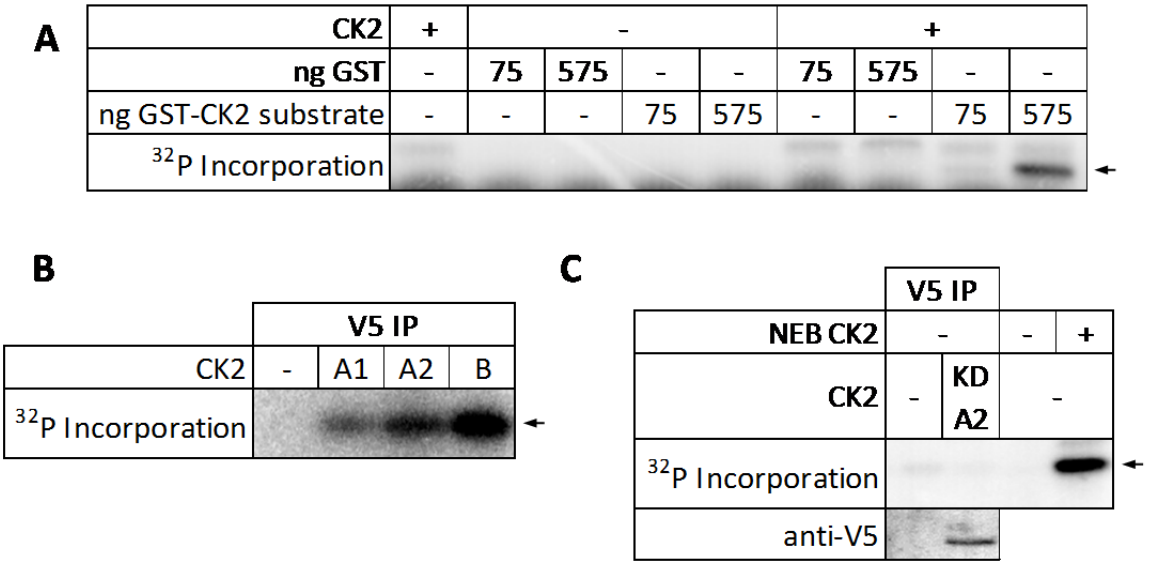

Figure 4.21 Immunoprecipitated CK2 subunits phosphorylate a CK2 substrate in vitro and activity is dependent on CK2 catalytic activity.

(A) CK2 (1 µl) was incubated in 1X CK2 buffer with 1.67 mM ATP, 5 fCi ATP-γ-^{32}P , and the amounts of each substrate shown for 1 hour. The reactions were stopped by addition of 5X SDS loading buffer and run on a SDS-PAGE gel. The gel was dried and a PhosphorImager Screen was exposed overnight and visualized with a Typhoon Imager. The arrow shows the position of the GST-CK2 substrate. (B) Lysate (20 µg) from 293T cells or 293T cells stably expressing CK2α-V5, CK2α'-V5, or CK2β-V5 were immunoprecipitated with magnetic anti-V5 beads and a kinase assay was performed as in (A) on the beads with 1150 µg GST-CK2 substrate. (C) Lysate (40 µg) from 293T cells or 293T cells stably expressing kinase dead CK2α'-V5 immunoprecipitated with magnetic anti-V5 beads and the beads were split for the kinase assay as performed in (B)and western blot analysis.

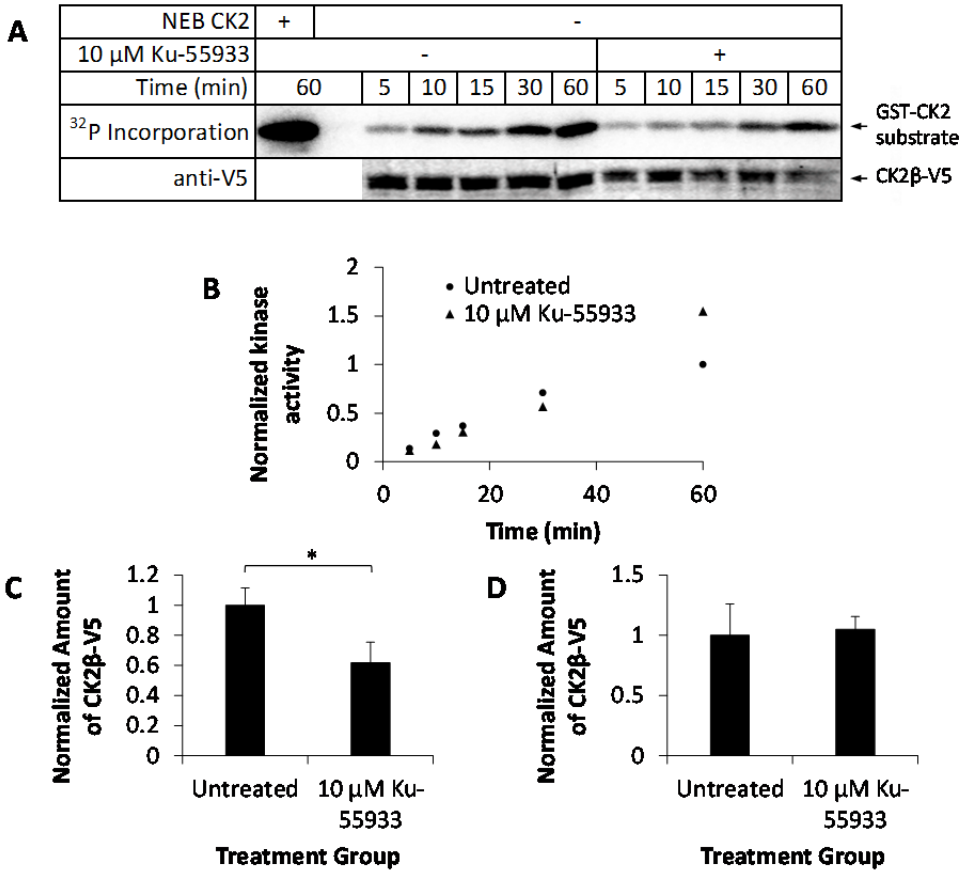

Figure 4.22 ATM inhibition affects CK2β-V5 immunoprecipitation but not the activity of CK2β-V5.

(A) 293T cells stably expressing CK2β-V5 were treated with 10 µM Ku-55933 or an equivalent amount of DMSO for 16 hours and then lysed with 1X Cell Lysis Buffer (Cell Signaling Technology). Lysate (12.5 µg) from each sample was immunoprecipitated with magnetic anti-V5 beads and split into 5 tubes. Kinase reactions were performed as in Figure 4.21 and stopped at the specified time points. The reactions were run on a gel, transferred to PVDF, probed for V5 levels by western blot, and exposed to a PhosphorImager Screen. (B) Quantitation of the results from (A) with kinase activity normalized to protein level. (C) Normalized amount of immunoprecipitated CK2β-V5 from (A) with the levels of CK2β-V5 in untreated cells defined as 1. (D) Quantitation by western blot of CK2β-V5 in lysates from untreated and 10 µM Ku-55933 treated 293T-CK2β-V5 cells. Levels were normalized to KAP1 and the average level of CK2β-V5 in untreated cells was defined as 1. Averages and standard deviations were calculated from two independent experiments and used for t-tests. P-values: * < 0.05

similar amount of CK2β-V5 in the input lysates of the untreated and Ku-55933 treated cells (Figure 4.22D). Thus ATM inhibition reduces the efficiency of CK2β immunoprecipitation and corresponding levels of CK2 activity.

CK2A' AND CK2B AGGREGATE IN CELLS WITH INACTIVE ATM

CK2 has been shown to undergo aggregation in vitro and in cells [160-164]. This aggregation may prevent CK2β-V5 immunoprecipitation and explain the difference in the in vitro kinase assay in inhibitor-treated cells. To test this hypothesis, I performed a sucrose gradient to compare the migration of CK2β-V5 from 293T cells with or without treatment by 10 μM Ku-55933. CK2β-V5 from untreated cells shows a primary peak centered around fractions 6 and 7 which is similar to CK2β-V5 from cells treated with 10 μM Ku-55933 (Figure 4.23A). Fractions 6 and 7 correspond to ~40 kDa while 8 and 9 correspond to ~240 suggesting fractions 6-10 range from a dimer of CK2β-V5 to the holoenzyme consisting of two CK2A subunits and two CK2β-V5 subunits. Although the peaks occur in fractions 6 and 7 with or without Ku-55933, when quantitated and normalized across all fractions there is a shift in the percentage of CK2β-V5 to later fractions in the presence of ATM inhibitor, suggesting there is an increased amount of aggregation occurring in the absence of ATM activity (Figure 4.23B). However, the lysis was performed in the presence of detergent (1% Triton X-100) and pelleted at high speeds so some aggregates may have been lost.

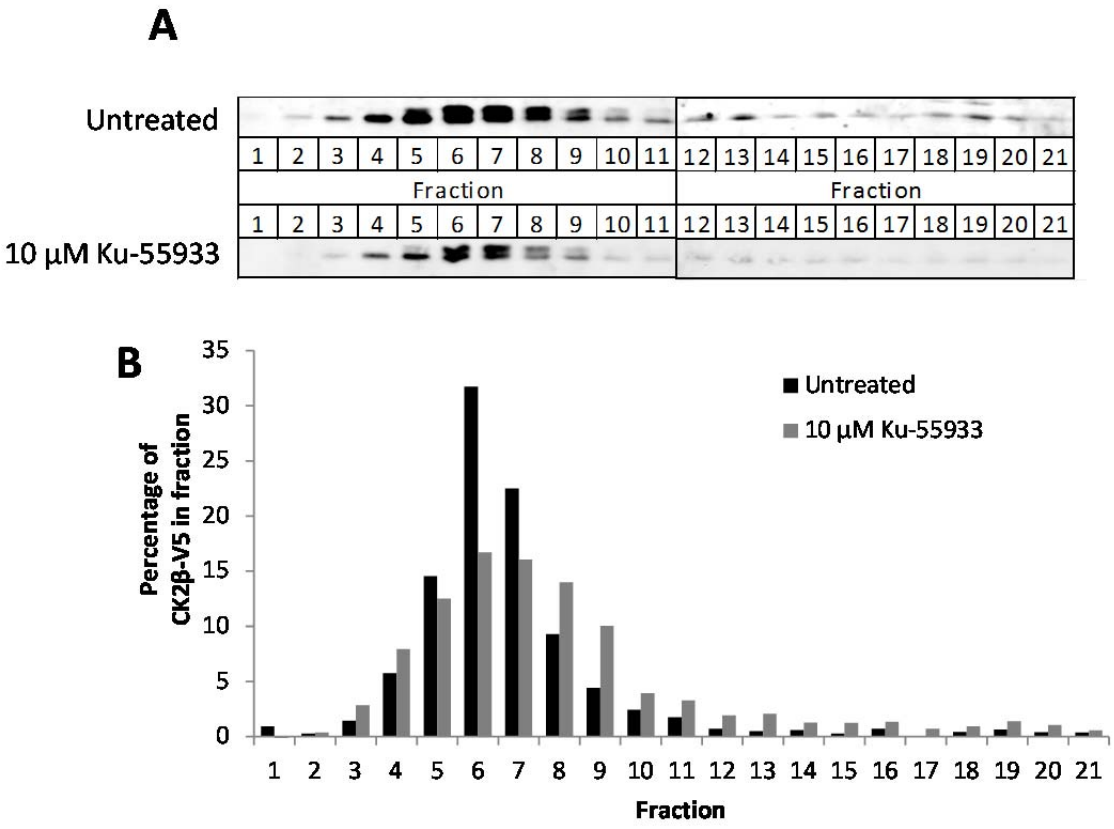

Figure 4.23 CK2β-V5 shifts to later fractions after cellular treatment with ATM inhibitor.

(A) Lysates from 293T cells were treated with 10 µM Ku-55933 or an equivalent amount of DMSO and lysed. Equal amounts of the lysates (10 µg) were added to the top of identical sucrose gradients consisting of 1 ml layers of 5-50% sucrose, 150 mM NaCl, and 20 mM Tris, pH 7.4 in 5% increments. A western blot was performed on the fractions with anti-V5. (B) Quantitation of results from (A).

To reduce the loss of any aggregates during sample processing, a gentle lysis buffer without detergent was used and the lysates were not pelleted. Lysates from HEK-293T cells expressing CK2α, CK2α', or CK2β treated with or without ATM inhibitor were run on a sucrose gradient as in Figure 4.23 and the fractions were analyzed by western blot and quantitated (Figure 4.24). CK2α-V5 shows very little response to ATM inhibition. However, both CK2α'-V5 and CK2β-V5 show a dramatic shift to the denser fractions, including a doubling of the amount in the last fraction (Figure 4.24B-C). The same lysis and sucrose gradient procedures were used on lysates from AT1ABR cells expressing wild-type-ATM or C2991L-ATM (Figure 4.25). Although CK2α showed similar distributions in both cell lines, CK2β again showed a marked shift, most evident in the last fraction. CK2α' was not visible in these conditions. This is similar to previously seen aggregation and may provide an explanation for the reduction in overall CK2 activity in the presence of ATM with the C2991L mutation.

SUMMARY

ATM is activated by oxidative stress in the absence of DNA damage and affects many cellular processes beyond the DNA repair pathway [4]. Here, I found 8% of the proteome was vastly reduced in cells expressing ATM with separation-of-function mutations. Analysis of a subset of these proteins revealed that some exhibit changes in their sedimentation rates in sucrose gradients with ATM inhibition, potentially from aggregation. ATM has been shown previously to phosphorylate multiple heat shock proteins [12]. Phosphorylation of Hsp27 promotes its interaction with glucose-6-phosphate dehydrogenase and increases the metabolic flow through the

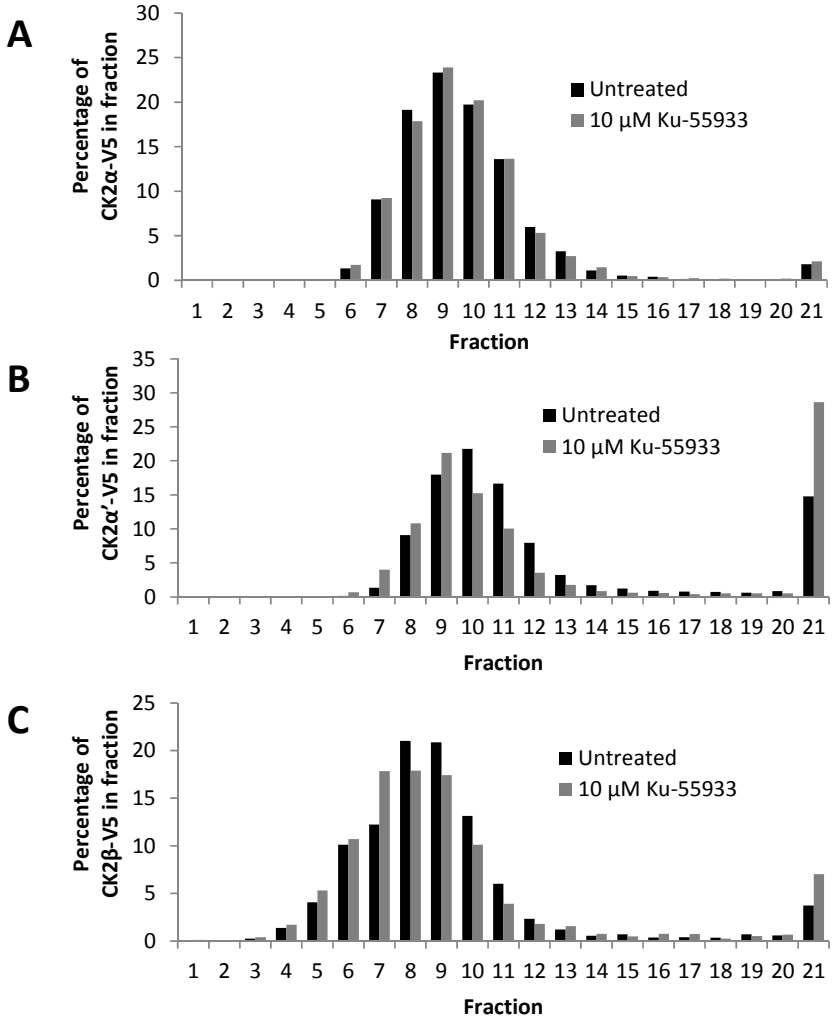

Figure 4.24 Gentle lysis reveals CK2α' and CK2β aggregation in 293T cells treated with ATM inhibitor.

(A) 293T cells expressing CK2α-V5 were treated with 10 μM Ku-55933 or an equivalent amount of DMSO for 16 hours, harvested, and lysed in the absence of detergent. 1 mg of lysate in 500 μl lysis buffer total was added to the top of a sucrose gradient made with 1 ml layers of 50% to 5% sucrose in 5% increments. After ultracentrifugation, 500 μl fractions were collected and analyzed by western blot. (B) Cell treatment and sucrose gradient as in (A) with 293T cells expressing CK2α'-V5. (C) Cell treatment and sucrose gradient as in (A) with 293T cells expressing CK2β-V5.

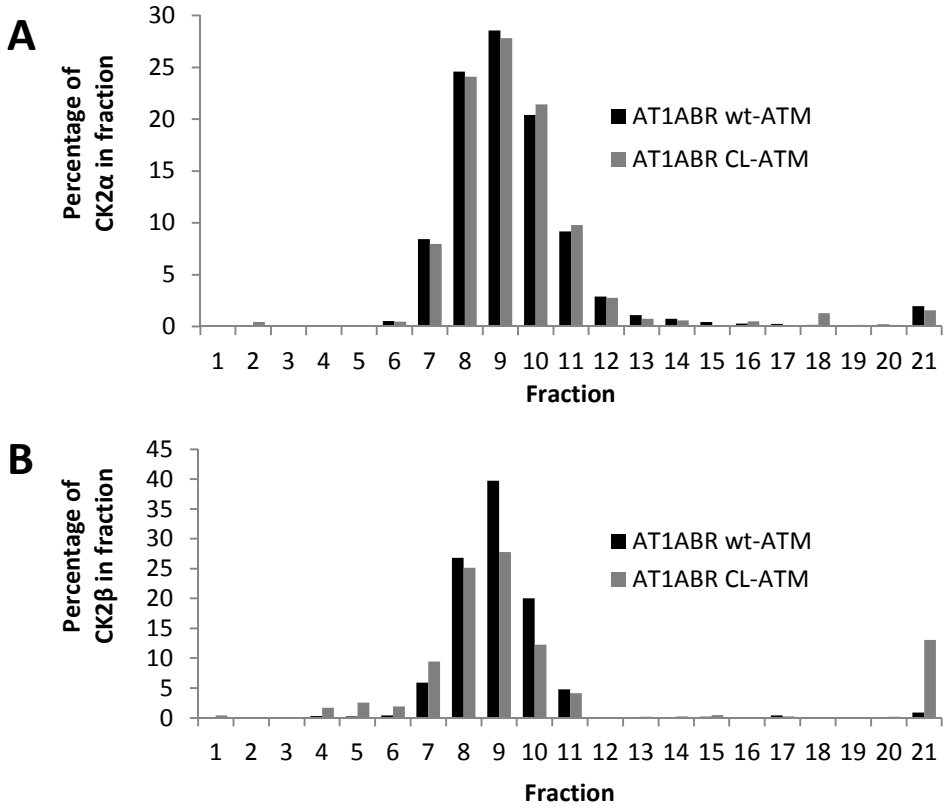

Figure 4.25 Gentle lysis shows CK2β shifts to higher molecular weight complexes in AT1ABR cells expressing C2991L-ATM.

(A) Induced AT1ABR cells expressing wild-type- or C2991L-ATM were harvested and lysed in the absence of detergent. Lysate (1 mg) in 500 µl lysis buffer total was added to the top of a sucrose gradient made with 1 ml layers of 50% to 5% sucrose in 5% increments. After ultracentrifugation, 500 µl fractions were collected and 16 µl each fraction was analyzed by western blot for CK2a (45 kDa), (B) Sucrose gradient and western blot performed as in (A) with 2 mg lysate and 120 µl each fraction probed for CK2β (25 kDa). Quantitation was performed on the Licor system using Image Studio Ver 4.0.

pentose phosphate pathway [222]. It will be interesting to determine how this and other phosphorylation events affect the activity or substrates of these chaperones.

ATM has been shown to be activated in cells over-expressing a form of GFP that aggregates [223]. Similarly, known ATM substrates were phosphorylated in fibroblasts from patients with Huntington's disease, a neurodegenerative disease associated with aggregation of the huntington protein. This evidence of ATM activation during aggregation suggests that these cellular states are also associated with oxidative stress and that ATM may aid in the clearance of aggregates.

Although some proteins appear to undergo aggregation, this does not fully explain the differences between the AT1ABR cells with wild-type-ATM versus C2991L-ATM. The increased oxidative stress in C2991L-ATM cells may be causing oxidative modifications on the proteins that prevent their identification by mass spectrometry. Interestingly, two of the eight known proteins involved in ferroptosis – glutathione peroxidase 4, and acyl-CoA synthetase family member 2 – were in the DIM group. Ferroptosis is an iron-dependent form of cell death that is associated with large amounts of oxidative damage in the cell [224]. Here, oxidative damage to proteins may be modifying them beyond recognition. Notably, some of the proteins in the DIM group had some peptides that showed normal levels, but drastically reduced levels of other peptides, suggesting site-specific modifications.

Proteins in the DIM group were enriched for localization to the mitochondria. Previously, cells lacking functional ATM were shown to have defective mitochondria and increased ROS levels [205]. My results show separation-of-function mutations in either pathway affect the levels of proteins involved in mitochondrial homeostasis. Notably, AT1ABR cells expressing wild-type-ATM had large increases

in mitochondrial mass relative to the parental cell line. C2991L-ATM expressing cells had an intermediate level of mitochondrial mass suggesting both activation pathways of ATM are important for mitochondrial health. The ROS levels in both wild-type- and C2991L-ATM expressing cells were increased relative to the parental AT1ABR cell line. Notably, our lab has previously characterized the long-term ROS levels of a MEF cell line with an inducible ATM knockout. Initially, ATM knockout causes an increase in ROS but over time the cells adapt to the absence of ATM and lower their ROS levels below the cells heterozygous for ATM (S Zhang, unpublished observations). This adaptation could include an increased induction of SLC7A11 as was seen here.

Examination of the phosphoproteomes from all six cell lines revealed a group of 315 phosphopeptides that were lower in the cells expressing C2991L- or R2579A/R2580A/C2991L-ATM. This pattern suggests that a defect in ATM activation by oxidative stress is the cause. Motif analysis of the phosphopeptides revealed an enrichment of sites predicted to be phosphorylated by CK2. A Kolmogorov-Smirnov analysis of the levels of these phosphopeptides in wild-type-ATM and C2991L-ATM containing AT1ABR cells relative to the entire phosphoproteome again showed a statistically significant lower amount of phosphorylation in C2991L-ATM AT1ABR cells.

Further analysis with 293T cells expressing V5-tagged CK2β showed an increased portion of CK2 was unable to be immunoprecipitated after treatment with an ATM inhibitor. Sucrose gradients of lysates from these cells revealed this coincided with a shift of CK2β-V5 to denser fractions. Similarly, AT1ABR cells expressing C2991L-ATM showed a shift of CK2β corresponding to changes in

aggregation state. However, CK2α was not shown to undergo this change suggesting the components of the CK2 holoenzyme may be differentially affected.

Substrates of the calcium/calmodulin-dependent protein kinase II (CaMKII) were also found to be less phosphorylated in AT1ABR cells expressing C2991L-ATM. Interestingly, experiments in U2OS cells with V5-CaMKIIδ showed ATM inhibition affects immunoprecipitation and not kinase activity, similar to CK2 (data not shown). Additionally, V5-CaMKIIδ shifted to more dense fractions upon ATM inhibition in these cells. This suggests changes in aggregation state induced by ATM inhibition or C2991L-ATM expression may affect the activity of multiple kinases through a type of auto-sequestration.

CHAPTER 5: DISCUSSION

THE CANONICAL ROLE OF ATM

The role of ATM in the cellular response to DNA double-strand breaks has been well described [4]. ATM is activated minutes after a DSB and phosphorylates hundreds of substrates to halt the cell cycle, initiate DNA repair, and regulate gene transcription [4]. In vitro studies and cellular assays have demonstrated this pathway of ATM activation requires the protein complex Mre11/Rad50/Nbs1 (MRN) [8, 33, 34, 71, 74]. Patients with hypomorphic mutations in Mre11, Nbs1, and Rad50 lead to Ataxia-telangiectasia-like disorder, Nijmegen breakage syndrome, and Nijmegen breakage syndrome-like disorder [73, 75, 76]. Patients with these diseases manifest some of the symptoms characteristic of A-T such as chromosomal instability and sensitivity to ionizing radiation but have slower progressing or absent cerebellar ataxia and ocular telangiectasia.

MRN REQUIREMENTS FOR DSB ACTIVATION OF ATM

Some of the enzymatic activities and domains of the components of MRN required for activation of ATM have been uncovered. Expression of a nuclease-deficient Mre11 in mouse cells demonstrated the Mre11 nuclease activity is dispensable for ATM activation but necessary for DNA repair [191]. In vitro kinase assays in the absence of Mre11 nuclease activity also stimulated ATM activity [34]. The C-terminus of Nbs1 is necessary for the recruitment of ATM to DSBs [55], and the coiled-coils of Rad50 were also shown to be important as deletions within this domain reduce ATM activation [225]. Previously it was shown that a mutation in the

Walker A motif of Rad50 that abrogates ATP-dependent functions of Rad50 was unable to activate ATM [34]. However, it was unclear from this mutant whether ATP binding alone or binding followed by hydrolysis was necessary for the activation of ATM.

Mre11/Rad50 Complexes Undergo ATP-Dependent Conformational Changes

Recent structural analyses of the catalytic heads of archaeal and bacterial Mre11 and Rad50 in the presence or absence of various nucleotides have demonstrated a large conformational shift upon ATP binding [65, 66, 85]. In the absence of ATP, Rad50 is in an "open" configuration with Mre11 bridging the catalytic heads (Figure 5.1) [85]. In the presence of ATP, the Rad50 head domains come together and Mre11 is flipped relative to the Rad50 dimer to form the "closed" conformation [66]. Several functions of MRN are dependent on ATP binding and/or hydrolysis including DNA end-binding, DNA tethering, and resection (Figure 5.1) [70]. Recent studies have shown the nuclease activity in the MR complex of *Pyrococcus furiosus* requires transitioning from the "closed" form back to the "open" form and the enzyme in the closed state does not exhibit nuclease activity [62].

ATP-Driven Conformational Changes of MRN Control ATM Activation

Here, I showed that ATP binding, but not hydrolysis, by Rad50 was required for ATM activation by the MRN complex. This agrees with previous results showing the preference of DNA ends for the ATP-bound form of MRN, the required DNA substrate for ATM activation. Notably, the ATP-bound form of Rad50 is long-lived as it hydrolyzes 0.1 ATP molecules/minute [174, 192]. ATP binding and hydrolysis may act as a molecular switch to trigger new activities within the complex instead of

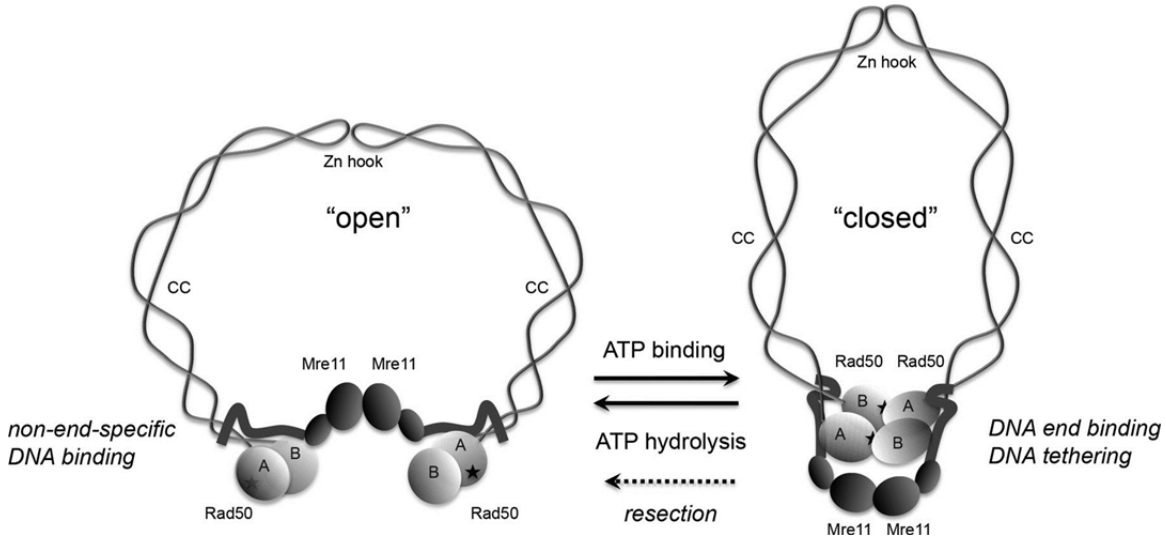

Figure 5.1 Schematic model of MRN in the absence (open) or presence of ATP (closed).

Rad50 is shown as light gray globular domains containing Walker A (A) and Walker B (B) motifs connected by intramolecular, antiparallel coiled-coils (CC), that attach to each other through the zinc hook motifs (Zn hook). Stars indicate the approximate positions of the ATP-binding residues in Rad50. Mre11 is shown as dark gray globular domains representing the nuclease/dimerization domain and the capping domain, connected to the linker that binds to the coiled-coils of Rad50. The closed state is associated with a higher affinity for DNA ends and with DNA tethering, while the movement from the closed to the open state is required for Mre11 nuclease activity and promotion of resection. The zinc hook is shown attached here, but the complex has also been observed with hooks unattached, both in solution and bound to DNA. This research was originally published in in Journal of Biological Chemistry. Lee JH, Mand MR, Deshpande RA, Kinoshita E, Yang SH, Wyman C, Paull TT. Ataxia Telangiectasia-Mutated (ATM) Kinase Activity Is Regulated by ATP-driven Conformational Changes in the Mre11/Rad50/Nbs1 (MRN) Complex. Journal of Biological Chemistry. 2013; 288:12840-12851. © the American Society for Biochemistry and Molecular Biology.

the normal function of ATP as an energy source. After binding ATP, MRN functions in DNA end-binding, DNA tethering, and ATM activation. Upon ATP hydrolysis, the nuclease activity of MRN is initiated and it binds DNA non-specifically [62]. The conformational and functional changes in MRN upon ATP binding and subsequent hydrolysis allow MRN to be temporally regulated to perform distinct functions.

NON-CANONICAL ROLES OF ATM IN CELLULAR HOMEOSTASIS

ATM has many roles in addition to its canonical role in the cellular response to DNA double-strand breaks. A-T patients show hypersensitivity to ionizing radiation consistent with the deficiency in DSB repair, but other symptoms such as cerebellar degeneration, ocular telangiectasia, and diabetes seem unrelated to this dysfunction [205]. A-T cells also display phenotypes that appear unconnected to the DNA repair deficiency including defective mitochondria, changes in insulin signaling, and increased oxidative stress [4]. ATM has been shown to phosphorylate substrates in the absence of DNA damage in response to hypoxia [6], hyperthermia [7], mitosis [9], and oxidative stress [5, 226, 227]. These other ATM-activating conditions may explain some of the other symptoms of A-T.

To more completely address the other pathways affected by ATM, I compared the proteomes and phosphoproteomes of lymphoblasts from a healthy person, A-T lymphoblasts, and A-T lymphoblasts re-expressing various ATM constructs. Separation-of-function mutations that prevent in vitro activation of ATM by DSBs (R2579A/R2580A-ATM), oxidative stress (C2991L-ATM), or both (R2579A/R2580A/C2991L-ATM) were used to distinguish the effect each pathway has on ATM downstream effects [5].

The proteomes in cells expressing any of the mutant ATM proteins underwent an apparent loss of many proteins. This *D*own *I*n *M*utants (DIM) group of 362 proteins had significantly reduced spectral counts in the LC-MS/MS. However, western blotting of a subset of this group revealed similar levels of protein between wild-type- and C2991L-ATM expressing cells, suggesting the total protein levels were the same but the proteins were not being identified during LC-MS/MS. Analysis at the peptide level showed some of these proteins had peptides that were systemically lower while other proteins had only a small subset of peptides that were lower. I investigated several of the proteins with systematic reductions in peptide levels and found these exhibited changes in their sedimentation coefficients in sucrose gradients corresponding to large increases in molecular weight or aggregation. These proteins may form aggregates after expression of ATM deficient in one or both of the activation pathways. ACLY, a protein that showed lower levels of only some of its peptides, did not have a shift in the sucrose gradient in AT1ABR cells expressing C2991L-ATM. It is also possible that the peptides with lower levels from the other DIM proteins may be due to oxidative modifications that prevent identification by LC-MS/MS. We are continuing to characterize the modifications of these proteins in lysates from the AT1ABR cells and particularly from the last fraction of the sucrose gradients.

The cerebellar neurodegeneration in A-T may be partially explained by protein aggregation, which is a common occurrence in neurodegenerative diseases [228]. Notably, a combination of increased oxidative stress, chaperone dysfunction, and reduced ability to clear aggregates through autophagy are thought to be responsible for protein aggregation [228, 229]. ATM may play in role in all three

mechanisms for managing protein aggregation (Figure 5.2). Oxidative stress activates ATM and prevention of this activation leads to increased oxidative stress [5]. Active ATM increases the production of the antioxidant NADPH through activation of the pentose phosphate pathway [222]. Promotion of the pentose phosphate pathway by ATM occurs through phosphorylation of the protein chaperone Hsp27, which then binds and stimulates G6PD [222]. Additionally, multiple heat shock proteins important for protein folding and chaperone-mediated autophagy have been identified in screens for ATM substrates [11, 12]. Furthermore, ATM itself co-purifies with a chaperone (unpublished observations). ATM also activates autophagy through the phosphorylation of LKB, which activates a pathway leading to stimulation of TSC2 [14]. TSC2 is a negative regulator of the autophagy-suppressing protein mTORC1. Notably, inhibition of mTORC1 in A-T cells with rapamycin reduced the levels of oxidative stress, suggesting that unregulated mTORC1 is at least partially responsible for changes in ROS [14]. In the absence of ATM kinase activity, inhibition of autophagy by mTORC1 may prevent the normal clearance of aggregates. Notably, expression of a polyglutamine-expanded protein induced activation of ATM through both oxidative stress and DNA damage, directly tying both activation pathways to protein aggregate clearance [223]. Thus all three methods of managing protein aggregation may be compromised in cells expressing mutant ATM.

The proteins in the DIM group were enriched for mitochondrial proteins and further analysis demonstrated increased oxidative stress and reduced mitochondrial mass in cells expressing C2991L-ATM relative to wild-type-ATM. Oxidative modification or changes in the aggregation state of these proteins could

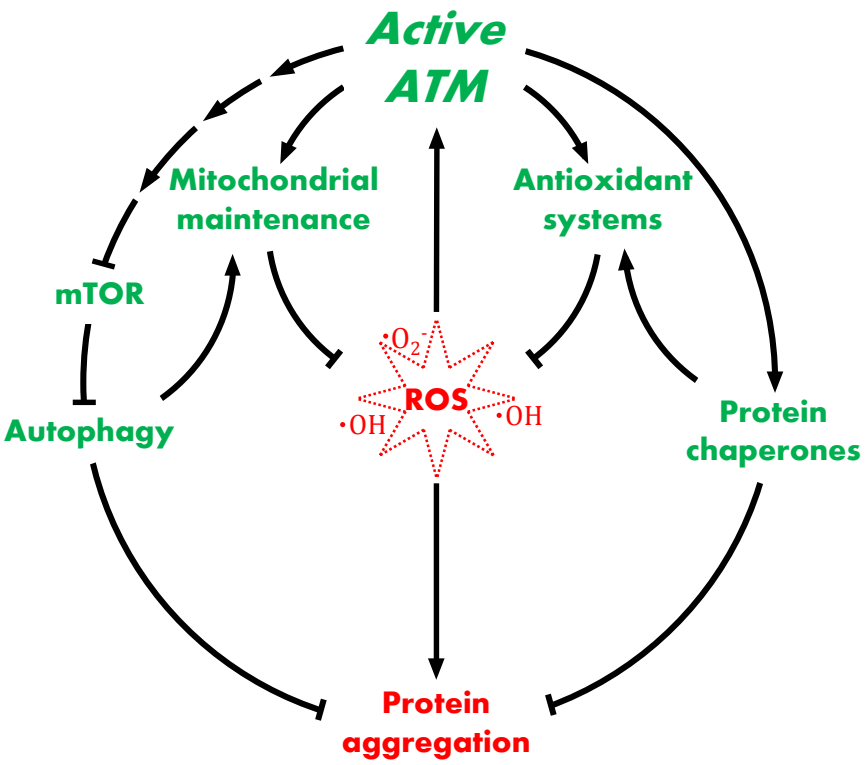

Figure 5.2 Model of ATM-mediated prevention of aggregation.

Multiple pathways downstream of ATM reduce oxidative stress and protein aggregation.

potentially explain the defects seen in mitochondria from A-T cells. Furthermore, the general chaperone defect will be interesting to pursue. Future experiments include the identification of the binding partners of the heat shock proteins in various conditions with or without ATM and the characterization of the importance of the S/TQ sites in chaperone function.

I also compared the phosphoproteomes of the normal lymphoblasts, A-T cells, and A-T cells expressing ATM. There were few putative ATM substrate

phosphopeptides (pS/pTQ) identified in the screen and these had little differences in their levels. However, there was a deficiency in the phosphorylation of putative CK2 substrates in cells expressing ATM with the C2991L mutation. There was no change in the levels of CK2α or CK2β by western blotting but under gentle lysis conditions a portion of CK2β pelleted in a sucrose gradient suggesting formation of aggregates. Similarly, CK2β-V5 from cells treated with an ATM inhibitor showed a shift in the sucrose gradient similar to C2991L-ATM expressing AT1ABR cells. These results suggest a similar mechanism of aggregation can cause changes in the phosphoproteome of A-T cells unrelated to the known downstream kinase targets of ATM.

CK2 interacts with the protein chaperone system in cells. HSP90 binding has been shown to prevent CK2 aggregation and increase its kinase activity [230]. Interestingly, CK2 has been shown to phosphorylate HSP90 and its co-chaperone cdc37 [231]. While CK2 phosphorylation of HSP90 appears to attenuate its activity, phosphorylation of cdc37 increases its binding to multiple kinases [231, 232]. CK2 also interacts with and is activated by HSPA1A (HSP72) [233]. In addition, CK2 can aid in the clearance of misfolded and ubiquitinated proteins through phosphorylation of HDAC6 to activate its deacetylase activity [234]. Thus, there could be a feedback loop whereby aggregation of CK2 reduces its kinase activity, HDAC6 is less active, and more aggregation occurs. Furthermore, CK2α has been shown to be carbonylated in the presence of oxidative stress [157]. There may be more modifications of CK2 in A-T cells that affect its activity and these are currently being explored.

DETRIMENTAL EFFECTS OF THE EXPRESSION OF INACTIVE ATM

The inhibition of ATM kinase activity has been shown to have effects that are distinct from the absence of ATM protein. White et al. demonstrated a loss of sister chromatid exchange in cells with wild-type ATM after treatment with an ATM inhibitor [235]. Notably, A-T cells had levels of sister chromatid exchange similar to wild-type cells and the addition of ATM inhibitor to A-T cells had no effect, so the presence of inactive ATM prevented sister chromatid exchange. Similarly, Gamper et al. found ATM inhibition, but not ATM depletion, decreases DNA synthesis through an interaction with PCNA [236]. The disparity is even more pronounced in mice as ATM knockout mice recapitulate some of the symptoms of A-T but the expression of kinase-dead ATM causes embryonic lethality [22, 237]. In my studies, in the absence of exogenous stress stimuli, inactivating mutations in ATM appear to have dominant negative effects, including apparent changes in the aggregation state of some proteins.

CONCLUDING REMARKS

The studies described here provide insights into the nature of ATM activation by MRN as well as the cellular effects of ATM separation-of-function mutations in the normal cellular environment. The activation of ATM by MRN in the presence of DSBs has been carefully analyzed in vitro to show the requirement of ATP binding by MRN for ATM activation. In the normal cellular environment, the separation-of-function mutations in ATM prevented the identification of a large number of proteins by LC-MS/MS. Although the proteins were present in similar levels in the lysate, the loss of LC-MS/MS identification was accompanied by a shift in the sedimentation rates of some of these proteins suggestive of aggregation. The

proteins from this group may also have oxidative modifications that prevent their identification by LC-MS/MS. In the phosphoproteome, phosphopeptides predicted to be phosphorylated by CK2 were shown to have lower levels in cells expressing ATM with the C2991L mutation. This was also accompanied by a shift in the sedimentation rates of the CK2α' and CK2β subunits similar to those seen in the proteome. Together these studies further characterize the mechanism of ATM activation by DSBs and suggest ATM helps prevent aggregation in the absence of exogenous stress.

REFERENCES

1. Kurz, E.U. and S.P. Lees-Miller, *DNA damage-induced activation of ATM and ATM-dependent signaling pathways.* DNA Repair, 2004. **3**(8-9): p. 889-900.
2. van Gent, D.C. and M. van der Burg, *Non-homologous end-joining, a sticky affair.* Oncogene, 2007. **26**(56): p. 7731-40.
3. Symington, L.S. and J. Gautier, *Double-Strand Break End Resection and Repair Pathway Choice.* Annual Review of Genetics, 2011. **45**(1): p. 247-271.
4. Shiloh, Y. and Y. Ziv, *The ATM protein kinase: regulating the cellular response to genotoxic stress, and more.* Nat Rev Mol Cell Biol, 2013. **14**(4): p. 197-210.
5. Guo, Z., et al., *ATM Activation by Oxidative Stress.* Science, 2010. **330**(6003): p. 517-521.
6. Bencokova, Z., et al., *ATM Activation and Signaling under Hypoxic Conditions.* Mol. Cell. Biol., 2009. **29**(2): p. 526-537.
7. Hunt, C.R., et al., *Hyperthermia activates a subset of ataxia-telangiectasia mutated effectors independent of DNA strand breaks and heat shock protein 70 status.* Cancer Res, 2007. **67**(7): p. 3010-7.
8. Bakkenist, C.J. and M.B. Kastan, *DNA damage activates ATM through intermolecular autophosphorylation and dimer dissociation.* Nature, 2003. **421**(6922): p. 499-506.
9. Yang, C., et al., *Aurora-B mediated ATM serine 1403 phosphorylation is required for mitotic ATM activation and the spindle checkpoint.* Mol Cell, 2011. **44**(4): p. 597-608.
10. Bennetzen, M.V., et al., *Site-specific Phosphorylation Dynamics of the Nuclear Proteome during the DNA Damage Response.* Molecular & Cellular Proteomics, 2010. **9**(6): p. 1314-1323.
11. Bensimon, A., et al., *ATM-Dependent and -Independent Dynamics of the Nuclear Phosphoproteome After DNA Damage.* Sci. Signal., 2010. **3**(151).
12. Matsuoka, S., et al., *ATM and ATR Substrate Analysis Reveals Extensive Protein Networks Responsive to DNA Damage.* Science, 2007. **316**(5828): p. 1160-1166.
13. Perl, A., et al., *Oxidative stress, inflammation and carcinogenesis are controlled through the pentose phosphate pathway by transaldolase.* Trends in Molecular Medicine, 2011. **17**(7): p. 395-403.
14. Alexander, A., et al., *ATM signals to TSC2 in the cytoplasm to regulate mTORC1 in response to ROS.* Proceedings of the National Academy of Sciences, 2010.
15. Yang, D.-Q. and M.B. Kastan, *Participation of ATM in insulin signalling through phosphorylation of eIF-4E-binding protein 1.* Nat Cell Biol, 2000. **2**(12): p. 893-898.

16. Halaby, M.J., et al., *ATM protein kinase mediates full activation of Akt and regulates glucose transporter 4 translocation by insulin in muscle cells.* Cell Signal, 2008. **20**(8): p. 1555-63.
17. Savitsky, K., et al., *A Single Ataxia Telangiectasia Gene with a Product Similar to PI-3 Kinase.* Science, 1995. **268**(5218): p. 1749-1753.
18. Khanna, K.K., *Cancer risk and the ATM gene: a continuing debate.* J Natl Cancer Inst, 2000. **92**(10): p. 795-802.
19. Athma, P., R. Rappaport, and M. Swift, *Molecular genotyping shows that ataxia-telangiectasia heterozygotes are predisposed to breast cancer.* Cancer Genet Cytogenet, 1996. **92**(2): p. 130-4.
20. Spring, K., et al., *Mice heterozygous for mutation in Atm, the gene involved in ataxia-telangiectasia, have heightened susceptibility to cancer.* Nat Genet, 2002. **32**(1): p. 185-90.
21. Barlow, C., et al., *Atm-deficient mice: a paradigm of ataxia telangiectasia.* Cell, 1996. **86**(1): p. 159-71.
22. Yamamoto, K., et al., *Kinase-dead ATM protein causes genomic instability and early embryonic lethality in mice.* J Cell Biol, 2012. **198**(3): p. 305-13.
23. Kim, S.T., et al., *Substrate specificities and identification of putative substrates of ATM kinase family members.* J Biol Chem, 1999. **274**(53): p. 37538-43.
24. Baretic, D. and R.L. Williams, *PIKKs--the solenoid nest where partners and kinases meet.* Curr Opin Struct Biol, 2014. **29**: p. 134-42.
25. Keith, C.T. and S.L. Schreiber, *PIK-related kinases: DNA repair, recombination, and cell cycle checkpoints.* Science, 1995. **270**(5233): p. 50-1.
26. Paull, T.T., *Mechanisms of ATM Activation.* Annu Rev Biochem, 2015.
27. Perry, J. and N. Kleckner, *The ATRs, ATMs, and TORs are giant HEAT repeat proteins.* Cell, 2003. **112**(2): p. 151-5.
28. Chook, Y.M. and G. Blobel, *Structure of the nuclear transport complex karyopherin-beta2-Ran x GppNHp.* Nature, 1999. **399**(6733): p. 230-7.
29. Groves, M.R., et al., *The structure of the protein phosphatase 2A PR65/A subunit reveals the conformation of its 15 tandemly repeated HEAT motifs.* Cell, 1999. **96**(1): p. 99-110.
30. Cingolani, G., et al., *Structure of importin-beta bound to the IBB domain of importin-alpha.* Nature, 1999. **399**(6733): p. 221-9.
31. Fernandes, N., et al., *DNA Damage-induced Association of ATM with Its Target Proteins Requires a Protein Interaction Domain in the N Terminus of ATM.* J. Biol. Chem., 2005. **280**(15): p. 15158-15164.
32. You, Z., et al., *ATM activation and its recruitment to damaged DNA require binding to the C terminus of Nbs1.* Mol Cell Biol, 2005. **25**(13): p. 5363-79.
33. Lee, J.-H. and T.T. Paull, *Direct Activation of the ATM Protein Kinase by the Mre11/Rad50/Nbs1 Complex.* Science, 2004. **304**(5667): p. 93-96.

34. Lee, J.-H. and T.T. Paull, *ATM Activation by DNA Double-Strand Breaks Through the Mre11-Rad50-Nbs1 Complex.* Science, 2005. **308**(5721): p. 551-554.
35. Bosotti, R., A. Isacchi, and E.L. Sonnhammer, *FAT: a novel domain in PIK-related kinases.* Trends Biochem Sci, 2000. **25**(5): p. 225-7.
36. Spagnolo, L., et al., *Three-dimensional structure of the human DNA-PKcs/Ku70/Ku80 complex assembled on DNA and its implications for DNA DSB repair.* Mol Cell, 2006. **22**(4): p. 511-9.
37. Lempiäinen, H. and T.D. Halazonetis, *Emerging common themes in regulation of PIKKs and PI3Ks.* The EMBO Journal, 2009. **28**(20): p. 3067-3073.
38. Jiang, X., et al., *The FATC domains of PIKK proteins are functionally equivalent and participate in the Tip60-dependent activation of DNA-PKcs and ATM.* J Biol Chem, 2006. **281**(23): p. 15741-6.
39. Mordes, D.A., et al., *TopBP1 activates ATR through ATRIP and a PIKK regulatory domain.* Genes & Development, 2008. **22**(11): p. 1478-1489.
40. Takahashi, T., et al., *Carboxyl-terminal region conserved among phosphoinositide-kinase-related kinases is indispensable for mTOR function in vivo and in vitro.* Genes Cells, 2000. **5**(9): p. 765-75.
41. Peterson, R.T., et al., *FKBP12-rapamycin-associated protein (FRAP) autophosphorylates at serine 2481 under translationally repressive conditions.* J Biol Chem, 2000. **275**(10): p. 7416-23.
42. Gilad, S., et al., *Genotype-phenotype relationships in ataxia-telangiectasia and variants.* Am J Hum Genet, 1998. **62**(3): p. 551-61.
43. Banin, S., et al., *Enhanced phosphorylation of p53 by ATM in response to DNA damage.* Science, 1998. **281**(5383): p. 1674-7.
44. Sekulic, A., et al., *A direct linkage between the phosphoinositide 3-kinase-AKT signaling pathway and the mammalian target of rapamycin in mitogen-stimulated and transformed cells.* Cancer Res, 2000. **60**(13): p. 3504-13.
45. Kumagai, A., et al., *TopBP1 activates the ATR-ATRIP complex.* Cell, 2006. **124**(5): p. 943-55.
46. Llorca, O., et al., *Electron microscopy and 3D reconstructions reveal that human ATM kinase uses an arm-like domain to clamp around double-stranded DNA.* Oncogene, 2003. **22**(25): p. 3867-74.
47. Rhodes, N., T.M. Gilmer, and T.J. Lansing, *Expression and purification of active recombinant ATM protein from transiently transfected mammalian cells.* Protein Expr Purif, 2001. **22**(3): p. 462-6.
48. Yang, H., et al., *mTOR kinase structure, mechanism and regulation.* Nature, 2013. **497**(7448): p. 217-23.
49. Sibanda, B.L., D.Y. Chirgadze, and T.L. Blundell, *Crystal structure of DNA-PKcs reveals a large open-ring cradle comprised of HEAT repeats.* Nature, 2010. **463**(7277): p. 118-21.

50. Walker, E.H., et al., *Structural Determinants of Phosphoinositide 3-Kinase Inhibition by Wortmannin, LY294002, Quercetin, Myricetin, and Staurosporine.* Molecular Cell, 2000. **6**(4): p. 909-919.
51. Dames, S.A., et al., *The Solution Structure of the FATC Domain of the Protein Kinase Target of Rapamycin Suggests a Role for Redox-dependent Structural and Cellular Stability.* J. Biol. Chem., 2005. **280**(21): p. 20558-20564.
52. Rivera-Calzada, A., et al., *Three-dimensional structure and regulation of the DNA-dependent protein kinase catalytic subunit (DNA-PKcs).* Structure, 2005. **13**(2): p. 243-55.
53. Williams, D.R., et al., *Cryo-EM structure of the DNA-dependent protein kinase catalytic subunit at subnanometer resolution reveals alpha helices and insight into DNA binding.* Structure, 2008. **16**(3): p. 468-77.
54. Chiu, C.Y., et al., *Cryo-EM imaging of the catalytic subunit of the DNA-dependent protein kinase.* J Mol Biol, 1998. **284**(4): p. 1075-81.
55. Falck, J., J. Coates, and S.P. Jackson, *Conserved modes of recruitment of ATM, ATR and DNA-PKcs to sites of DNA damage.* Nature, 2005. **434**(7033): p. 605-11.
56. Khalil, H., et al., *Targeting ATM pathway for therapeutic intervention in cancer.* Biodiscovery, 2012. **1**(3).
57. Miyamoto, S., *Nuclear initiated NF-[kappa]B signaling: NEMO and ATM take center stage.* Cell Res, 2011. **21**(1): p. 116-130.
58. Lim, D.S., et al., *ATM binds to beta-adaptin in cytoplasmic vesicles.* Proc Natl Acad Sci U S A, 1998. **95**(17): p. 10146-51.
59. Watters, D., et al., *Localization of a Portion of Extranuclear ATM to Peroxisomes.* Journal of Biological Chemistry, 1999. **274**(48): p. 34277-34282.
60. Li, J., et al., *Cytoplasmic ATM in Neurons Modulates Synaptic Function.* Current Biology, 2009. **19**(24): p. 2091-2096.
61. Boehrs, J.K., et al., *Constitutive expression and cytoplasmic compartmentalization of ATM protein in differentiated human neuron-like SH-SY5Y cells.* J Neurochem, 2007. **100**(2): p. 337-45.
62. Deshpande, R.A., et al., *ATP-driven Rad50 conformations regulate DNA tethering, end resection, and ATM checkpoint signaling.* Embo j, 2014. **33**(5): p. 482-500.
63. Stracker, T.H. and J.H.J. Petrini, *The MRE11 complex: starting from the ends.* Nat Rev Mol Cell Biol, 2011. **12**(2): p. 90-103.
64. Williams, R.S., J.S. Williams, and J.A. Tainer, *Mre11-Rad50-Nbs1 is a keystone complex connecting DNA repair machinery, double-strand break signaling, and the chromatin template.* Biochem Cell Biol, 2007. **85**(4): p. 509-20.

65. Lim, H.S., et al., *Crystal structure of the Mre11–Rad50–ATPγS complex: understanding the interplay between Mre11 and Rad50.* Genes & Development, 2011. **25**(10): p. 1091-1104.
66. Möckel, C., et al., *ATP driven structural changes of the bacterial Mre11:Rad50 catalytic head complex.* Nucleic Acids Research, 2011.
67. Williams, G.J., et al., *ABC ATPase signature helices in Rad50 link nucleotide state to Mre11 interface for DNA repair.* Nat Struct Mol Biol, 2011. **advance online publication**.
68. Desai-Mehta, A., K.M. Cerosaletti, and P. Concannon, *Distinct functional domains of nibrin mediate Mre11 binding, focus formation, and nuclear localization.* Mol Cell Biol, 2001. **21**(6): p. 2184-91.
69. Chapman, J.R. and S.P. Jackson, *Phospho-dependent interactions between NBS1 and MDC1 mediate chromatin retention of the MRN complex at sites of DNA damage.* EMBO Rep, 2008. **9**(8): p. 795-801.
70. Paull, T.T. and R.A. Deshpande, *The Mre11/Rad50/Nbs1 complex: recent insights into catalytic activities and ATP-driven conformational changes.* Exp Cell Res, 2014. **329**(1): p. 139-47.
71. Dupre, A., L. Boyer-Chatenet, and J. Gautier, *Two-step activation of ATM by DNA and the Mre11-Rad50-Nbs1 complex.* Nat Struct Mol Biol, 2006. **13**(5): p. 451-457.
72. Carney, J.P., et al., *The hMre11/hRad50 protein complex and Nijmegen breakage syndrome: linkage of double-strand break repair to the cellular DNA damage response.* Cell, 1998. **93**(3): p. 477-86.
73. Waltes, R., et al., *Human RAD50 Deficiency in a Nijmegen Breakage Syndrome-like Disorder.* The American Journal of Human Genetics, 2009. **84**(5): p. 605-616.
74. Uziel, T., et al., *Requirement of the MRN complex for ATM activation by DNA damage.* EMBO J, 2003. **22**(20): p. 5612-21.
75. Stewart, G.S., et al., *The DNA double-strand break repair gene hMRE11 is mutated in individuals with an ataxia-telangiectasia-like disorder.* Cell, 1999. **99**(6): p. 577-87.
76. Varon, R., et al., *Nibrin, a novel DNA double-strand break repair protein, is mutated in Nijmegen breakage syndrome.* Cell, 1998. **93**(3): p. 467-76.
77. Hopfner, K.P., et al., *Structural biochemistry and interaction architecture of the DNA double-strand break repair Mre11 nuclease and Rad50-ATPase.* Cell, 2001. **105**(4): p. 473-85.
78. Das, D., et al., *Crystal structure of the first eubacterial Mre11 nuclease reveals novel features that may discriminate substrates during DNA repair.* J Mol Biol, 2010. **397**(3): p. 647-63.
79. Park, Y.B., et al., *Crystal Structure of Human Mre11: Understanding Tumorigenic Mutations.* Structure, 2011. **19**(11): p. 1591-1602.

80. Williams, R.S., et al., *Nbs1 Flexibly Tethers Ctp1 and Mre11-Rad50 to Coordinate DNA Double-Strand Break Processing and Repair.* Cell, 2009. **139**(1): p. 87-99.
81. Lafrance-Vanasse, J., G.J. Williams, and J.A. Tainer, *Envisioning the dynamics and flexibility of Mre11-Rad50-Nbs1 complex to decipher its roles in DNA replication and repair.* Prog Biophys Mol Biol, 2015.
82. Tauchi, H., et al., *Nijmegen breakage syndrome gene, NBS1, and molecular links to factors for genome stability.* Oncogene, 2002. **21**(58): p. 8967-80.
83. Williams, G.J., S.P. Lees-Miller, and J.A. Tainer, *Mre11-Rad50-Nbs1 conformations and the control of sensing, signaling, and effector responses at DNA double-strand breaks.* DNA Repair. **In Press, Corrected Proof**.
84. Lee, J.H., et al., *Regulation of Mre11/Rad50 by Nbs1: effects on nucleotide-dependent DNA binding and association with ataxia-telangiectasia-like disorder mutant complexes.* J Biol Chem, 2003. **278**(46): p. 45171-81.
85. Lammens, K., et al., *The Mre11:Rad50 Structure Shows an ATP-Dependent Molecular Clamp in DNA Double-Strand Break Repair.* Cell, 2011. **145**(1): p. 54-66.
86. Reichenbach, J., et al., *Elevated oxidative stress in patients with ataxia telangiectasia.* Antioxid Redox Signal, 2002. **4**(3): p. 465-9.
87. Reichenbach, J., et al., *Anti-oxidative capacity in patients with ataxia telangiectasia.* Clin Exp Immunol, 1999. **117**(3): p. 535-9.
88. Kamsler, A., et al., *Increased oxidative stress in ataxia telangiectasia evidenced by alterations in redox state of brains from Atm-deficient mice.* Cancer Res, 2001. **61**(5): p. 1849-54.
89. Reliene, R. and R.H. Schiestl, *Antioxidant N-acetyl cysteine reduces incidence and multiplicity of lymphoma in Atm deficient mice.* DNA Repair, 2006. **5**(7): p. 852-859.
90. Ito, K., et al., *Regulation of reactive oxygen species by Atm is essential for proper response to DNA double-strand breaks in lymphocytes.* J Immunol, 2007. **178**(1): p. 103-10.
91. Yi, M., M.P. Rosin, and C.K. Anderson, *Response of fibroblast cultures from ataxia-telangiectasia patients to oxidative stress.* Cancer Lett, 1990. **54**(1-2): p. 43-50.
92. Green, M.H., et al., *Hypersensitivity of ataxia-telangiectasia fibroblasts to a nitric oxide donor.* Free Radic Biol Med, 1997. **22**(1-2): p. 343-7.
93. Barzilai, A., G. Rotman, and Y. Shiloh, *ATM deficiency and oxidative stress: a new dimension of defective response to DNA damage.* DNA Repair (Amst), 2002. **1**(1): p. 3-25.
94. Kozlov, S.V., et al., *Autophosphorylation and ATM Activation.* Journal of Biological Chemistry, 2011. **286**(11): p. 9107-9119.

95. Kozlov, S.V., et al., *Involvement of novel autophosphorylation sites in ATM activation.* Embo j, 2006. **25**(15): p. 3504-14.
96. So, S., A.J. Davis, and D.J. Chen, *Autophosphorylation at serine 1981 stabilizes ATM at DNA damage sites.* The Journal of Cell Biology, 2009.
97. Daniel, J.A., et al., *Multiple autophosphorylation sites are dispensable for murine ATM activation in vivo.* J Cell Biol, 2008. **183**(5): p. 777-83.
98. Pellegrini, M., et al., *Autophosphorylation at serine 1987 is dispensable for murine Atm activation in vivo.* Nature, 2006. **443**(7108): p. 222-225.
99. Tian, B., Q. Yang, and Z. Mao, *Phosphorylation of ATM by Cdk5 mediates DNA damage signalling and regulates neuronal death.* Nat Cell Biol, 2009. **11**(2): p. 211-8.
100. Lee, H.J., et al., *Tyrosine 370 phosphorylation of ATM positively regulates DNA damage response.* Cell Res, 2015. **25**(2): p. 225-36.
101. Shafman, T., et al., *Interaction between ATM protein and c-Abl in response to DNA damage.* Nature, 1997. **387**(6632): p. 520-3.
102. Baskaran, R., et al., *Ataxia telangiectasia mutant protein activates c-Abl tyrosine kinase in response to ionizing radiation.* Nature, 1997. **387**(6632): p. 516-9.
103. Wang, X., et al., *A positive role for c-Abl in Atm and Atr activation in DNA damage response.* Cell Death Differ, 2010.
104. Sun, Y., et al., *A role for the Tip60 histone acetyltransferase in the acetylation and activation of ATM.* Proc Natl Acad Sci U S A, 2005. **102**(37): p. 13182-7.
105. Sun, Y., et al., *DNA Damage-Induced Acetylation of Lysine 3016 of ATM Activates ATM Kinase Activity.* Mol. Cell. Biol., 2007. **27**(24): p. 8502-8509.
106. Kaidi, A. and S.P. Jackson, *KAT5 tyrosine phosphorylation couples chromatin sensing to ATM signalling.* Nature, 2013. **498**(7452): p. 70-4.
107. Beli, P., et al., *Proteomic Investigations Reveal a Role for RNA Processing Factor THRAP3 in the DNA Damage Response.* Molecular Cell.
108. Bensimon, A., R. Aebersold, and Y. Shiloh, *Beyond ATM: The protein kinase landscape of the DNA damage response.* FEBS Letters, 2011. **585**(11): p. 1625-1639.
109. Gatei, M., et al., *Ataxia-telangiectasia-mutated (ATM) and NBS1-dependent phosphorylation of Chk1 on Ser-317 in response to ionizing radiation.* J Biol Chem, 2003. **278**(17): p. 14806-11.
110. Melchionna, R., et al., *Threonine 68 is required for radiation-induced phosphorylation and activation of Cds1.* Nat Cell Biol, 2000. **2**(10): p. 762-5.
111. Ahn, J.Y., et al., *Threonine 68 phosphorylation by ataxia telangiectasia mutated is required for efficient activation of Chk2 in response to ionizing radiation.* Cancer Res, 2000. **60**(21): p. 5934-6.

112. Chen, B.P., et al., *Ataxia telangiectasia mutated (ATM) is essential for DNA-PKcs phosphorylations at the Thr-2609 cluster upon DNA double strand break.* J Biol Chem, 2007. **282**(9): p. 6582-7.
113. Xu, N., et al., *Akt: a double-edged sword in cell proliferation and genome stability.* J Oncol, 2012. **2012**: p. 951724.
114. Kroonen, J., et al., *Casein kinase 2 inhibition modulates the DNA damage response but fails to radiosensitize malignant glioma cells.* Int J Oncol, 2012. **41**(2): p. 776-82.
115. Siddiqui-Jain, A., et al., *CK2 inhibitor CX-4945 suppresses DNA repair response triggered by DNA-targeted anticancer drugs and augments efficacy: mechanistic rationale for drug combination therapy.* Mol Cancer Ther, 2012. **11**(4): p. 994-1005.
116. Litchfield, D.W., *Protein kinase CK2: structure, regulation and role in cellular decisions of life and death.* Biochem J, 2003. **369**(Pt 1): p. 1-15.
117. Burnett, G. and E.P. Kennedy, *The enzymatic phosphorylation of proteins.* J Biol Chem, 1954. **211**(2): p. 969-80.
118. Thornburg, W. and T.J. Lindell, *Purification of rat liver nuclear protein kinase NII.* J Biol Chem, 1977. **252**(19): p. 6660-5.
119. Lasa-Benito, M., et al., *Golgi apparatus mammary gland casein kinase: monitoring by a specific peptide substrate and definition of specificity determinants.* FEBS Lett, 1996. **382**(1-2): p. 149-52.
120. Padmanabha, R., et al., *Isolation, sequencing, and disruption of the yeast CKA2 gene: casein kinase II is essential for viability in Saccharomyces cerevisiae.* Mol Cell Biol, 1990. **10**(8): p. 4089-99.
121. Hanna, D.E., A. Rethinaswamy, and C.V. Glover, *Casein kinase II is required for cell cycle progression during G1 and G2/M in Saccharomyces cerevisiae.* J Biol Chem, 1995. **270**(43): p. 25905-14.
122. Lou, D.Y., et al., *The alpha catalytic subunit of protein kinase CK2 is required for mouse embryonic development.* Mol Cell Biol, 2008. **28**(1): p. 131-9.
123. Buchou, T., et al., *Disruption of the regulatory beta subunit of protein kinase CK2 in mice leads to a cell-autonomous defect and early embryonic lethality.* Mol Cell Biol, 2003. **23**(3): p. 908-15.
124. Xu, X., et al., *Globozoospermia in mice lacking the casein kinase II alpha' catalytic subunit.* Nat Genet, 1999. **23**(1): p. 118-21.
125. Tawfic, S., et al., *Protein kinase CK2 signal in neoplasia.* Histol Histopathol, 2001. **16**(2): p. 573-82.
126. Trembley, J.H., et al., *Protein kinase CK2 in health and disease: CK2: a key player in cancer biology.* Cell Mol Life Sci, 2009. **66**(11-12): p. 1858-67.
127. Meggio, F. and L.A. Pinna, *One-thousand-and-one substrates of protein kinase CK2?* Faseb j, 2003. **17**(3): p. 349-68.

128. Niefind, K., et al., *Crystal structure of human protein kinase CK2: insights into basic properties of the CK2 holoenzyme.* Embo j, 2001. **20**(19): p. 5320-31.
129. Bian, Y., et al., *Global screening of CK2 kinase substrates by an integrated phosphoproteomics workflow.* Sci Rep, 2013. **3**: p. 3460.
130. Kuenzel, E.A., et al., *Substrate specificity determinants for casein kinase II as deduced from studies with synthetic peptides.* J Biol Chem, 1987. **262**(19): p. 9136-40.
131. Bodenbach, L., et al., *Recombinant human casein kinase II. A study with the complete set of subunits (alpha, alpha' and beta), site-directed autophosphorylation mutants and a bicistronically expressed holoenzyme.* Eur J Biochem, 1994. **220**(1): p. 263-73.
132. Vilk, G., et al., *Protein kinase CK2 catalyzes tyrosine phosphorylation in mammalian cells.* Cell Signal, 2008. **20**(11): p. 1942-51.
133. Donella-Deana, A., et al., *Autocatalytic tyrosine-phosphorylation of protein kinase CK2 alpha and alpha' subunits: implication of Tyr182.* Biochem J, 2001. **357**(Pt 2): p. 563-7.
134. Basnet, H., et al., *Tyrosine phosphorylation of histone H2A by CK2 regulates transcriptional elongation.* Nature, 2014. **516**(7530): p. 267-71.
135. Ahmed, K., D.A. Gerber, and C. Cochet, *Joining the cell survival squad: an emerging role for protein kinase CK2.* Trends Cell Biol, 2002. **12**(5): p. 226-30.
136. Canton, D.A. and D.W. Litchfield, *The shape of things to come: an emerging role for protein kinase CK2 in the regulation of cell morphology and the cytoskeleton.* Cell Signal, 2006. **18**(3): p. 267-75.
137. Li, P.F., et al., *Phosphorylation by protein kinase CK2: a signaling switch for the caspase-inhibiting protein ARC.* Mol Cell, 2002. **10**(2): p. 247-58.
138. Olsen, B.B., et al., *Protein kinase CK2 localizes to sites of DNA double-strand break regulating the cellular response to DNA damage.* BMC Mol Biol, 2012. **13**: p. 7.
139. Hari, F.J., et al., *A divalent FHA/BRCT-binding mechanism couples the MRE11-RAD50-NBS1 complex to damaged chromatin.* EMBO Rep, 2010. **11**(5): p. 387-392.
140. Spycher, C., et al., *Constitutive phosphorylation of MDC1 physically links the MRE11-RAD50-NBS1 complex to damaged chromatin.* J Cell Biol, 2008. **181**(2): p. 227-40.
141. Kim, S.T., *Protein kinase CK2 interacts with Chk2 and phosphorylates Mre11 on serine 649.* Biochem Biophys Res Commun, 2005. **331**(1): p. 247-52.
142. Ayoub, N., et al., *HP1-beta mobilization promotes chromatin changes that initiate the DNA damage response.* Nature, 2008. **453**(7195): p. 682-6.
143. Yata, K., et al., *Plk1 and CK2 act in concert to regulate Rad51 during DNA double strand break repair.* Mol Cell, 2012. **45**(3): p. 371-83.

144. Hjerrild, M., et al., *Phosphorylation of murine double minute clone 2 (MDM2) protein at serine-267 by protein kinase CK2 in vitro and in cultured cells.* Biochem J, 2001. **355**(Pt 2): p. 347-56.
145. Gotz, C., et al., *Identification of a CK2 phosphorylation site in mdm2.* Eur J Biochem, 1999. **266**(2): p. 493-501.
146. Allende-Vega, N., et al., *Phosphorylation of the acidic domain of Mdm2 by protein kinase CK2.* Mol Cell Biochem, 2005. **274**(1-2): p. 85-90.
147. Rao, F., et al., *Inositol pyrophosphates mediate the DNA-PK/ATM-p53 cell death pathway by regulating CK2 phosphorylation of Tti1/Tel2.* Mol Cell, 2014. **54**(1): p. 119-32.
148. Hurov, K.E., C. Cotta-Ramusino, and S.J. Elledge, *A genetic screen identifies the Triple T complex required for DNA damage signaling and ATM and ATR stability.* Genes Dev, 2010. **24**(17): p. 1939-50.
149. Horejsi, Z., et al., *CK2 phospho-dependent binding of R2TP complex to TEL2 is essential for mTOR and SMG1 stability.* Mol Cell, 2010. **39**(6): p. 839-50.
150. Takai, H., et al., *Tel2 regulates the stability of PI3K-related protein kinases.* Cell, 2007. **131**(7): p. 1248-59.
151. Shanware, N.P., et al., *Coregulated ataxia telangiectasia-mutated and casein kinase sites modulate cAMP-response element-binding protein-coactivator interactions in response to DNA damage.* J Biol Chem, 2007. **282**(9): p. 6283-91.
152. Luo, H., et al., *Regulation of intra-S phase checkpoint by ionizing radiation (IR)-dependent and IR-independent phosphorylation of SMC3.* J Biol Chem, 2008. **283**(28): p. 19176-83.
153. Niefind, K., J. Raaf, and O.G. Issinger, *Protein kinase CK2 in health and disease: Protein kinase CK2: from structures to insights.* Cell Mol Life Sci, 2009. **66**(11-12): p. 1800-16.
154. Keller, D.M. and H. Lu, *p53 serine 392 phosphorylation increases after UV through induction of the assembly of the CK2.hSPT16.SSRP1 complex.* J Biol Chem, 2002. **277**(51): p. 50206-13.
155. Mottet, D., et al., *Role for casein kinase 2 in the regulation of HIF-1 activity.* Int J Cancer, 2005. **117**(5): p. 764-74.
156. Gerber, D.A., et al., *Heat-induced relocalization of protein kinase CK2. Implication of CK2 in the context of cellular stress.* J Biol Chem, 2000. **275**(31): p. 23919-26.
157. Murtaza, I., et al., *Down-regulation of catalase and oxidative modification of protein kinase CK2 lead to the failure of apoptosis repressor with caspase recruitment domain to inhibit cardiomyocyte hypertrophy.* J Biol Chem, 2008. **283**(10): p. 5996-6004.

158. Ghavidel, A. and M.C. Schultz, *TATA binding protein-associated CK2 transduces DNA damage signals to the RNA polymerase III transcriptional machinery.* Cell, 2001. **106**(5): p. 575-84.
159. Johnston, I.M., et al., *CK2 forms a stable complex with TFIIIB and activates RNA polymerase III transcription in human cells.* Mol Cell Biol, 2002. **22**(11): p. 3757-68.
160. Kumar, R. and M. Tao, *Multiple forms of casein kinase from rabbit erythrocytes.* Biochim Biophys Acta, 1975. **410**(1): p. 87-98.
161. Hathaway, G.M. and J.A. Traugh, *Cyclic nucleotide-independent protein kinases from rabbit reticulocytes. Purification of casein kinases.* J Biol Chem, 1979. **254**(3): p. 762-8.
162. Glover, C.V., *A filamentous form of Drosophila casein kinase II.* J Biol Chem, 1986. **261**(30): p. 14349-54.
163. Valero, E., et al., *Quaternary structure of casein kinase 2. Characterization of multiple oligomeric states and relation with its catalytic activity.* J Biol Chem, 1995. **270**(14): p. 8345-52.
164. Hubner, G.M., et al., *Evidence for aggregation of protein kinase CK2 in the cell: a novel strategy for studying CK2 holoenzyme interaction by BRET(2).* Mol Cell Biochem, 2014. **397**(1-2): p. 285-93.
165. Poole, A., et al., *A global view of CK2 function and regulation.* Mol Cell Biochem, 2005. **274**(1-2): p. 163-70.
166. Lolli, G., L.A. Pinna, and R. Battistutta, *Structural determinants of protein kinase CK2 regulation by autoinhibitory polymerization.* ACS Chem Biol, 2012. **7**(7): p. 1158-63.
167. Niefind, K. and O.G. Issinger, *Primary and secondary interactions between CK2alpha and CK2beta lead to ring-like structures in the crystals of the CK2 holoenzyme.* Mol Cell Biochem, 2005. **274**(1-2): p. 3-14.
168. Schnitzler, A., et al., *The protein kinase CK2(Andante) holoenzyme structure supports proposed models of autoregulation and trans-autophosphorylation.* J Mol Biol, 2014. **426**(9): p. 1871-82.
169. Mamrack, M.D., *Stimulation of enzymatic activity in filament preparations of casein kinase II by polylysine, melittin, and spermine.* Mol Cell Biochem, 1989. **85**(2): p. 147-57.
170. Boldyreff, B., et al., *Reconstitution of normal and hyperactivated forms of casein kinase-2 by variably mutated beta-subunits.* Biochemistry, 1993. **32**(47): p. 12672-7.
171. Sarno, S., et al., *Basic residues in the 74-83 and 191-198 segments of protein kinase CK2 catalytic subunit are implicated in negative but not in positive regulation by the beta-subunit.* Eur J Biochem, 1997. **248**(2): p. 290-5.

172. Krehan, A., et al., *Interaction sites between catalytic and regulatory subunits in human protein kinase CK2 holoenzymes as indicated by chemical cross-linking and immunological investigations.* Biochemistry, 1996. **35**(15): p. 4966-75.
173. Mu, J.-J., et al., *A Proteomic Analysis of Ataxia Telangiectasia-mutated (ATM)/ATM-Rad3-related (ATR) Substrates Identifies the Ubiquitin-Proteasome System as a Regulator for DNA Damage Checkpoints.* Journal of Biological Chemistry, 2007. **282**(24): p. 17330-17334.
174. Bhaskara, V., et al., *Rad50 adenylate kinase activity regulates DNA tethering by Mre11/Rad50 complexes.* Mol Cell, 2007. **25**(5): p. 647-61.
175. Paull, T.T. and M. Gellert, *The 3' to 5' exonuclease activity of Mre 11 facilitates repair of DNA double-strand breaks.* Mol Cell, 1998. **1**(7): p. 969-79.
176. Paull, T.T. and M. Gellert, *Nbs1 potentiates ATP-driven DNA unwinding and endonuclease cleavage by the Mre11/Rad50 complex.* Genes Dev, 1999. **13**(10): p. 1276-88.
177. Lee, J.H. and T.T. Paull, *Purification and biochemical characterization of ataxia-telangiectasia mutated and Mre11/Rad50/Nbs1.* Methods Enzymol, 2006. **408**: p. 529-39.
178. Zhang, N., et al., *Isolation of full-length ATM cDNA and correction of the ataxia-telangiectasia cellular phenotype.* Proceedings of the National Academy of Sciences of the United States of America, 1997. **94**(15): p. 8021-8026.
179. Wenger, C.D., et al., *COMPASS: a suite of pre- and post-search proteomics software tools for OMSSA.* Proteomics, 2011. **11**(6): p. 1064-74.
180. de Hoon, M.J., et al., *Open source clustering software.* Bioinformatics, 2004. **20**(9): p. 1453-4.
181. Saldanha, A.J., *Java Treeview--extensible visualization of microarray data.* Bioinformatics, 2004. **20**(17): p. 3246-8.
182. Chou, M.F. and D. Schwartz, *Biological sequence motif discovery using motif-x.* Curr Protoc Bioinformatics, 2011. **Chapter 13**: p. Unit 13.15-24.
183. Schwartz, D. and S.P. Gygi, *An iterative statistical approach to the identification of protein phosphorylation motifs from large-scale data sets.* Nat Biotechnol, 2005. **23**(11): p. 1391-8.
184. Xue, Y., et al., *GPS 2.1: enhanced prediction of kinase-specific phosphorylation sites with an algorithm of motif length selection.* Protein Eng Des Sel, 2011. **24**(3): p. 255-60.
185. Pfaffl, M.W., G.W. Horgan, and L. Dempfle, *Relative expression software tool (REST) for group-wise comparison and statistical analysis of relative expression results in real-time PCR.* Nucleic Acids Res, 2002. **30**(9): p. e36.
186. Shah, K., et al., *Engineering unnatural nucleotide specificity for Rous sarcoma virus tyrosine kinase to uniquely label its direct substrates.* Proceedings of the National Academy of Sciences of the United States of America, 1997. **94**(8): p. 3565-3570.

187. Kodama, M., et al., *Requirement of ATM for Rapid p53 Phosphorylation at Ser46 without Ser/Thr-Gln Sequences.* Molecular and Cellular Biology, 2010. **30**(7): p. 1620-1633.
188. Costanzo, V., et al., *Mre11 assembles linear DNA fragments into DNA damage signaling complexes.* PLoS Biol, 2004. **2**(5): p. E110.
189. Shiotani, B. and L. Zou, *Single-stranded DNA orchestrates an ATM-to-ATR switch at DNA breaks.* Mol Cell, 2009. **33**(5): p. 547-58.
190. Hopfner, K.P., et al., *Structural biology of Rad50 ATPase: ATP-driven conformational control in DNA double-strand break repair and the ABC-ATPase superfamily.* Cell, 2000. **101**(7): p. 789-800.
191. Buis, J., et al., *Mre11 Nuclease Activity Has Essential Roles in DNA Repair and Genomic Stability Distinct from ATM Activation.* Cell, 2008. **135**(1): p. 85-96.
192. de Jager, M., et al., *DNA end-binding specificity of human Rad50/Mre11 is influenced by ATP.* Nucleic Acids Res, 2002. **30**(20): p. 4425-31.
193. Hopfner, K.P., et al., *The Rad50 zinc-hook is a structure joining Mre11 complexes in DNA recombination and repair.* Nature, 2002. **418**(6897): p. 562-6.
194. Wiltzius, J.J., et al., *The Rad50 hook domain is a critical determinant of Mre11 complex functions.* Nat Struct Mol Biol, 2005. **12**(5): p. 403-7.
195. Hohl, M., et al., *The Rad50 coiled-coil domain is indispensable for Mre11 complex functions.* Nat Struct Mol Biol, 2011. **advance online publication**.
196. He, J., et al., *Rad50 zinc hook is important for the Mre11 complex to bind chromosomal DNA double-stranded breaks and initiate various DNA damage responses.* J Biol Chem, 2012. **287**(38): p. 31747-56.
197. de Jager, M., et al., *Human Rad50/Mre11 is a flexible complex that can tether DNA ends.* Mol Cell, 2001. **8**(5): p. 1129-35.
198. Kinoshita, E., et al., *RAD50, an SMC family member with multiple roles in DNA break repair: how does ATP affect function?* Chromosome Res, 2009. **17**(2): p. 277-88.
199. Williams, R.S., et al., *Mre11 dimers coordinate DNA end bridging and nuclease processing in double-strand-break repair.* Cell, 2008. **135**(1): p. 97-109.
200. Fang, Y., et al., *Phosphatidic acid-mediated mitogenic activation of mTOR signaling.* Science, 2001. **294**(5548): p. 1942-5.
201. McKinnon, P.J. and L.A. Burgoyne, *Altered cellular morphology and microfilament array in ataxia-telangiectasia fibroblasts.* Eur J Cell Biol, 1985. **39**(1): p. 161-6.
202. Bhattacharyya, S., et al., *Cystathionine beta-synthase (CBS) contributes to advanced ovarian cancer progression and drug resistance.* PLoS One, 2013. **8**(11): p. e79167.

203. Huang da, W., B.T. Sherman, and R.A. Lempicki, *Systematic and integrative analysis of large gene lists using DAVID bioinformatics resources.* Nat Protoc, 2009. **4**(1): p. 44-57.
204. Huang da, W., B.T. Sherman, and R.A. Lempicki, *Bioinformatics enrichment tools: paths toward the comprehensive functional analysis of large gene lists.* Nucleic Acids Res, 2009. **37**(1): p. 1-13.
205. Ambrose, M. and R.A. Gatti, *Pathogenesis of ataxia-telangiectasia: the next generation of ATM functions.* Blood, 2013. **121**(20): p. 4036-45.
206. Ambrose, M., J.V. Goldstine, and R.A. Gatti, *Intrinsic mitochondrial dysfunction in ATM-deficient lymphoblastoid cells.* Hum Mol Genet, 2007. **16**(18): p. 2154-64.
207. Valentin-Vega, Y.A., et al., *Mitochondrial Dysfunction in Ataxia-Telangiectasia.* Blood, 2012. **119**(6): p. 1490-1500.
208. Eaton, J.S., et al., *Ataxia-telangiectasia mutated kinase regulates ribonucleotide reductase and mitochondrial homeostasis.* J Clin Invest, 2007. **117**(9): p. 2723-34.
209. Canman, C.E., et al., *The p53-dependent G1 cell cycle checkpoint pathway and ataxia-telangiectasia.* Cancer Res, 1994. **54**(19): p. 5054-8.
210. Jung, M., et al., *Correction of radiation sensitivity in ataxia telangiectasia cells by a truncated I kappa B-alpha.* Science, 1995. **268**(5217): p. 1619-21.
211. Beamish, H., et al., *Defect in multiple cell cycle checkpoints in ataxia-telangiectasia postirradiation.* J Biol Chem, 1996. **271**(34): p. 20486-93.
212. Barlow, C., et al., *Loss of the ataxia-telangiectasia gene product causes oxidative damage in target organs.* Proc Natl Acad Sci U S A, 1999. **96**(17): p. 9915-9.
213. Fu, X., et al., *Etoposide induces ATM-dependent mitochondrial biogenesis through AMPK activation.* PLoS One, 2008. **3**(4): p. e2009.
214. Cano, M., et al., *Oxidative stress induces mitochondrial dysfunction and a protective unfolded protein response in RPE cells.* Free Radic Biol Med, 2014. **69**: p. 1-14.
215. Wu, Z., et al., *Mechanisms controlling mitochondrial biogenesis and respiration through the thermogenic coactivator PGC-1.* Cell, 1999. **98**(1): p. 115-24.
216. Bannai, S., et al., *Enhancement of glutathione levels in mouse peritoneal macrophages by sodium arsenite, cadmium chloride and glucose/glucose oxidase.* Biochim Biophys Acta, 1991. **1092**(2): p. 175-9.
217. Jiang, L., et al., *Ferroptosis as a p53-mediated activity during tumour suppression.* Nature, 2015. **520**(7545): p. 57-62.
218. Sweeney, T.E., et al., *Differential regulation of the PGC family of genes in a mouse model of Staphylococcus aureus sepsis.* PLoS One, 2010. **5**(7): p. e11606.

219. Soyal, S., et al., *PGC-1alpha: a potent transcriptional cofactor involved in the pathogenesis of type 2 diabetes.* Diabetologia, 2006. **49**(7): p. 1477-88.
220. Xue, Y., et al., *GPS 2.0, a tool to predict kinase-specific phosphorylation sites in hierarchy.* Mol Cell Proteomics, 2008. **7**(9): p. 1598-608.
221. Penner, C.G., Z. Wang, and D.W. Litchfield, *Expression and localization of epitope-tagged protein kinase CK2.* J Cell Biochem, 1997. **64**(4): p. 525-37.
222. Cosentino, C., D. Grieco, and V. Costanzo, *ATM activates the pentose phosphate pathway promoting anti-oxidant defence and DNA repair.* EMBO J, 2010. **advance online publication**.
223. Giuliano, P., et al., *DNA damage induced by polyglutamine-expanded proteins.* Hum Mol Genet, 2003. **12**(18): p. 2301-9.
224. Dixon, S.J., et al., *Ferroptosis: an iron-dependent form of nonapoptotic cell death.* Cell, 2012. **149**(5): p. 1060-72.
225. Lee, J.H., et al., *Ataxia telangiectasia-mutated (ATM) kinase activity is regulated by ATP-driven conformational changes in the Mre11/Rad50/Nbs1 (MRN) complex.* J Biol Chem, 2013. **288**(18): p. 12840-51.
226. Guo, Z., R. Deshpande, and T.T. Paull, *ATM activation in the presence of oxidative stress.* Cell Cycle, 2010. **9**(24): p. 4805-4811.
227. Ditch, S. and T.T. Paull, *The ATM protein kinase and cellular redox signaling: beyond the DNA damage response.* Trends in Biochemical Sciences.
228. Ciechanover, A. and Y.T. Kwon, *Degradation of misfolded proteins in neurodegenerative diseases: therapeutic targets and strategies.* Exp Mol Med, 2015. **47**: p. e147.
229. Tabner, B.J., et al., *Protein aggregation, metals and oxidative stress in neurodegenerative diseases.* Biochem Soc Trans, 2005. **33**(Pt 5): p. 1082-6.
230. Miyata, Y. and I. Yahara, *The 90-kDa heat shock protein, HSP90, binds and protects casein kinase II from self-aggregation and enhances its kinase activity.* J Biol Chem, 1992. **267**(10): p. 7042-7.
231. Miyata, Y. and E. Nishida, *CK2 binds, phosphorylates, and regulates its pivotal substrate Cdc37, an Hsp90-cochaperone.* Mol Cell Biochem, 2005. **274**(1-2): p. 171-9.
232. Mollapour, M., et al., *Threonine 22 phosphorylation attenuates Hsp90 interaction with cochaperones and affects its chaperone activity.* Mol Cell, 2011. **41**(6): p. 672-81.
233. Duan, Y., et al., *HspA1A facilitates DNA repair in human bronchial epithelial cells exposed to Benzo[a]pyrene and interacts with casein kinase 2.* Cell Stress Chaperones, 2014. **19**(2): p. 271-9.
234. Watabe, M. and T. Nakaki, *Protein kinase CK2 regulates the formation and clearance of aggresomes in response to stress.* J Cell Sci, 2011. **124**(Pt 9): p. 1519-32.

235. White, J.S., S. Choi, and C.J. Bakkenist, *Transient ATM kinase inhibition disrupts DNA damage-induced sister chromatid exchange.* Sci Signal, 2010. **3**(124): p. ra44.
236. Gamper, A.M., et al., *ATM protein physically and functionally interacts with proliferating cell nuclear antigen to regulate DNA synthesis.* J Biol Chem, 2012. **287**(15): p. 12445-54.
237. Daniel, J.A., et al., *Loss of ATM kinase activity leads to embryonic lethality in mice.* J Cell Biol, 2012. **198**(3): p. 295-304.